
Individual Pitch Control for Load Mitigation

Master's Thesis
Stefan Jespersen & Randy Oldenbürger

Aalborg University, Esbjerg, 2017
Department of Energy Technology



Department of Energy Technology
Aalborg University, Esbjerg
<http://www.et.aau.dk>

AALBORG UNIVERSITY

STUDENT REPORT

Title:

Individual Pitch Control for Load Mitigation

Project Period:

September 2016 - June 2017

Group Members:

Stefan Jespersen
Randy Oldenbürger

Supervisor:

Mohsen Soltani

Page Numbers: 94

Date of Completion:

June 8, 2017

Abstract:

The objective of this report is the development of an individual pitch controller to mitigate loads on a wind turbine. This includes the development of a non-linear mathematical model, containing structural and aerodynamic properties. The structural model consists the fore-aft movement of the tower and the flap- and edgewise movement of the blades. For the modelling of the aerodynamics the Blade Element Momentum Theory (BEMT) has been used and implemented. The non-linear model has been used to make a linearization, to develop a linear model for control purposes.

Firstly, a collective PI controller has been developed to maintain steady power output, whereafter an individual PI controller has been implemented to even out the loads on the rotor caused by shear wind.

A successful MPC was not implemented due to time limitations.

Todo list

Preface

This report contains the documentation of a master project within the study programme M.Sc. in Offshore Energy Systems at Aalborg University Esbjerg, Denmark.

The thesis contains the modelling of a wind turbine and implementation of control systems, proposed by Vestas as a student project.

The purpose of this thesis has been *Individual Pitch Control using MPC*. But as this goal not has been reached, the title was changed to "*Individual Pitch Control for Load Mitigation*", as the implementation of an individual PI controller has been successful.

In this project NREL's aeroelastic computer-aided engineering (CAE) tool FAST is used. The original download folder contains a certified set-up of a 5 MW wind turbine, which was used for simulation purposes and verification of the developed control systems in this project.

As part of this project, several MATLAB scripts and Simulink models were developed and uploaded the database of Aalborg university. The content and the explanation of the files can be found on the first appendix page in this report

Last but not least, we would like to thank our Supervisor Mohsen Soltani for support and guidance through the project period. Furthermore we would also like to thank Tobias Gybel Hovgaard and Keld Hammerum from Vestas Wind Systems for the project proposal and guidance.

Aalborg University, Esbjerg, June 8, 2017

Stefan Jespersen

Randy Oldenbürger

Contents

List of Figures	vi
1 Introduction	2
1.1 Background and Motivation	2
1.2 Individual Pitch Control	3
1.3 State of the Art	3
1.4 Objectives and Contributions	4
2 Wind Turbine System	6
2.1 Horizontal-Axis Wind Turbines	6
2.2 NREL 5 MW Wind Turbine	7
2.3 Project Delimitation	8
3 Modelling	11
3.1 Model Degree of Freedoms	12
3.2 Blade Element Momentum Theory	13
3.2.1 Prandtl's Tip Loss Correction	18
3.2.2 Glauert Correction	18
3.2.3 BEMT Comparison with FAST Aerodyn Module	19
3.3 Pitch Actuator	21
3.4 Drive Train	22
3.5 Generator Model	23
3.6 Tower Dynamics	24
3.7 Blade Dynamics	28
3.7.1 Flapwise Dynamics	30
3.7.2 Edgewise Dynamics	34
3.7.3 Combined Dynamics	36
3.7.4 Blade Mode Shapes	37
3.8 State Space of Structural Dynamics	39
3.9 Blade Root Sensor Modelling	40

4	Linearization	42
4.1	Model Validation	47
5	Collective Pitch Control	50
5.0.1	Filtering	50
5.1	Collective Pitch Control using PI	51
5.1.1	Test of Collective Pitch Control	56
6	Individual Pitch Control	58
6.1	Individual Pitch Control using PI	58
6.1.1	Find loads on Hub	58
6.1.2	Filtering	60
6.1.3	Control Strategy	60
6.2	Comparison between Collective PI and Individual PI Control	61
6.2.1	Tower loads	63
6.2.2	Load on Blades	64
6.2.3	Load on Pitch Bearings	65
6.2.4	Load on Hub	66
6.2.5	Load on Low-Speed-Shaft	66
6.2.6	Power output	67
6.3	Individual Pitch Control using MPC	69
7	Discussion	71
8	Conclusion	73
A	Appendix	76
A.1	BEMT Verification	78
A.2	Drive Train Tuning	86
A.3	BEM Linear Approximations	88
A.4	Validation of Linearization	91
	Linearization Matrices	93

List of Figures

- 1.1 Illustration of wind shear. 2
- 2.1 Illustration of nacelle including its components [10]. 7
- 2.2 Wind turbine operation regions. 9
- 3.1 Flowchart showing the wind turbine model structure. 12
- 3.2 An annular control volume showing the discretization used in BEMT. 14
- 3.3 Illustration of angles and velocity components used in BEMT calculation. 15
- 3.4 Comparison between FAST and BEM code at 16 m/s. 20
- 3.5 Comparison between FAST and BEM code at 18 m/s. 21
- 3.6 Mechanical model of the drivetrain [5]. 22
- 3.7 Generator Torque comparison between FAST and SIMULINK. 24
- 3.8 illustration of tower modelling. 25
- 3.9 fore-aft deflection of tower top and rotor thrust. 26
- 3.10 nacelle displacement without aerodynamic influence. 27
- 3.11 Definition of ψ 29
- 3.12 Illustration of coordinate system used for blades. 29
- 3.13 Illustration blade model. 31
- 3.14 Flapwise deflection, root bending moment and edgewise deflection 32
- 3.15 Flapwise eigenfrequency and damping. 33
- 3.16 Edgewise deflection, root bending moment and edgewise deflection 35
- 3.17 Edgewise eigenfrequency and damping. 36
- 3.18 Illustration of shapes for first flapwise and first edgewise eigenmode. 38
- 4.1 Linear approximation of the edgewise moment. 47
- 4.2 Dynamics of Tower deflection using step wind. 48
- 4.3 Dynamics of blade deflection using step wind. 49
- 4.4 Blade root moment sensor output. 49
- 5.1 Plot of the calculated points of power sensitivity to pitch and the corresponding best linear fit. 55
- 5.2 Plot of gain scheduled proportional and integral gains. 56

5.3	Test of gain scheduled PI controller.	57
6.1	Control structure for individual PI pitch control.	58
6.2	Rotor illustration	60
6.3	Wind speed at hub height used for verification.	62
6.4	Pitch angle and pitch rate using collective and individual pitch control.	62
6.5	Comparison of tower deflection and the rotor thrust.	63
6.6	Flap- and edgewise blade deflection for blade 1, 2 and 3.	64
6.7	FFT analysis of blade deflection.	65
6.8	tilt- and yaw moments on hub using collective and individual pitch control.	66
6.9	Comparison of torsion of low-speed-shaft.	67
6.10	Comparison of power output.	67
6.11	Blade pitch angle using MPC.	69
6.12	Rotor speed using MPC.	70
A.1	Rotor speed as commanded in FAST.	78
A.2	Pitch angle ramp used for validation.	79
A.3	Aerodynamic Thust comparison between Aerodyn and the simulink BEM model.	80
A.4	Aerodynamic Thust comparison between Aerodyn and the simulink BEM model.	80
A.5	Comparison between aerodynamic torque calculated by FAST Aerodyn module and BEM code in Simulink/MATLAB function.	81
A.6	In-plane bending moment comparison with Elastodyn.	82
A.7	Out-of plane bending moment comparison with Elastodyn.	82
A.8	Comparison at 14 m/s.	83
A.9	Comparison at 16 m/s.	84
A.10	Comparison at 18 m/s.	84
A.11	Generator speed before Tuning.	86
A.12	Generator speed before Tuning.	87
A.13	Linear approximation with respect to rotor speed.	88
A.14	Linear approximation with respect to wind speed.	89
A.15	Linear approximation with respect to pitch angle.	90
A.16	Blade dynamics with respect to pitch step.	91
A.17	blade root bending moment with respect to pitch step.	92
A.18	Tower dynamics with respect to pitch step.	92

Chapter 1

Introduction

1.1 Background and Motivation

Today's wind turbine design tends towards increasing rotor size. Meanwhile the wind velocity increases with height - a phenomenon also known as wind shear, see figure 1.1. As the rotors grow in size, the wind speed that a blade experiences varies significantly in its path from the upper half of the rotor to the bottom half. If collective pitch is used, all the blades are pitched the same angle at a given time, and the whole rotor will therefore experience an uneven loading. This increases the wear of the hub and blade bearings and thereby reduces the lifetime of the wind turbine components. Short component life time increases the cost of energy production. To circumvent this individual pitch control can be used.

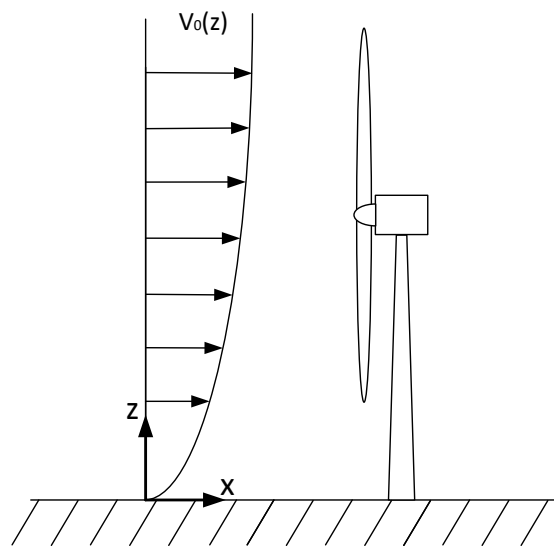


Figure 1.1: Illustration of wind shear.

1.2 Individual Pitch Control

Modern wind turbines can pitch the blades individually. This gives the possibility of evening out the loads on the rotor. Smaller and/or more even loads can prolong the life time of components or even make it possible to use lighter components, thus reducing the overall cost of the wind turbine. However, the individual pitch control might also affect the power production and as the purpose of the wind turbine is to produce power; a degradation in the amount and steadiness of the power produced is unwanted. Thus, the objective of the individual pitch controller is to maintain the power output while reducing the cost of components, service and repairs.

1.3 State of the Art

As the wind speed can vary in the different sections of the rotor of a wind turbine, asymmetric loads will affect the rotor – causing non-uniform stresses in the rotor bearing, tower etc. and thereby reducing the lifetime of the components. Today's wind turbines are able to pitch all three blades individually, which can be used to counteract asymmetric loads on the rotor and thereby extend the lifetime of the wind turbine. This is referred to as individual pitch control (IPC). Load mitigation using individual pitch control has been studied using many different control strategies. For instance, the classical PI-controller was used in [8], whereas LQR was the control strategy chosen in [9]. In [1] PI and LQI was used for collective pitch control where LQI yielded a steadier power output and PI was used for the individual pitch control which showed improved load mitigation. Thus, both classical methods such as PI has been investigated but also modern control such as LQR and LQG [2] have been considered. The advantage of the modern control is that the state space formulation makes it possible to control internal states of the system, not directly visible in the input output relations of transfer functions. In [4] the authors considered the use of MPC for individual pitch control. The feed forward control was based on predictions of the wind speed estimated from the blade root moment using a Kalman filter. The previous wind estimates were stored, shifted in time and used as input to the next passing blade. The individual pitch MPC proved to dampen tower and blade deflections and mitigate the drivetrain loads. The comparison was made with a PID controller for collective pitch. In [6] LIDAR was used in the MPC formulation. LIDAR makes it possible to measure the wind speed in front of the wind turbine, which could be a great advantage for control purposes. However, this technology is not widely used on wind turbines yet.

In [9] focus was put on modelling the wake, to reduce loads resulting from a wind turbine feeling or partially feeling the wake from the wind turbine in front of it. The wind field was modelled in Fast using turbsim. No turbulence model was incorporated, instead the focus was put on the wake and vertical shear. In [4] the wind was modelled as a time varying wind field with velocity components originating from a mean wind, wind shear, tower shading and a simple wake model, to consider the effect of other turbines. The simple wake model and the wind shear model had stochastic components.

1.4 Objectives and Contributions

The purpose of this project was to reduce the loads on the wind turbine by use of individual pitch control. To achieve this, an individual PI controller was chosen to be developed, with the objective to reduce the uneven loads on the rotor. Hereafter it was planned to use MPC as the control strategy - not only since it uses the state space formulation of the system, but also due to its ability to handle constraints. Also, the cost function in the MPC formulation can be minimized by means of optimization methods to improve the total life time of the wind turbine.

As it is hardly possible to verify a controller on a real wind turbine, computer software was used to validate the effect of the controller. Therefore, a simple mathematical model was developed, which was validated in FAST - which is a high fidelity wind turbine aero-elastic simulation software provided by NREL. Aeroelastic codes are used for wind turbine design and verification in industry. The validated simple model was used to design a PI-controller for collective and individual pitch control, respectively. The collective PI-controller was used as the baseline to which the individual pitch control was compared. Finally, the non-linear model was linearized over a set of operating points in the above rated region. The intention was to use these linearized models for design of a model predictive controller.

For modelling of the wind, the stochastic inflow turbulence tool TurbSim provided by NREL is used, which makes it possible to design a wind field containing both turbulence and wind shear.

Using FAST as simulation software together with a wind field constructed in TurbSim, the developed controllers were tested and validated. The aim was a MPC formulation which took into consideration the stress or fatigue of the pitch bearings, main shaft, blade flapwise and edgewise deflection and the tower deflection. The fatigue of the pitch actuator system should also be taken into consideration, to prevent the lifetime of the included components to be reduced too much and thereby increase the maintenance costs of the wind turbine. A successful controller should also be able to keep the power output at least as steady as the baseline PI controller. Furthermore, one has to choose which sensors should be used for the control system. As LIDAR is not a widely used technology, it will not be used in this project. Since some modern wind turbines are equipped with strain gauges capable of measuring the blade root bending moment, this project focuses on using those for estimation purposes, as it facilitates improvement of already existing systems. Therefore a lot of work was spent on making a wind turbine simulation model with the ability to simulate the blade dynamics and the root-bending moments.

The intention of this project was to firstly compare collective PI control to individual PI control, to even out the loads on the main bearing. The final step was supposed to be the comparison between individual PI control and MPC to see whether this more advanced controller could improve the results even more.

In conclusion, this thesis revolves around *design and evaluation of a MPC controller capable of mitigating loads while maintaining acceptable power output, by means of commonly used sensors e.g.*

blade root strain gauges.

This thesis falls in the following objectives:

- A non-linear wind turbine model resembling FAST aeroelastic code.
- A linearised model for control design.
- Development of a collective pitch controller using PI.
- Development of an individual pitch controller using PI.
- Design of an individual pitch controller using MPC.

Chapter 2

Wind Turbine System

In this chapter the general structure of a horizontal axis wind-turbine will be presented in section 2.1. More specifically this thesis revolves around the NREL 5 MW wind turbine, and a brief description of this wind turbine model is given in section 2.2. In section 2.3 the delimitation of this project is mentioned.

2.1 Horizontal-Axis Wind Turbines

If the wind turbine blades are connected to a horizontal shaft, the wind turbine is called a horizontal-axis wind turbine or HAWT for short. However, HAWT's can still vary in design. Wind turbines can differ in the number of blades, rotor diameter, hub height, rated power and the control strategy [13].

Rotors are usually two or three bladed. The two-bladed rotor is not rigidly connected to the shaft but is mounted on the shaft through a hinge - a teetering mechanism. This teetering mechanism ensures that no bending moments are transferred from the rotor to the shaft. The three-bladed rotors, on the other hand, are rigidly connected and are thus more vulnerable to uneven loads. The wind turbine rotor rotates with rotational speeds of approximately 10 to 50 RPM, which is much slower than the shaft speed of most generators - which is around 1,000 to 3,000 RPM. To achieve a transition from low rotational speed at the rotor side to the high rotational speed at the generator side, a gearbox is installed. Some generators can run with low speeds due to a multipole design, so no gearbox is needed. The rated power is the maximum power which can be safely produced by the generator and a control system is needed to saturate the power output at rated for high wind speeds.

Wind turbine rotors are designed to have the wind coming in perpendicular to the rotor. Most wind turbines are equipped with a wind vane (see fig 2.1), which measures the direction of the wind relative to the turbine. A yaw motor is used to continuously turn the nacelle into the wind. If the rotor is not facing the wind perpendicularly, there will be a power loss. The misalignment of the nacelle and the wind is also called a yaw error. In addition, an anemometer is positioned on the nacelle which measures the wind speed. The pitching of the

blades depends on which region of wind speed the turbine is currently operating in. To brake the rotor the blades can be pitched out of the wind until they reach stall conditions. In addition to the aerodynamic brake a mechanical brake is also installed as seen in 2.1.

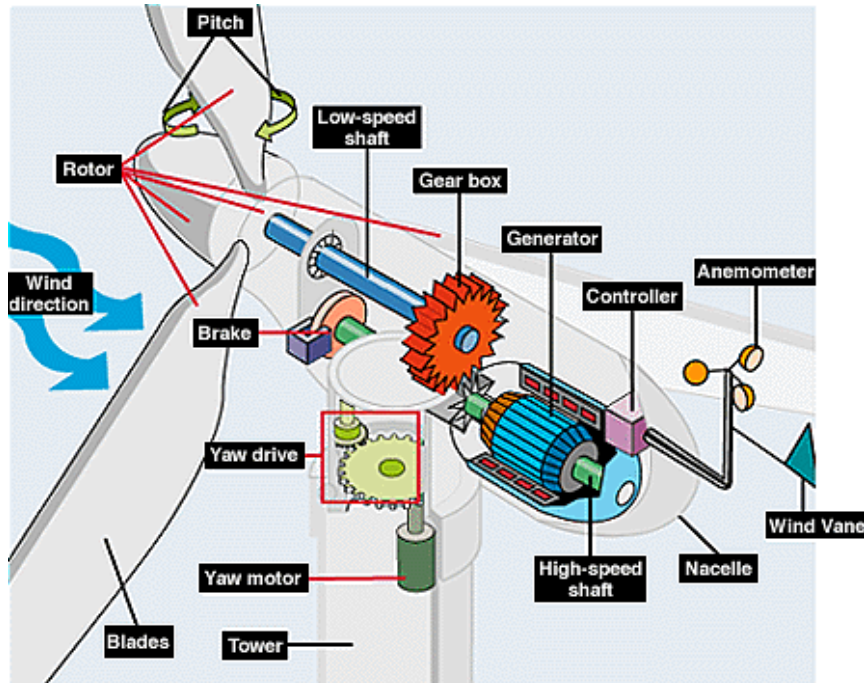


Figure 2.1: Illustration of nacelle including its components [10].

2.2 NREL 5 MW Wind Turbine

The turbine considered in this thesis is the NREL 5 MW wind turbine. All information in this section is based on the Technical Report *Definition of a 5-MW Reference Wind Turbine for Offshore System Development* (referred to as [3]) and gives a summation of all important specifications used in this project. In table 2.1 different information about the wind turbine is given.

The NREL 5MW turbine has been chosen, because it is a conventional three-bladed upwind variable-speed turbine. The turbine model already comes with a control system, which in this case is a collective pitch control - meaning that all the pitching systems of the blades are given the same signal and are thus pitched simultaneously and equally.

The wind turbine operates in 3 main regions, where 3 different control structures are used.

- Region 1 refers to wind speeds below the cut-in speed, where the wind turbine does not produce any power. In this region the goal is to accelerate the rotor and ultimately reach start up of the wind turbine.

Rating	5 MW
Rotor Orientation, Configuration	Upwind, 3 Blades
Control	Variable Speed, Collective Pitch
Drivetrain	High Speed, Multiple-Stage Gearbox
Rotor, Hub Diameter	126 m, 3 m
Hub Height	90 m
Cut-In, Rated, Cut-Out Wind Speed	3 m/s 11.4 m/s, 25 m/s
Cut-In, Rated Rotor Speed	6.9 rpm, 12.1 rpm
Overhang, Shaft Tilt, Precone	5 m, 5°, 2.5°
Rotor Mass	110,000 kg
Nacelle Mass	240,000 kg
Tower Mass	347,460 kg

Table 2.1: NREL 5MW turbine properties [3].

- Region 2 refers to the region between the cut-in speed and the rated wind Speed. Here the wind turbine operates with a pitch angle of 0° . Here a controller is designed to control the generator torque and generator/rotor speed to maximize power output.
- Region 3 refers to wind speeds above rated wind speed until cut-out speed. Here the generator torque is inverse proportional to the generator speed to maintain the rated power output. Here the pitch controller is used to adjust the torque applied to the rotor and thereby the speed of the rotor/generator, in order to keep it constant at the rated speed.
- At wind speeds above the cut-out speed the wind turbine is shut down for safety reasons and does not produce any power.

The cut-in, rated and cut-out wind speeds are given in table 2.1 as 3, 11.4 and 25 m/s, respectively. An illustration of the power output and the pitch angle is given in figure 2.2.

As for the mathematical modelling in chapter 3 some more information is needed; some specifications from the blades, rotor, drivetrain and generator is given in table 2.2

2.3 Project Delimitation

Certain aspects of modelling will be omitted due to time limitations and is instead referred to as possible future work. This includes:

- Only the above rated wind speed region (region 3) will be examined. This is the region where the power output is limited and individual pitch control can be implemented without without reduction of power output.

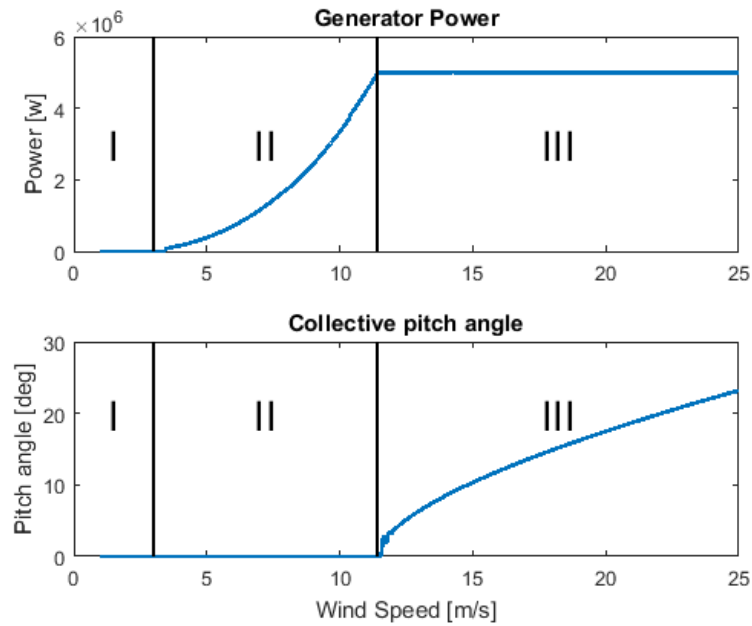


Figure 2.2: Wind turbine operation regions.

- No yaw error will be considered, meaning that it is assumed that the wind is always flowing perpendicularly to the rotor.
- A detailed fatigue estimation is not given, but would be favourable for the design and validation of the controller.
- The turbine model has only been linearized at a specific operating point - meaning, that it not necessarily can be used at higher or lower wind speed

The delimitation to the above rated wind region gives the definition of what was meant by an acceptable power output:

- The power output using MPC should be at least as steady as the power output of the IPC using PI.

Blade length	61.5 m
Blade mass (pr. blade)	17.740 kg
Blade First Mass Moment of inertia (w.r.t Root)	363,231 kg·m
Blade Second Mass Moment of inertia (w.r.t Root)	11,776,047 kg·m ²
CM Location of blade (w.r.t. Root along Preconed Axis)	20.475 m
Hub Mass	56,780 kg
Hub Intertia about Low-Speed Shaft	115,926 kg·m ²
Rated Generator Speed	1173.7 rpm
Gearbox ratio	97:1
Electrical Generator Efficiency	94.4 %
Generator Inertia about High-Speed Shaft	534,116 kg·m ²
Equivalent Drive-Shaft Torsional-Spring Constant	867,637,000 N·m/rad
Equivalent Drive-Shaft Torsional-Damping Constant	6,215,000 N·m/(rad/s)
Corner Frequency of Generator-Speed Low-Pass Filter	0.25 Hz
Maximum Absolute Blade Pitch Rate	8 °/s

Table 2.2: NREL 5MW turbine specifications [3].

Chapter 3

Modelling

In chapter 2.1 the general structure of a horizontal axis wind turbine was presented. In this chapter, these subsystems are presented in the form of mathematical models, which are then combined to yield a full system wind turbine model. An overview of the model structure can be seen in figure 3.1 with a description of its variables in table 3.1.

In section 3.1 the degrees of freedom used in the model are described. Section 3.2 covers a description of the Blade Element Momentum Theory (BEMT), used to find the aerodynamic forces on the blades. In section 3.3, 3.4 and 3.5 the modelling of the Pitch actuator, Drive train and Generator is described. Section 3.6 and 3.7 covers the structural modelling of the tower and the blades.

θ_b :	pitch angle given to blade b
$V_0(z)$:	wind speed, dependent on height above ground
ω_r :	angular velocity of rotor
ω_g :	angular velocity of generator
T_r :	Rotor torque
T_g :	generator torque
F_t :	Thrust force on rotor hub
V_t :	nacelle velocity
$V_{o,b}$:	out-of-plane velocity of blade b
$V_{i,b}$:	in-plane velocity of blade b
$M_{i,b}$:	in-plane moment given to blade b
$M_{o,b}$:	out-of-plane moment given to blade b
$M_{f,b}$:	measured flapwise moment of blade b
$M_{e,b}$:	measured edgewise moment of blade b
P_{out} :	measured power output from generator

Table 3.1: Description of the nomenclature used in figure 3.1.

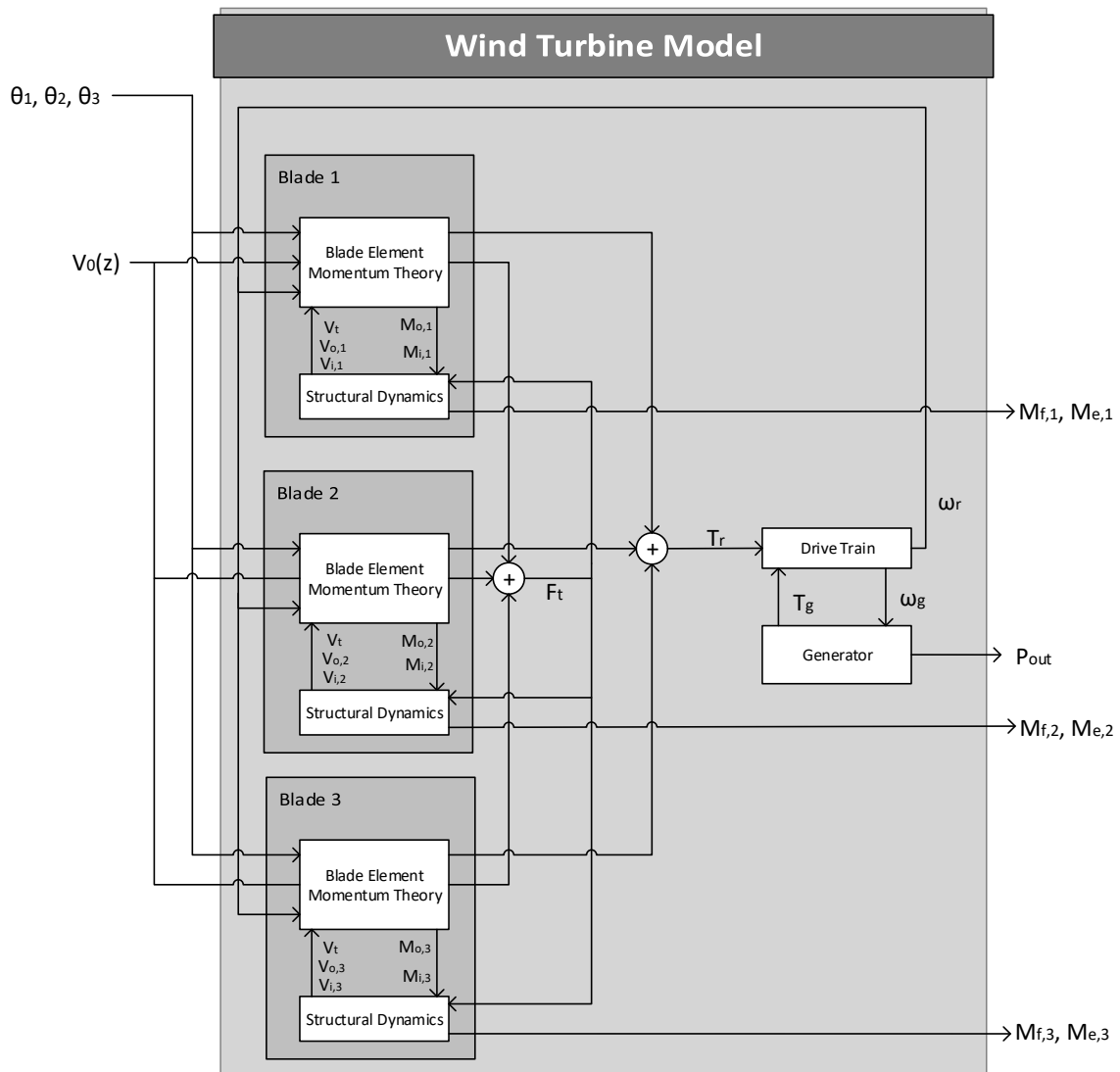


Figure 3.1: Flowchart showing the wind turbine model structure.

3.1 Model Degree of Freedoms

When modelling a wind turbine it is important to decide which degrees of freedom (DOF) the model should contain. Depending on the purpose of the project it should be decided what degrees of freedom are necessary and which degrees of freedom are negligible.

As the movement of the nacelle has a notable effect on the effective wind speed on the rotor, it has been decided to model the first fore-aft tower bending mode. The side-side movement

of the tower and the Yaw DOF was not chosen to be modelled. The wind is assumed to be flowing perpendicularly to the rotor; the vertical and lateral components of the wind field thus being zero.

The generator DOF is needed to calculate the torque given from the generator and the generator speed and thereby also the power output and the angular velocity of the rotor.

The Drivetrain rotational flexibility was chosen to be modelled, as its dynamics influence the generator and the rotor.

It was also chosen to model the first flapwise blade mode and the first edgewise blade mode, as those have an influence in the aerodynamics calculated by the blade element momentum theory. Furthermore the root bending moments of the blades are calculated by means of the tip displacement of each blade.

In table 3.2 a list of the available DOFs in FAST, and which of those have been modelled in this project, are shown.

Available DOF's in FAST	DOF's used in model
First flapwise blade mode	True
Second flapwise blade mode	False
First edgewise blade mode	True
Drivetrain rotational-flexibility	True
Generator	True
Yaw	False
First fore-aft tower bending-mode	True
Second fore-aft tower bending-mode	False
First side-side tower bending-mode	False
Second side-side tower bending-mode	False

Table 3.2: Degrees of freedom used in modelling.

Additionally it was also chosen to model the pitch actuator, which is not included in FAST. The modelling of the pitch actuator might add some delay to the pitch angle, which could have an influence when using individual pitch control.

3.2 Blade Element Momentum Theory

In this section the classical Blade Element Momentum Method (BEM) by Glauert (1935) will be presented. The content in this section is based on chapter six from *Aerodynamics of Wind Turbines* (referred to as [13]). Through the BEM model the steady thrust, rotor torque and power can be calculated for different wind speeds, rotational speeds and pitch angles.

The blade element momentum method is based on the one-dimensional momentum theory. However, whereas the simple one-dimensional momentum theory only considers the rotor as a permeable disk, BEM also takes into consideration the number of blades, the blade twist and the chord distribution. In BEM, the same streamtube as introduced in one-dimensional

momentum theory is divided into N annular elements of differential height dr . BEM is based on the following assumptions

- There is no radial dependency, i.e. an element cannot feel any influence from the other elements.
- The force from the blades on the flow is constant in each annular element corresponding to a rotor with an infinite number of blades.

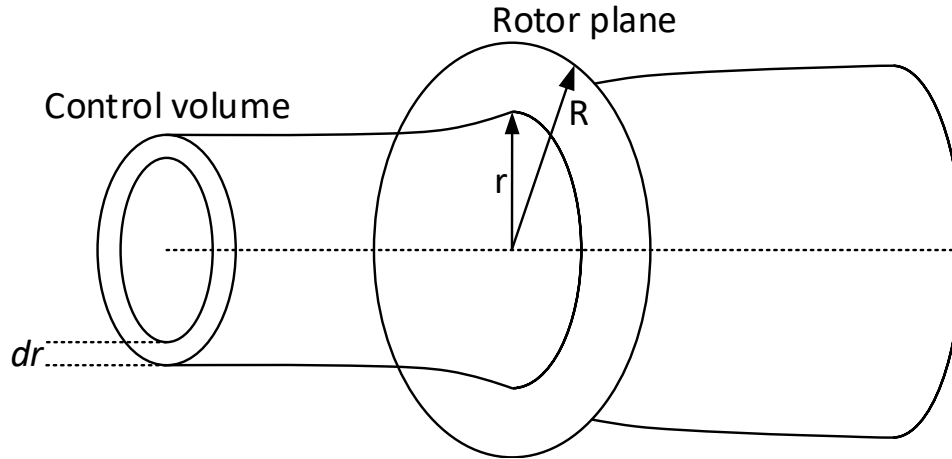


Figure 3.2: An annular control volume showing the discretization used in BEMT.

The assumption of each annular element being independent, makes it possible to calculate the contribution from each annular element independently. Thus, the solution is found at one radius before calculating the solution at the next radius. In the implementation, the blades are discretized into a number of points at which aerodynamic properties and blade dimensions are known. The method can be considered as being composed of the following eight steps as found in [13].

1. Initialize a and a' , typically $a = a' = 0$
2. Compute the flow angle ϕ from the equation

$$\tan(\phi) = \frac{(1 - a)V_0}{(1 + a')\omega r} \quad (3.1)$$

Where

- V_0 is the free stream air velocity.
- ω is the angular velocity of the rotor in radians per second.
- r is the radial distance of the current blade node.

3. Compute the local angle of attack α using the equation

$$\alpha = \phi - \theta \quad (3.2)$$

Where θ is the local pitch angle, i.e. the angle between the chord of the section and the plane of rotation as illustrated in figure 3.3. The local pitch is the sum of the blade twist β and the pitch angle θ_p .

$$\theta = \theta_p + \beta \quad (3.3)$$

The pitch angle θ_p is the angle between the tip chord and the plane of rotation. The twist is given relative to the tip chord.

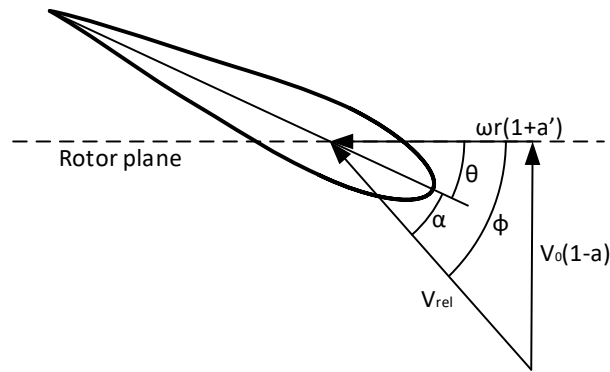


Figure 3.3: Illustration of angles and velocity components used in BEMT calculation.

4. Read the Lift Coefficient $C_l(\alpha)$ and the Drag Coefficient $C_d(\alpha)$ from a look-up table. The blade is discretized into a number of nodes each having their own airfoil shape. The $C_l(\alpha)$ and $C_d(\alpha)$ curves for the different nodes were imported into MATLAB and linear interpolation is used between the data points.
5. Compute the Normal Coefficient C_n and the Tangential Coefficient C_t from the equations

$$C_n = C_l \cos(\phi) + C_d \sin(\phi) \quad (3.4)$$

$$C_t = C_l \sin(\phi) - C_d \cos(\phi) \quad (3.5)$$

6. Calculate a and a' from the equations

$$a = \frac{1}{\frac{4 \sin(\phi)^2}{\sigma C_n} + 1} \quad (3.6)$$

$$a' = \frac{1}{\frac{4 \sin(\phi) \cos(\phi)}{\sigma C_t} - 1} \quad (3.7)$$

Where, σ is the solidity, given as the ratio of total chord length to circumference at the given radius. It represents the fraction of the rotor plane area in the annular control volume which is covered by blades.

$$\sigma(r) = \frac{Bc(r)}{2\pi r} \quad (3.8)$$

7. If the change in a and a' is less than some tolerance go to step 8 - else go back to step 2.
8. Compute the local loads on the blade segment p_N and p_T by multiplication with the dynamic pressure and the chord length

$$p_N = \frac{1}{2}\rho V_{rel}^2 C_n c \quad (3.9)$$

$$p_T = \frac{1}{2}\rho V_{rel}^2 C_t c \quad (3.10)$$

This is the tangential force and normal force per unit length, respectively.

The first 7 steps are thus carried out for each blade node iteratively, until a and a' has converged, before the local loads are calculated in step 8. From the loads, the important outputs such as aerodynamic torque, thrust force, in-plane moments and out-plane moments can be calculated.

Since p_N is the normal force per unit length, multiplication with the number of blades B and the differential radial distance dr gives the normal force acting on a control volume of thickness dr :

$$dF_t = Bp_N dr \quad (3.11)$$

In order to find the total thrust force a linear variation of p_N between nodes is assumed

$$p_N = A_i r + B_i \quad (3.12)$$

Where A_i is the slope between the nodes i and $i + 1$

$$A_i = \frac{p_{N,i+1} - p_{N,i}}{r_{i+1} - r_i} \quad (3.13)$$

and B_i is the intercept given by

$$B_i = \frac{p_{N,i} r_{i+1} - p_{N,i+1} r_i}{r_{i+1} - r_i} \quad (3.14)$$

Integration of this yields the given elements contribution to the total thrust force

$$F_{t|i,i+1} = B \int_{r_i}^{r_{i+1}} p_N dr = B \int_{r_i}^{r_{i+1}} (A_i r + B_i) dr = B \left(\left[\frac{1}{2} A_i r^2 \right]_{r_i}^{r_{i+1}} + [B_i r]_{r_i}^{r_{i+1}} \right) \quad (3.15)$$

$$= B \left(\frac{1}{2} A_i (r_{i+1}^2 - r_i^2) + B_i (r_{i+1} - r_i) \right) \quad (3.16)$$

The summation of all $N - 1$ elements gives the total thrust force

$$F_t = \sum_1^{N-1} F_{t|i,i+1} \quad (3.17)$$

To calculate the aerodynamic torque, the following approach is used:

Assume that the distribution of the tangential force p_T is linear between nodes

$$p_T = A_i r + B_i \quad (3.18)$$

Where A_i is the slope between the nodes i and $i + 1$

$$A_i = \frac{p_{T,i+1} - p_{T,i}}{r_{i+1} - r_i} \quad (3.19)$$

and B_i is the intercept given by

$$B_i = \frac{p_{T,i} r_{i+1} - p_{T,i+1} r_i}{r_{i+1} - r_i} \quad (3.20)$$

The torque for a differential length of the blade dr is given by

$$dT_r = r p_T dr = r(A_i r + B_i) dr = (A_i r^2 + B_i r) dr \quad (3.21)$$

Integration over one element yields:

$$T_{r|i,i+1} = \int_{r_i}^{r_{i+1}} (A_i r^2 + B_i r) dr = \left(\left[\frac{1}{3} A_i r^3 \right]_{r_i}^{r_{i+1}} + \left[\frac{1}{2} B_i r^2 \right]_{r_i}^{r_{i+1}} \right) \quad (3.22)$$

$$= \left(\frac{1}{3} A_i (r_{i+1}^3 - r_i^3) + \frac{1}{2} B_i (r_{i+1}^2 - r_i^2) \right) \quad (3.23)$$

Multiplying by the blade number B and summing contributions from each element yields the total aerodynamic torque:

$$T_r = \sum_1^{N-1} T_{r|i,i+1} \quad (3.24)$$

The calculation of the in-plane aerodynamic blade root moment is identical to the calculation of the aerodynamic torque. The difference between the two comes from the difference in the applied radial vector. For the calculation of aerodynamic torque, the radial distance is to the center of the hub, whereas for the blade root moment, it is the distance to the blade root.

Similarly, for calculation of the aerodynamic out-of-plane blade root bending moment the normal load is used instead of the tangential load and the radial vector gives the distance from the blade nodes to the blade root. However, it should be noted that the in-plane and out-of-plane moments calculated are the moments which affects the blades due to the aerodynamic forces distributed along the blade. Those, bending moments is what drives the blade dynamics which is discussed in section 3.7.

3.2.1 Prandtl's Tip Loss Correction

Two corrections are needed for the BEM method presented until now. The first one to consider is Prandtl's tip loss factor which corrects the assumption of an infinite number of blades. The solidity has already been introduced, but the vortex system in the wake is different for a rotor with a finite number of blades which is what is given in reality. A correction factor F is introduced as:

$$F = \frac{2}{\pi} \cos(e^{-f})^{-1} \quad (3.25)$$

where f is given by:

$$f = \frac{B}{2} \frac{R - r}{r \sin(\phi)} \quad (3.26)$$

Using this correction factor, the expression for a and a' becomes

$$a = \frac{1}{\frac{4F \sin(\phi)^2}{\sigma C_n} + 1} \quad (3.27)$$

$$a' = \frac{1}{\frac{4F \sin(\phi) \cos(\phi)}{\sigma C_t} - 1} \quad (3.28)$$

The equations 3.27 and 3.28 should replace equation 3.6 and 3.7 [13].

3.2.2 Glauert Correction

When the axial induction factor a becomes larger than 0.2 – 0.4 the simple momentum equations begin to lose their validity. In order to calculate the induced velocities for larger values of the thrust coefficient a correction is needed. Different empirical relations have been made for the thrust coefficient as a function of the axial induction factor. Based on one such relation the following expressions for a :

$$k = \frac{\sigma \cdot C_n}{4 \cdot F \cdot \sin(\phi)^2} \quad (3.29)$$

if $k \leq 2/3$

$$a = \frac{k}{1+k} \quad (3.30)$$

else

$$g1 = 2 \cdot F \cdot k - \left(\frac{10}{9} - F\right) \quad (3.31)$$

$$g2 = 2 \cdot F \cdot k - \left(\frac{4}{3} \cdot F\right) \cdot F \quad (3.32)$$

$$g3 = 2 \cdot F \cdot k - \left(\frac{25}{9} - 2 \cdot F\right) \quad (3.33)$$

if $\text{abs}(g3) < 10^{-6}$

$$a = 1 - \frac{1}{2} \cdot \sqrt{g2} \quad (3.34)$$

else

$$a = \frac{(g1 - \sqrt{g2})}{g3} \quad (3.35)$$

end

end

To incorporate the Glauert correction, equation 3.27 should be replaced by the above equations. Notice that for $k \leq 2/3$ the equation for a is the same as 3.27 [15].

3.2.3 BEMT Comparison with FAST Aerodyn Module

As the scope of the project is to design pitch control and validating the design with FAST aeroelastic code, it would be preferable if the aerodynamics of the simulation model is similar to the one used in FAST. The Glauert corrections used to correct the classical momentum theory are empirical, which means that there exists many different relations. In FAST source code the correction used is the Glauert(Buhl) correction. So for simplicity the same correction has been implemented in the BEMT code of the simple model presented in this thesis.

The iterative process of calculating the induction factors a and a' is implemented as described in the previous sections where, the airfoil data for each blade node is taken from FAST to ensure that the wind turbine properties are the same. The data implemented in the MATLAB code is the chord distributions and lift and drag coefficients for each airfoil and the radial distance where the airfoils are positioned along the blade.

The proposed wind turbine simulation model consists of several components interacting where the aerodynamics delivers the driving force. Therefore, it is convenient to validate the aerodynamics block on its own. To do this, all degrees of freedom in FAST were deactivated and the rotor speed was set to the rated rotor speed.

To test the aerodynamics module, a comparison is carried out for different wind speeds and different pitch angles. For each test the wind speed is held constant whereas the pitch is given a ramp signal.

The input into the BEM calculation is the free-stream velocity V_0 , the pitch angle θ_p and the rotational speed ω_{rot} . The tower velocity and the blade velocities at the blade node points can also be given as inputs, but are set to zero for the purpose of this verification.

The pitch angle was given as a ramp with an initial pitch angle of -20 deg and a slope of 1 deg/s. The simulation was run for 50 s which yields a pitch varying from -20 deg to 30 deg.

The verification for 16 m/s and 18 m/s can be seen in figure 3.4 and 3.5, respectively.

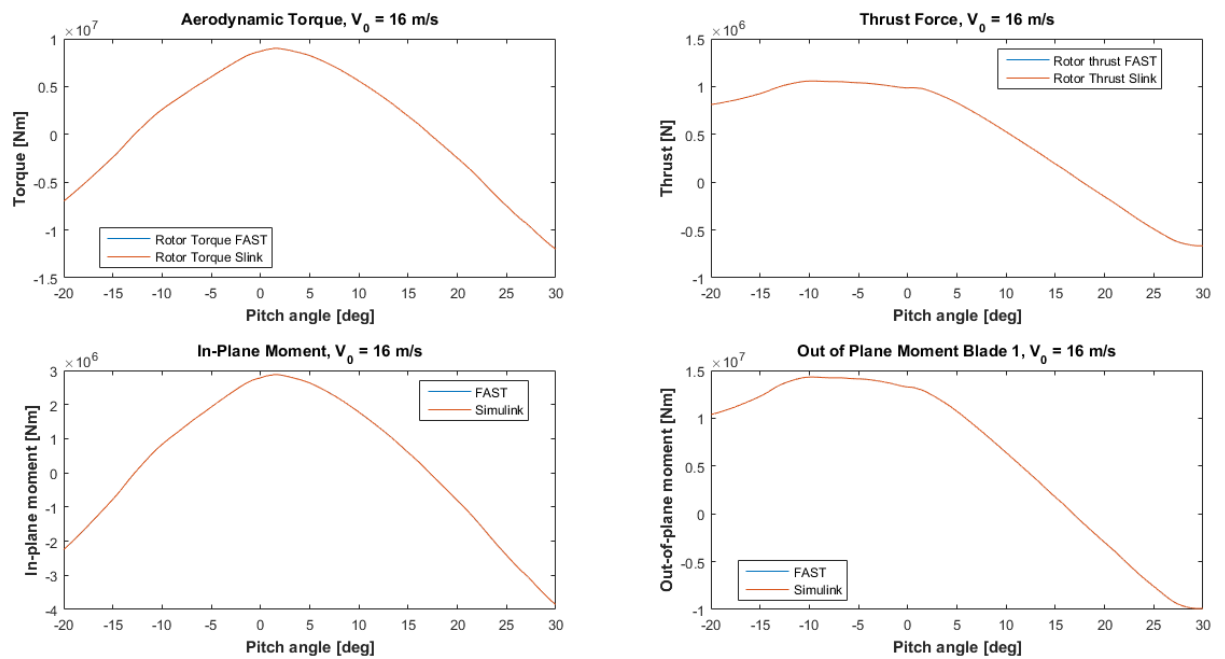


Figure 3.4: Comparison between FAST and BEM code at 16 m/s.

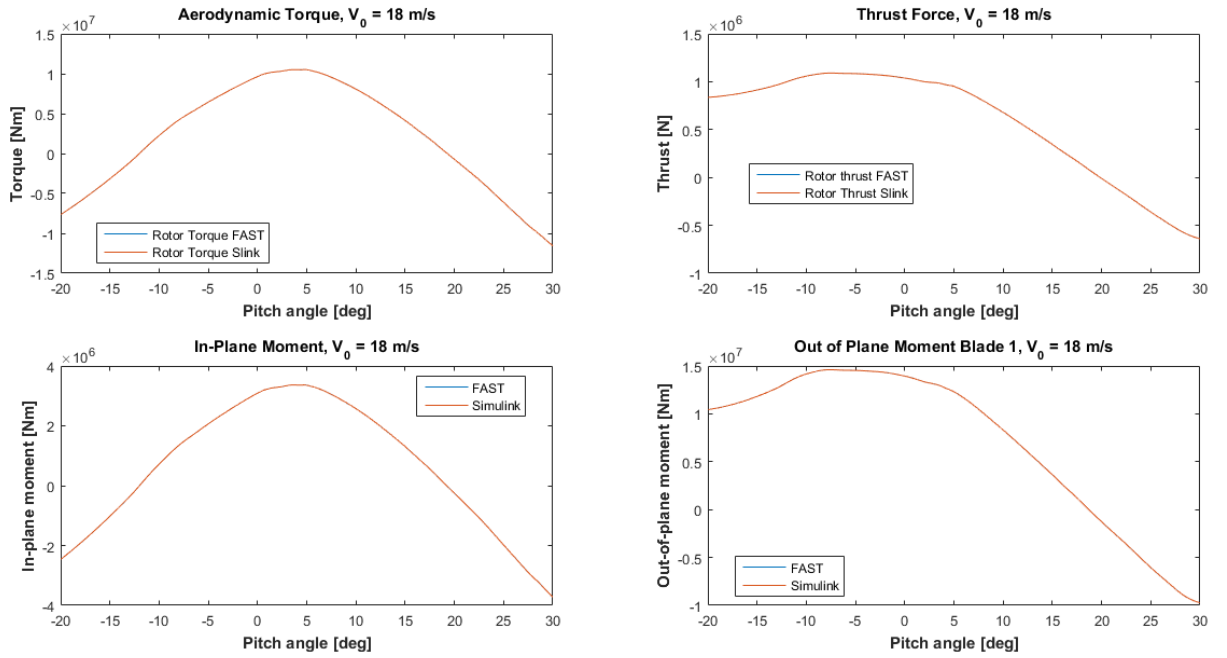


Figure 3.5: Comparison between FAST and BEM code at 18 m/s.

It is noticed that the curves from FAST and Simulink are indistinguishable and the BEM code is thus sufficient as a representation of the aerodynamics in this operating region. For more validation plots see appendix A.1.

3.3 Pitch Actuator

As the pitch angle of a blade from a wind turbine cannot change immediately, the dynamics of the pitch actuator has to be modelled. The input to the model is the reference angle θ_{ref} , which is the pitch angle determined by the pitch controller. θ is the output pitch angle given into the model. To keep it simple, the pitch actuator has been modelled as a 1st order system, given as

$$\dot{\theta} = \theta_{ref} \frac{1}{\tau_{\theta}} - \theta \frac{1}{\tau_{\theta}} \quad (3.36)$$

Or equivalently in transfer function form

$$\frac{\theta}{\theta_{ref}} = \frac{1}{\tau_{\theta} \cdot s + 1} \quad (3.37)$$

Since no other information were given, the timeconstant for the pitch actuator has been estimated to be $\tau_{\theta} = 0.3$.

3.4 Drive Train

The model of the drive train describes the connection between the rotor and the generator. In this project the drive train has been modelled, as it can be seen in figure 3.6.

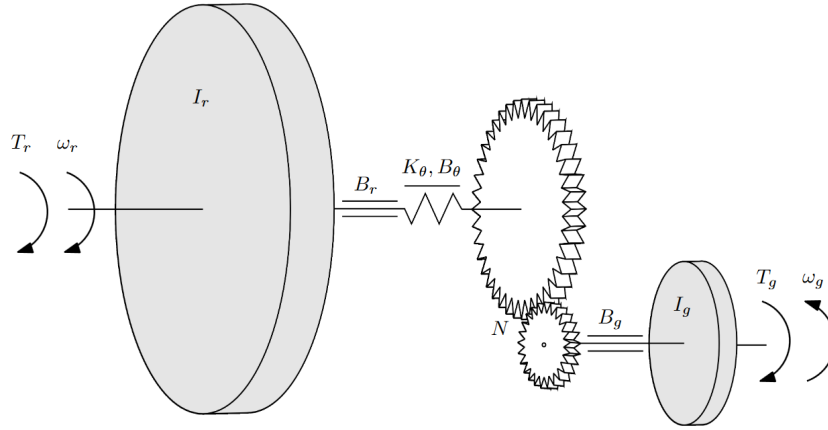


Figure 3.6: Mechanical model of the drivetrain [5].

The rotor is described as a rotating disc with inertia J_r and is affected by the aerodynamic torque T_r . The torque T_r arise from the aerodynamic forces acting on the blades. The angle of the disc is given as θ_r . The rotor is connected by a Low Speed Shaft (LSS) to a gearbox with ratio N_g . On the other side of the gearbox there is a High Speed Shaft (HSS), connecting the gearbox with the generator, which has inertia J_g and is affected by the counter torque from the generator T_g . The angle of the generator is denoted by θ_g .

As both the HSS, gearbox and LSS are not fully stiff bodies, they can be modelled as flexible systems. In this project it has been chosen to neglect the flexibility of both the gearbox and the HSS, whereas the dynamics of the LSS were modelled as a rotational mass-spring-damper system. The spring constant K_s and damping coefficient D_s are given in section 2.2.

The modelling of the drive train has been split up into two parts. The first part describes the connection of the rotor and the mass-spring-damper system, which is given as

$$J_r \ddot{\theta}_r = T_r - \left(\dot{\theta}_r - \frac{\dot{\theta}_g}{N_g} \right) D_s - \left(\theta_r - \frac{\theta_g}{N_g} \right) K_s \quad (3.38)$$

The second part of the drive train describes the connection between the mass-spring-damper and the generator, which also includes the gearbox and is given as

$$J_g N_g \ddot{\theta}_g = -T_g N_g + \left(\dot{\theta}_r - \frac{\dot{\theta}_g}{N_g} \right) D_s + \left(\theta_r - \frac{\theta_g}{N_g} \right) K_s \quad (3.39)$$

As the rotor inertia not directly is given, it has been estimated by means of the second mass moment of inertia (w.r.t. root) from the blades and the hub inertia about the LSS

$$J_r = 3 \cdot J_{blade} + J_{hub} \quad (3.40)$$

Where J_{blade} is the second mass moment of inertia (w.r.t. root) and J_{hub} is the hub inertia about LSS. It has to be mentioned that the root from the blades have some distance to the LSS due to the hub diameter, but this was chosen to be negligible in this report.

A validation of the drivetrain can be seen in appendix A.2.

3.5 Generator Model

The wind turbine generator is the transducer which converts the kinetic energy of the shaft into electrical energy. For simplicity the wind turbine generator is modelled as a first order transfer function.

$$\frac{T_g}{T_{ref}} = \frac{1}{\tau_g \cdot s + 1} \quad (3.41)$$

Where, τ_g is the generator time constant. The reference torque T_{ref} is inverse proportional to the generator rotational speed in region 3:

$$T_{ref} = \frac{P_{ref}}{\omega_g} \quad (3.42)$$

and P_{ref} is the rated mechanical power.

Furthermore, the generator has efficiency η_g , so

$$P_{ref} = \frac{P_{rated}}{\eta_g} \quad (3.43)$$

where P_{rated} is the rated power of the wind turbine.

The output power is calculated as

$$P_{out} = T_g \cdot \omega_g \cdot \eta_g \quad (3.44)$$

As there have not been found any time constant for the model of the generator, τ_g has been estimated and compared with the generator model used in the certification test for the NREL 5MW wind turbine in FAST.

Here a simulation in FAST has been carried out, where all DOFs were activated and a step wind was used as input ($V_0 = 16m/s$ for $t < 40s$ and $V_0 = 17m/s$ for $t > 40s$). Here the generator speed data from FAST has been used as input into the model. The outputs of the model, which are the generator torque and the generator power, were compared with the data from FAST. The time constant τ was tuned using trial and error until the generator model was sufficient for the purpose of the project.

The time constant found in this simulation is $\tau_g = 0.633$, which gave following results as shown in figure 3.7.

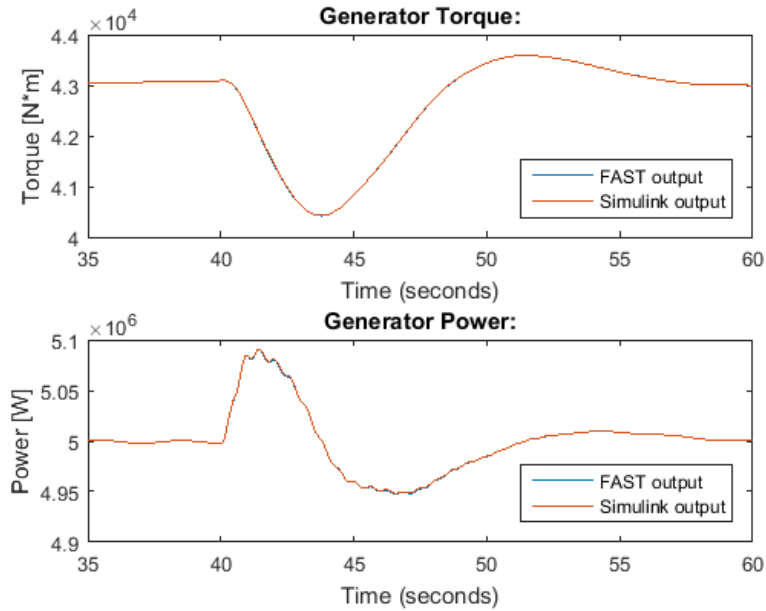


Figure 3.7: Generator Torque comparison between FAST and SIMULINK.

As it can be seen in the comparison, there can be seen no significant difference between the 1st order generator model used in this project, and the generator model used in FAST.

3.6 Tower Dynamics

As the movement of the tower has some influences in the resulting windspeed on the blades, the fore-aft movement of the tower was chosen to be modelled.

In this project only the 1st eigenmode of the fore-aft movement will be modelled, since it influences the nacelle movement significantly and thereby influences the resulting windspeed on the blades. The 2nd eigenmode of the fore-aft movement has not been modelled in this project, since its influence to the nacelle movement has been chosen to be negligible. The side-to-side movement has been chosen to be negligible aswell, as in this project the windfield will be kept simple and not include significant forces to influence the side-to-side movement of the nacelle.

The fore-aft movement of the nacelle has been modelled as mass-spring-damper system with only 1 DOF, which is the deflection in x-direction. The governing equation is thereby given as

$$m_t \ddot{x}_t + c_t \dot{x}_t + k_t x_t = F_t \quad (3.45)$$

where

- x_t is the displacement of the tower top (Nacelle displacement)

- k_t is the spring constant of the tower
- c_t is the damping coefficient of the tower
- m_t is the equivalent mass of the tower top
- F_t is the force acting on the top of the tower

An illustration of the model can be seen in figure 3.8

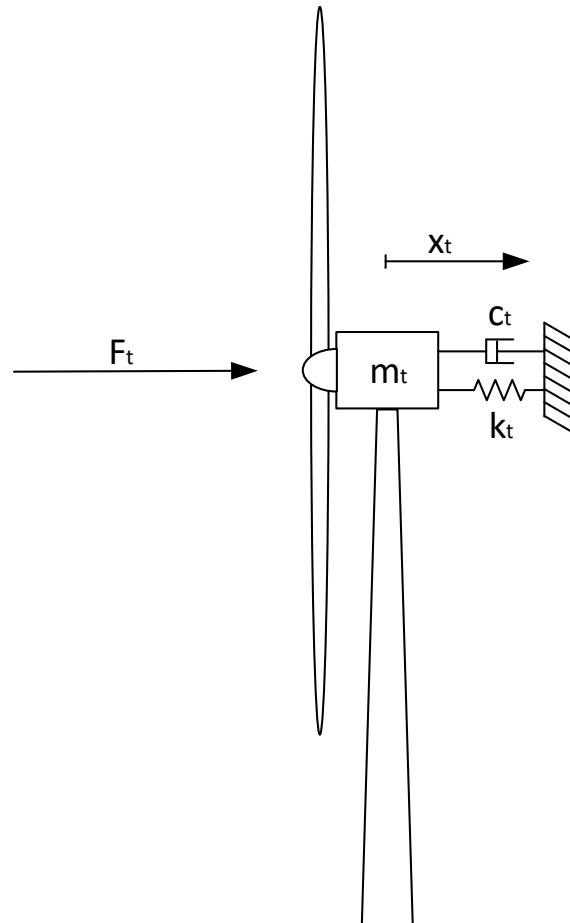


Figure 3.8: illustration of tower modelling.

The Force F_t is the input given from the Blade Element Momentum theory, which is described in 3.2. As the values for m_t , c_t and k_t are unknown, they have to be estimated by means of some simulations using FAST. Here it has to be mentioned that all degrees of freedom, except the first fore-aft tower bending-mode, has been deactivated to avoid influence from any other degrees of freedom.

To find the spring constant k_t an experiment was made in FAST, during which a constant wind velocity of 17 m/s was applied and the fore-aft deflection of the tower was examined. In

figure 3.9 the fore-aft displacement x_t and the thrust force of the rotor F_t can be seen.

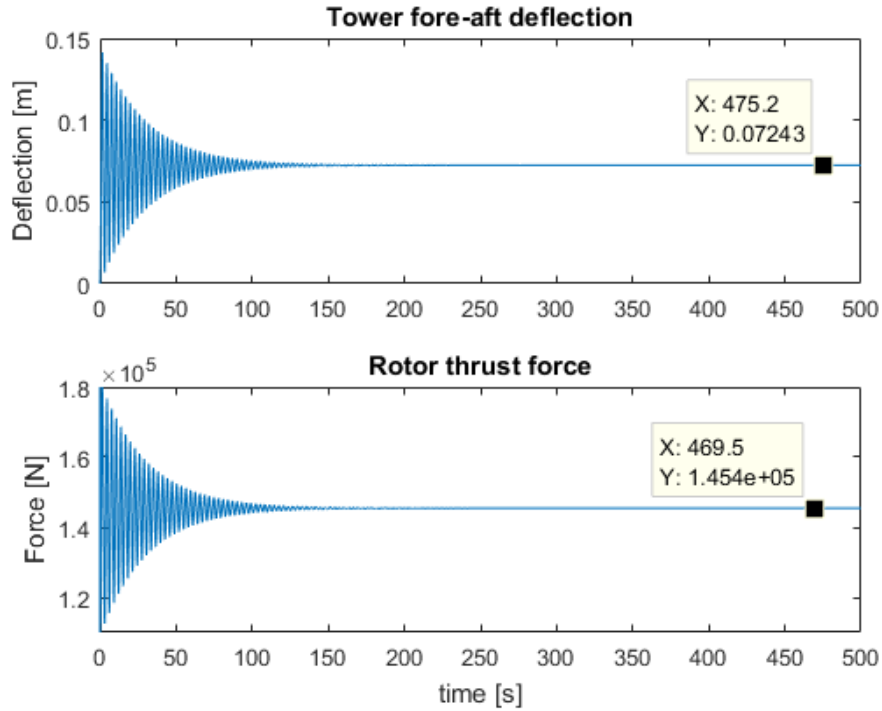


Figure 3.9: fore-aft deflection of tower top and rotor thrust.

Here the nacelle displacement reaches some steady state value after a specific amount of time, due to the constant windfield. From these tests the steady state rotor thrust $F_{t,ss}$ and the steady state nacelle displacement $x_{t,ss}$ is found. From this the spring constant k_t can be found as

$$k_t = \frac{F_{t,ss}}{x_{t,ss}} = 2.008 \cdot 10^6 \frac{N}{m} \quad (3.46)$$

m_t and c_t can be found by estimating the damped frequency ω_d and damping ratio ζ .

To estimate ω_d and ζ a simulation was carried out in FAST, where the nacelle has been given an initial displacement and released to see the dynamics. The result of the nacelle displacement can be seen in figure 3.10. To avoid aerodynamic damping, the aerodynamics was deactivated.

The simulation contains following data:

- Initial displacement: $A_0 = 1$
- Initial time: $t_0 = 0$
- number of counted oscillations $n = 50$
- time after n oscillation: $t_n = 152.5$

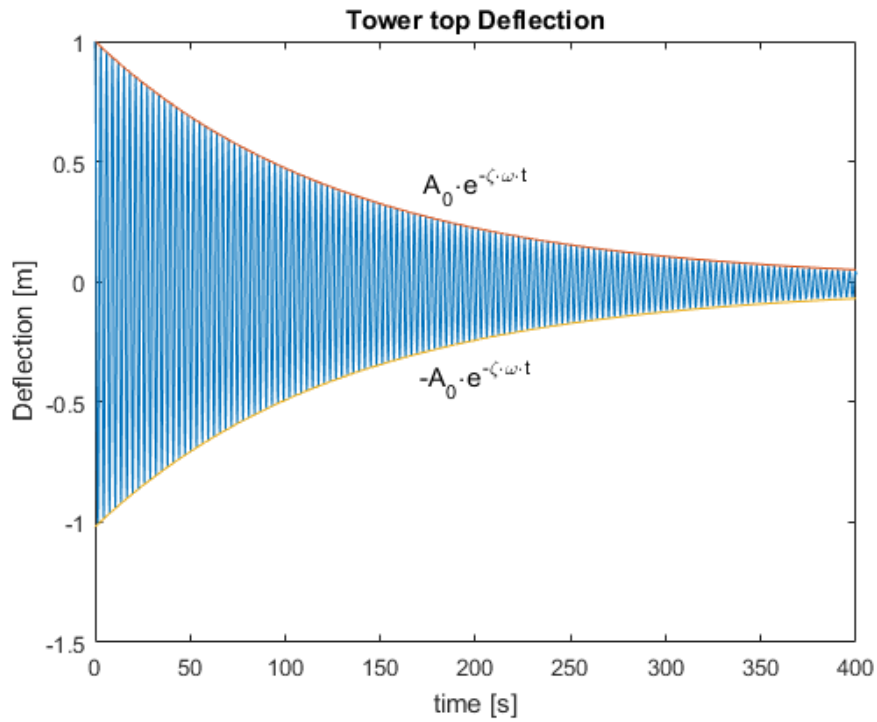


Figure 3.10: nacelle displacement without aerodynamic influence.

- Amplitude after n oscillations: $A_n = 0.3185$

The damping ratio ζ is given as [14]

$$\zeta = \frac{\sigma}{\sqrt{(2 \cdot \pi)^2 + \sigma^2}} \quad (3.47)$$

where

$$\sigma = \frac{1}{n} \cdot \ln\left(\frac{A_0}{A_n}\right) \quad (3.48)$$

The damped eigenfrequency can be found as

$$\omega_d = 2\pi \cdot \frac{n}{t_n - t_0} \quad (3.49)$$

with which the natural eigenfrequency ω_n can be calculated

$$\omega_n = \frac{\omega_d}{\sqrt{1 - \zeta^2}} \quad (3.50)$$

The equivalent mass can be found from

$$m = \frac{k}{\omega_n^2} \quad (3.51)$$

Where, $k = k_t$ from before.

The critical damping coefficient c_c can be found as

$$c_c = 2m\omega_n \quad (3.52)$$

and the actual damping coefficient c can be found

$$c = c_c \cdot \zeta \quad (3.53)$$

The equivalent mass and damping coefficient for the tower were found to be

$$m_t = 4.7338 \cdot 10^5 \text{ kg} \quad (3.54)$$

$$c_t = 7.1012 \cdot 10^3 \frac{\text{N} \cdot \text{s}}{\text{m}} \quad (3.55)$$

For the later use in a state space equation the governing equation 3.45 is rewritten as

$$\ddot{x}_t = -\frac{k_t}{m_t}x_t - \frac{c_t}{m_t}\dot{x}_t + \frac{F_t}{m_t} \quad (3.56)$$

The tower dynamics does not include any influence from the blade dynamics for simplicity reasons.

3.7 Blade Dynamics

As the movements of the blades have some influence on the aerodynamics, it has been chosen to model the first flapwise and the first edgewise blade mode. Furthermore the deflection of the blades is used to simulate the root bending moment, which is used for blade root sensor modelling in section 3.9. The two DOFs were assumed to be independent.

In the BEM calculations from section 3.2 the aerodynamic in-plane and out-of-plane moment for each blade is given. In this section the modelling of a single blade is described. In the modelling it is assumed that all blades are equal.

Beyond the aerodynamic moments from the BEM, also the gravitational force has been implemented. This affects only the in-plane moment, given as

$$M_i = M_{i,BEM} + I_1 \cdot g \cdot \sin(\psi) \quad (3.57)$$

where

- M_i is the in-plane moment.
- $M_{i,BEM}$ is the in-plane moment given from the BEMT calculations.

- I_1 is the first mass-moment of inertia for the blade.
- ψ is the azimuth angle of the actual blade.
- g is the gravitational acceleration.

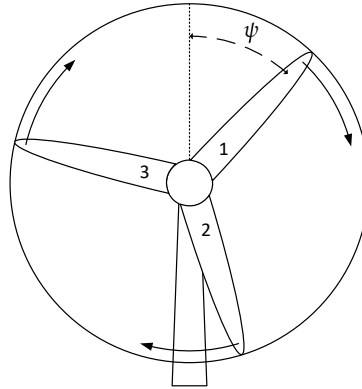


Figure 3.11: Definition of ψ .

The azimuth angle is defined to be 0, when the blade is standing in an upright position, while the azimuth angle increases during operation. An illustration is given in figure 3.11.

The in- and out-of-plane moments are transformed to moments acting on the blades in flapwise and edgewise directions, which are the inputs to the state space model. The output of the state space model is the tip deflection and velocity of each blade in both edge- and flapwise direction. The tip velocities are then transferred back into in-plane and out-of-plane velocities, which are used as input in the BEM calculations. The edge- and flapwise tip deflections are used to calculate the root bending moment of the blade, which can be seen in section 3.9.

The positive definition of in-plane, out-of-plane, edgewise and flapwise deflection can be seen in figure 3.12 (left), together with the positive definition of the corresponding moment vectors (right).

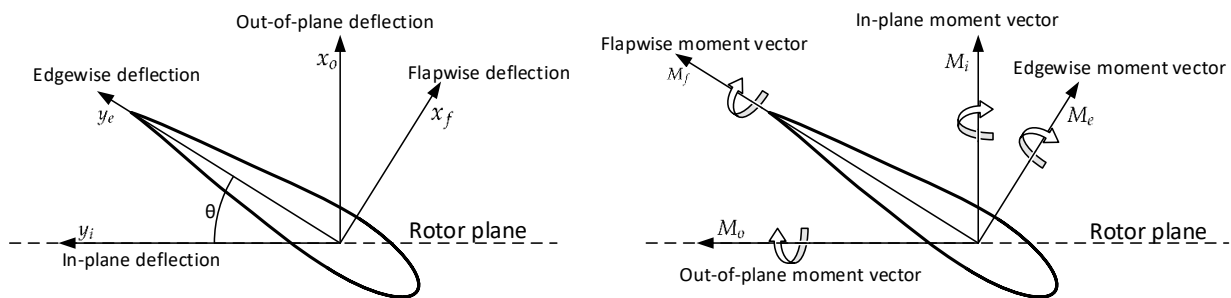


Figure 3.12: Illustration of coordinate system used for blades.

The calculations from in-plane and out-of-plane moments, as given from BEMT, to moments in edgewise and flapwise direction are given as

$$M_e = M_i \cos(\theta) - M_o \sin(\theta) \quad (3.58)$$

$$M_f = M_o \cos(\theta) + M_i \sin(\theta) \quad (3.59)$$

while the calculation from edgewise and flapwise deflection to in-plane and out-of-plane deflection is given as

$$x_o = x_f \cos(\theta) + y_e \sin(\theta) \quad (3.60)$$

$$y_i = y_e \cos(\theta) - x_f \sin(\theta) \quad (3.61)$$

As for the deflection, the same equations can also be used for velocities. These are used to calculate the flap- and edgewise velocities to in- and out-of-plane velocities to be used in the BEM calculations

The modelling of the blades is very similar to the modelling of the tower, described in section 3.6. Here it is instead assumed that an equivalent mass is placed at the tip of the blade, whereas an equivalent force, spring constant, damping coefficient and mass is found for the flap- and edgewise DOF. An illustration of the principle is shown in figure 3.13.

As the velocity from different places is needed, the velocities are calculated by means of the tip velocity. More about this can be read in subsection 3.7.4 about the blade mode shapes.

3.7.1 Flapwise Dynamics

As the flapwise deflection is modelled as spring-mass-damper system, the governing equation is given as

$$m_f \ddot{x}_f + c_f \dot{x}_f + k_f x_f = F_f \quad (3.62)$$

where

- x_f represents the tip deflection in flapwise direction.
- m_f is the equivalent mass needed to accelerate the tip.
- c_f is the damping coefficient of the flapwise movement.
- k_f is the spring constant of the flapwise deflection.
- F_f is the equivalent force acting on the tip of the blade.

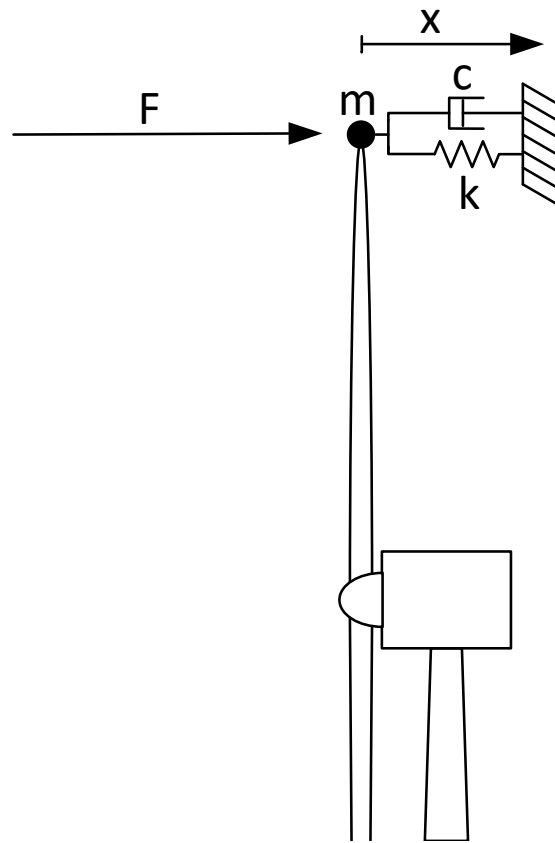


Figure 3.13: Illustration blade model.

To find the coefficients needed for the governing equation, the same theory as in previous section, equation 3.46 to 3.53 is used.

The equivalent spring constant k_f has been found in a test in FAST, where azimuth angle of one blade was set to 90° , the pitch angle of the blade was fixed to 90° and aerodynamics were deactivated. All structural degrees of freedom (except the first flapwise blade mode) were deactivated to avoid any other influences.

This causes the blade to fluctuate and go into steady state after some time with a positive deflection due to the gravity acting on the blade. In figure 3.14 the flapwise tip deflection and the flapwise root bending moment (moment around the blade y-axis) can be seen.

The equivalent force acting on the tip of the blade in flapwise direction is calculated by means of the moment acting in flapwise direction:

$$F_f = \frac{M_f}{L_{Blade}} \quad (3.63)$$

where L_{Blade} is the length of the blade, previously given as 61.5 m. The spring constant k_f is then found as

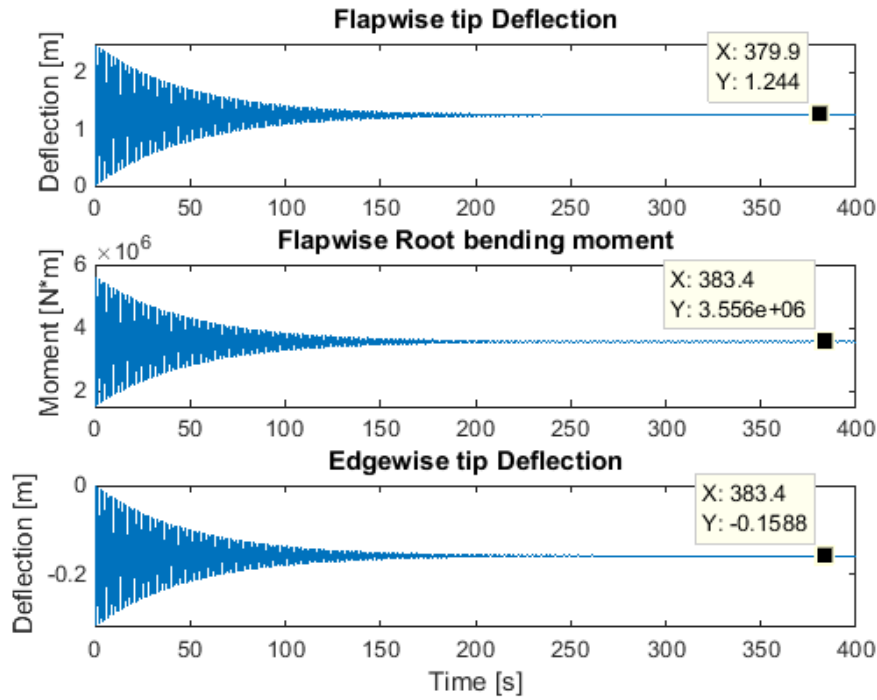


Figure 3.14: Flapwise deflection, root bending moment and edgewise deflection using only first flapwise blade mode.

$$k_f = \frac{F_{f,ss}}{x_{f,ss}} = 4.647 \cdot 10^4 \frac{N}{m} \quad (3.64)$$

where $F_{f,ss}$ is the steady state force and $x_{f,ss}$ is the steady state deflection. In figure 3.14 it also can be seen that the flapwise deflection causes some edgewise deflection, showing the same dynamics as the flapwise deflection. Here it is assumed that the first flapwise blade mode has some influence on the edgewise tip deflection, which is given as

$$y_{e,f} = \frac{y_{e,ss}}{x_{f,ss}} = -0.1276 \quad (3.65)$$

where $y_{e,ss}$ is the steady state tip deflection in edgewise direction.

To find the damping and the eigenfrequency, the fluctuations in the beginning of the experiment were analysed, which also can be seen in figure 3.15.

The key information of this simulation is:

- Initial displacement: $A_0 = 2.4702$
- Initial time: $t_0 = 0.74$
- number of counted oscillations $n = 50$

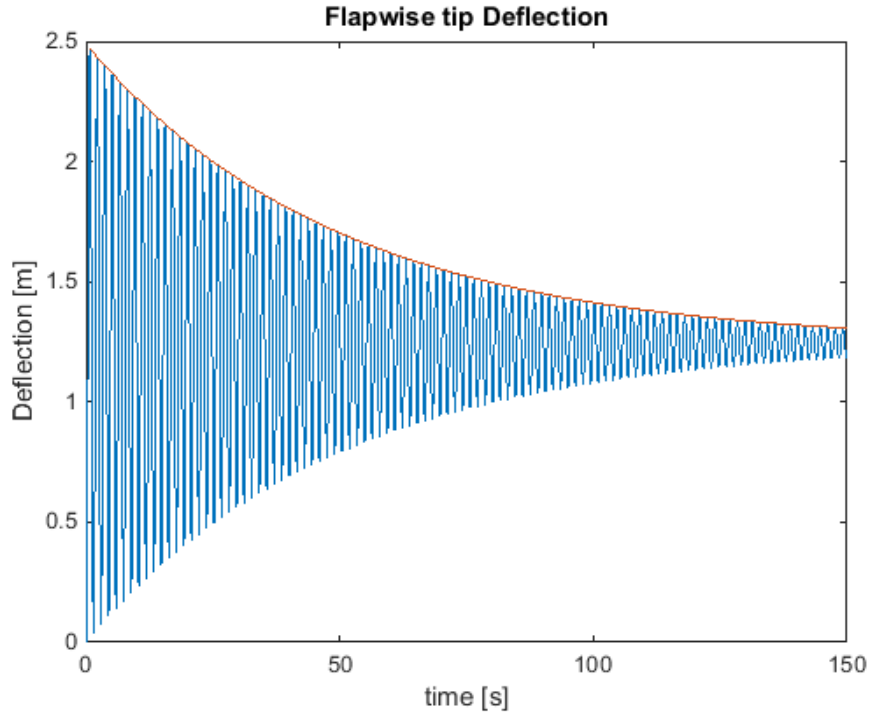


Figure 3.15: Flapwise eigenfrequency and damping.

- time after n oscillation: $t_n = 74.97$
- Amplitude after n oscillations: $A_n = 1.5192$

To find the equivalent mass m_f and damping coefficient c_f equation 3.47 to 3.53 is used. Here it has to be mentioned that, due to a steady state deflection $x_{f,ss}$, σ is calculated as

$$\sigma = \frac{1}{n} \cdot \ln\left(\frac{A_0 - x_{f,ss}}{A_n - x_{f,ss}}\right) \quad (3.66)$$

The equivalent mass m_f and damping coefficient c_f are then calculated to be

$$m_f = 2.2177 \cdot 10^4 \text{ kg} \quad (3.67)$$

$$c_f = 105.5448 \frac{\text{N} \cdot \text{s}}{\text{m}} \quad (3.68)$$

The governing equation for use in section 3.8 is rewritten as

$$\ddot{x}_f = -\frac{k_f}{m_f} x_f - \frac{c_f}{m_f} \dot{x}_f + \frac{F_f}{m_f} \quad (3.69)$$

3.7.2 Edgewise Dynamics

The modelling of the edgewise deflection of the blade is very similar to modelling of the flapwise deflection.

The governing equation is given as

$$m_e \ddot{y}_e + c_e \dot{y}_e + k_e y_e = F_e \quad (3.70)$$

where

- y_e represents the tip deflection in edgewise direction.
- m_e is the equivalent mass needed to accelerate the tip.
- c_e is the damping coefficient of the edgewise movement.
- k_e is the spring constant of the edgewise deflection.
- F_e is the equivalent force acting on the tip of the blade.

To find the equivalent spring constant for the edgewise deflection k_e there has been made a simulation in FAST, similar to the one in previous section about the flapwise deflection. Here the blade was given an azimuth angle of 270° and a pitch angle of 0° . Aerodynamics and all structural DOFs (except the first edgewise blade mode) were deactivated to avoid any other influences.

As described in previous subsection, this causes the blade to fluctuate and get into steady state due to gravity. In figure 3.16 the edgewise tip deflection and the edgewise root bending moment, which is equal to the moment around the x-axis in the coordinate system given in figure 3.12, can be seen.

The equivalent force acting on the tip of the blade is given as

$$F_e = \frac{-M_e}{L_{Blade}} \quad (3.71)$$

The reason for the minus sign can be seen in fig. 3.12 where positive moment (by the right-hand-rule convention) around the x_f -axis (i.e. edgewise moment) would result in a negative equivalent force in the y_e -direction.

The equivalent spring constant for the edgewise tip deflection is thereby

$$k_e = \frac{F_{e,ss}}{y_{e,ss}} = 1.3197 \cdot 10^5 \frac{N}{m} \quad (3.72)$$

where $F_{e,ss}$ is the steady state force and $y_{e,ss}$ is the steady state tip deflection. In figure 3.16 it also can be seen, that the first edgewise blade mode has an influence in the flapwise direction. Here it is also assumed that the first flapwise blade mode has some influence on the edgewise tip deflection, which is given as

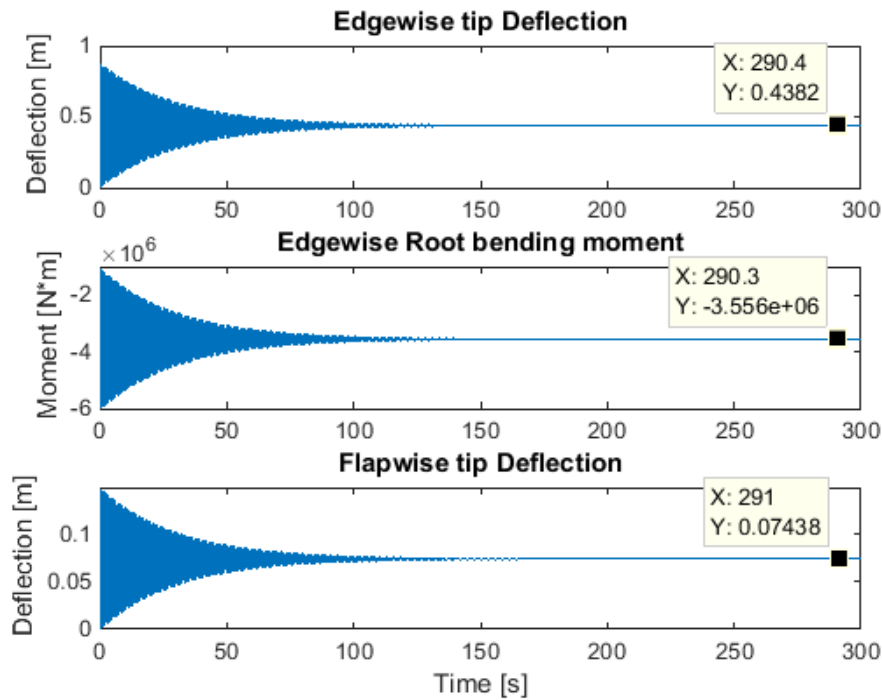


Figure 3.16: Edgewise deflection, root bending moment and flapwise deflection using only first Edgewise blade mode.

$$x_{f,e} = \frac{x_{f,ss}}{y_{e,ss}} = 0.1697 \quad (3.73)$$

where $x_{f,ss}$ is the steady state tip deflection in flapwise direction.

To find the damping and the eigenfrequency, the fluctuations in the beginning of the experiment were analysed, which also can be seen in figure 3.17.

The key information of this simulation is:

- Initial displacement: $A_0 = 0.8696$
- Initial time: $t_0 = 0.46$
- number of counted oscillations $n = 50$
- time after n oscillation: $t_n = 45.66$
- Amplitude after n oscillations: $A_n = 0.5378$

to find the equivalent mass m_f and damping coefficient c_f , again equation 3.47 to 3.53 is used. Here it has to be mentioned that, due to a steady state deflection, σ is calculated as following

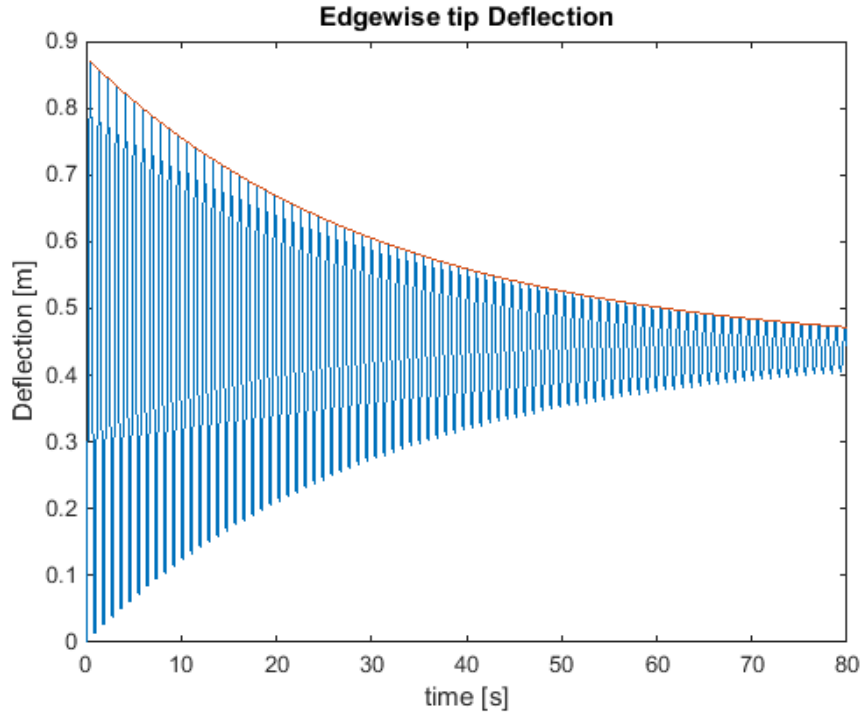


Figure 3.17: Edgewise eigenfrequency and damping.

$$\sigma = \frac{1}{n} \cdot \ln\left(\frac{A_0 - y_{e,ss}}{A_n - y_{e,ss}}\right) \quad (3.74)$$

The equivalent mass m_e and damping coefficient c_e are then calculated to be

$$m_e = 2.7876 \cdot 10^3 \text{ kg} \quad (3.75)$$

$$c_e = 179.0125 \frac{\text{N} \cdot \text{s}}{\text{m}} \quad (3.76)$$

The governing equation for later use is given as

$$\ddot{y}_e = -\frac{k_e}{m_e} y_e - \frac{c_e}{m_e} \dot{y}_e + \frac{F_e}{m_e} \quad (3.77)$$

3.7.3 Combined Dynamics

The models in section 3.7.1 and 3.7.2 describes the blade motion as two uncoupled systems, whereas it was seen that a deflection in flapwise direction gave rise to a deflection in edgewise direction and vice versa. The following approach incorporates this interconnection in the model

by transferring the fraction K_{F2E} from flapwise to edgewise direction and similarly the fraction K_{E2F} from edgewise to flapwise direction.

$$\ddot{x}_f = -\frac{k_f}{m_f}(x_f - K_{E2F} \cdot y_e) - \frac{c_f}{m_f}(\dot{x}_f - K_{E2F} \cdot \dot{y}_e) + \frac{F_f}{m_f} \quad (3.78)$$

$$\ddot{y}_e = -\frac{k_e}{m_e}(y_e - K_{F2E} \cdot x_f) - \frac{c_e}{m_e}(\dot{y}_e - K_{F2E} \cdot \dot{x}_f) + \frac{F_e}{m_e} \quad (3.79)$$

Notice that equations 3.69 and 3.77 are a special case of equations 3.78 and 3.79 with $K_{F2E} = K_{E2F} = 0$. The idea of using K_{F2E} and K_{E2F} came from $y_{e,f}$ and $x_{f,e}$ in sections 3.7.1 and 3.7.2 and have been tuned to satisfactory values. The two coefficients used are $k_{F2E} = 0.0653$ and $k_{E2F} = 1.7273$.

3.7.4 Blade Mode Shapes

As not only the tip velocity is needed as feedback into the BEM calculations, but also the velocity of the different sections of the blade, the shape of the blade has been simplified. FAST gives the possibility to see the deflection of different nodes on the blade. From the tests described in previous subsections, the steady state deflections of the different nodes on the blade were analysed and illustrated. Figure 3.18 a) illustrates the flapwise deflection found due to the simulation made in subsection 3.7.1, where only the first flapwise blademode was activated. Figure 3.18 b) illustrates the edgewise deflection found due to the simulation from subsection 3.7.2, where only the first edgewise blademode was activated.

Besides the illustration of the blade mode shapes, also a 3rd order and a 2nd order polynomial are compared to the flap- and edgewise blade mode shape, respectively. These polynomials were used in this project to find the velocity/deflection of every node on the blade easily.

To find the flap- and edgewise deflection of any point on the blade, following equations are used

$$x_f(r) = \frac{r^3}{L_{Blade}^3} \cdot x_f(L_{Blade}) \quad (3.80)$$

$$y_e(r) = \frac{r^2}{L_{Blade}^2} \cdot y_e(L_{Blade}) \quad (3.81)$$

where r is the radial distance to the actual node on the blade. Thereby $x_f(L_{Blade})$ and $y_e(L_{Blade})$ are the flap- and edgewise tip deflection, respectively.

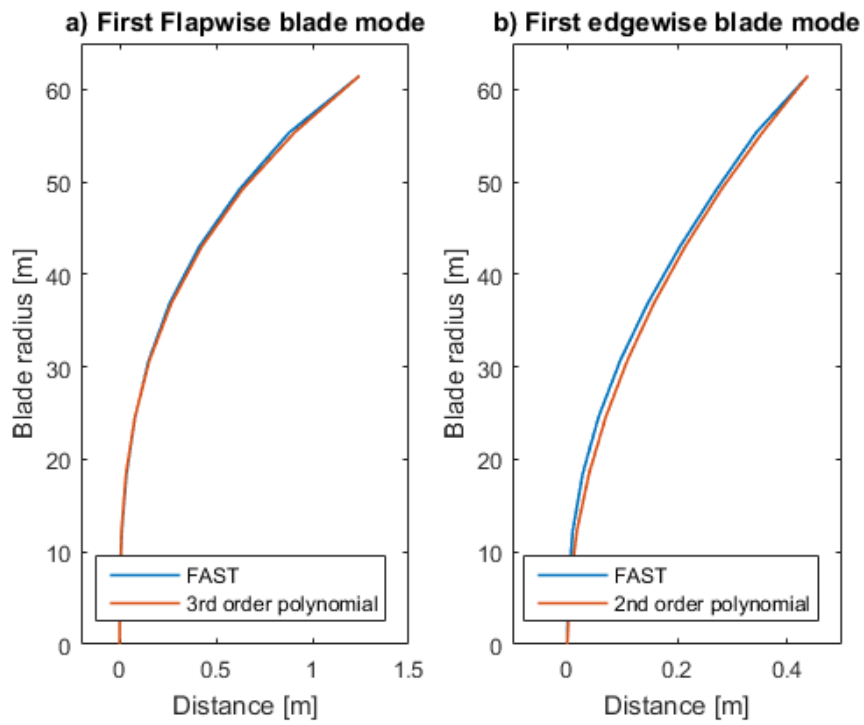


Figure 3.18: Illustration of shapes for first flapwise and first edgewise eigenmode.

3.8 State Space of Structural Dynamics

It has been chosen to model the tower and blade dynamics as a state space model. For the sake of manageability, it has been chosen to make 3 equal state space models, one for each blade and each including the tower dynamics. Here it is important to mention, that the dynamic influence of the blades to the tower were chosen to be negligible. The only influence on the tower is the thrust force, which is given by the aerodynamics of all blades. This makes sure, that the dynamics of the tower is the same in each state space model.

The representation of the state space model is given as

$$\dot{x} = Ax + Bu \quad (3.82)$$

$$y = Cx + \overset{0}{D}u \quad (3.83)$$

where D is zero, as the inputs do not affect the outputs directly.

The states are given as

$$\begin{aligned} x_1 &= x_t \\ x_2 &= \dot{x}_t \\ x_3 &= x_f \\ x_4 &= \dot{x}_f \\ x_5 &= y_e \\ x_6 &= \dot{y}_e \end{aligned} \quad (3.84)$$

and the inputs into the state space model are given as

$$\begin{aligned} u_1 &= F_t \\ u_2 &= F_f \\ u_3 &= F_e \end{aligned} \quad (3.85)$$

The governing equations for the tower and blade dynamics can be rewritten as the follow-

ing:

$$\dot{x}_1 = x_2 \quad (3.86)$$

$$\dot{x}_2 = -\frac{k_t}{m_t}x_1 - \frac{c_t}{m_t}x_2 + \frac{1}{m_t}u_1 \quad (3.87)$$

$$\dot{x}_3 = x_4 \quad (3.88)$$

$$\dot{x}_4 = -\frac{k_f}{m_f}x_3 - \frac{c_f}{m_f}x_4 - \frac{k_f}{m_f}K_{E2F} \cdot x_5 - \frac{c_f}{m_f}K_{E2F} \cdot x_6 + \frac{1}{m_f}u_2 \quad (3.89)$$

$$\dot{x}_5 = x_6 \quad (3.90)$$

$$\dot{x}_6 = -\frac{k_e}{m_e}K_{F2E} \cdot x_3 - \frac{c_e}{m_e}K_{F2E} \cdot x_4 - \frac{k_e}{m_e}x_5 - \frac{c_e}{m_e}x_6 + \frac{1}{m_e}u_3 \quad (3.91)$$

Which gives the state space representation of the tower top movement as

$$\begin{bmatrix} \dot{x}_1 \\ \dot{x}_2 \\ \dot{x}_3 \\ \dot{x}_4 \\ \dot{x}_5 \\ \dot{x}_6 \end{bmatrix} = \begin{bmatrix} 0 & 1 & 0 & 0 & 0 & 0 \\ -\frac{k_t}{m_t} & -\frac{c_t}{m_t} & 0 & 0 & 0 & 0 \\ 0 & 0 & 0 & 1 & 0 & 0 \\ 0 & 0 & -\frac{k_f}{m_f} & -\frac{c_f}{m_f} & -\frac{k_f}{m_f}K_{E2F} & -\frac{c_f}{m_f}K_{E2F} \\ 0 & 0 & 0 & 0 & 0 & 1 \\ 0 & 0 & -\frac{k_e}{m_e}K_{F2E} & -\frac{c_e}{m_e}K_{F2E} & -\frac{k_e}{m_e} & -\frac{c_e}{m_e} \end{bmatrix} \begin{bmatrix} x_1 \\ x_2 \\ x_3 \\ x_4 \\ x_5 \\ x_6 \end{bmatrix} + \begin{bmatrix} 0 & 0 & 0 \\ \frac{1}{m_t} & 0 & 0 \\ 0 & 0 & 0 \\ 0 & \frac{1}{m_f} & 0 \\ 0 & 0 & 0 \\ 0 & 0 & \frac{1}{m_e} \end{bmatrix} \begin{bmatrix} u_1 \\ u_2 \\ u_3 \end{bmatrix} \quad (3.92)$$

$$\begin{bmatrix} y_1 \\ y_2 \\ y_3 \\ y_4 \\ y_5 \\ y_6 \end{bmatrix} = \begin{bmatrix} 1 & 0 & 0 & 0 & 0 & 0 \\ 0 & 1 & 0 & 0 & 0 & 0 \\ 0 & 0 & 1 & 0 & 0 & 0 \\ 0 & 0 & 0 & 1 & 0 & 0 \\ 0 & 0 & 0 & 0 & 1 & 0 \\ 0 & 0 & 0 & 0 & 0 & 1 \end{bmatrix} \begin{bmatrix} x_1 \\ x_2 \\ x_3 \\ x_4 \\ x_5 \\ x_6 \end{bmatrix} \quad (3.93)$$

here the outputs of the state space model are the same as the states.

The validation of the non-linear model can be seen together with the validation of the linear model in section 4.1.

3.9 Blade Root Sensor Modelling

As mentioned in the introduction of this project, it is assumed that the wind turbine has installed strain gauges at the root of each blade, which can measure the compression/tension of the material at the root of the blades and thereby can estimate the blade root moments.

The calculation from the compression/tension of the material to get the root bending moment has not been dealt with in this report. Here it is assumed that that the root bending moment is linearly dependent on the tip deflection of the blade. The implementation of this

is simple, as both the tip deflection is given by the model and as the spring constants for the edge- and flapwise deflection are already known. The moment in flapwise direction (around the blades' local y-axis) is thereby given as

$$M_f = k_f \cdot x_f \cdot L_{Blade} \quad (3.94)$$

and the moment in edgewise direction (around the blades' local x-axis) is given as

$$M_e = -k_e \cdot y_e \cdot L_{Blade} \quad (3.95)$$

Chapter 4

Linearization

In this section the linear design model is derived. This model will be used for the design of the MPC controller in section 6.3.

From the equation of the pitch actuator we have

$$\dot{\theta} = -\frac{1}{\tau_{\theta}} \cdot \theta + \frac{1}{\tau_{\theta}} \cdot \theta_{ref} \quad (4.1)$$

For the drive-train the equations with individual pitching can be written as:

$$\dot{\omega}_r = -\frac{D_s}{J_r} \cdot \omega_r + \frac{D_s}{J_r \cdot N_g} \cdot \omega_g - \frac{K_s}{J_r} \cdot \Delta\phi + \frac{1}{J_r} \cdot T_r(V, \omega_r, \theta_1, \theta_2, \theta_3) \quad (4.2)$$

$$\dot{\omega}_g = \frac{D_s}{J_g \cdot N_g} \cdot \omega_r - \frac{D_s}{J_g \cdot N_g^2} \cdot \omega_g + \frac{K_s}{J_g \cdot N_g} \cdot \Delta\phi - \frac{1}{J_g} \cdot T_g \quad (4.3)$$

$$\Delta\dot{\phi} = \omega_r - \frac{\omega_g}{N_g} \quad (4.4)$$

For the generator the equation is

$$\dot{T}_g = -\frac{1}{\tau_g} \cdot T_g + \frac{1}{\tau_g} \cdot T_{ref} \quad (4.5)$$

The tower mass-spring-damper system is given by:

$$\ddot{x}_t = -\frac{k_t}{m_t} x_t - \frac{c_t}{m_t} \dot{x}_t + \frac{F_t(V, \omega_r, \theta_1, \theta_2, \theta_3)}{m_t} \quad (4.6)$$

and the blade dynamics are given by:

$$\ddot{x}_{f,k} = -\frac{k_f}{m_f} x_f - \frac{c_f}{m_f} \dot{x}_f + \frac{F_f(V, \omega_r, \theta_k)}{m_f} \quad (4.7)$$

and

$$\ddot{x}_{e,k} = -\frac{k_e}{m_e} x_e - \frac{c_e}{m_e} \dot{x}_e + \frac{F_e(V, \omega_r, \theta_k)}{m_e} \quad (4.8)$$

Where $k = 1, 2, 3$ denotes the blade number.

Notice that not all of these equations are linear. The non-linear parts arise from the aerodynamic inputs such as the rotor torque T_r and the aerodynamic "forces" F_t, F_f and F_e which are all functions of the wind speed V , the rotor speed ω_r and the pitch angles $\theta_1, \theta_2, \theta_3$.

This means that we have a set of non-linear equations on the form [11]

$$\dot{\mathbf{x}} = \mathbf{f}(\mathbf{x}, \mathbf{u}) \quad (4.9)$$

In the third region of the wind turbine operation a set of operating points or equilibrium points $\mathbf{x}_0, \mathbf{u}_0$ have been found, which satisfies $\dot{\mathbf{x}}_0 = \mathbf{0} = \mathbf{f}(\mathbf{x}_0, \mathbf{u}_0)$. In the operating points the equation can be expressed in terms of perturbations from the operating point as:

$$\dot{\mathbf{x}}_0 + \delta\dot{\mathbf{x}} \cong \mathbf{f}(\mathbf{x}_0, \mathbf{u}_0) + \mathbf{A}\delta\mathbf{x} + \mathbf{B}\delta\mathbf{u} \quad (4.10)$$

where \mathbf{A} and \mathbf{B} are the best linear fits at the equilibrium point

$$\mathbf{A} = \left[\frac{\partial \mathbf{f}}{\partial \mathbf{x}} \right]_{\mathbf{x}_0, \mathbf{u}_0} \quad \text{and} \quad \mathbf{B} = \left[\frac{\partial \mathbf{f}}{\partial \mathbf{u}} \right]_{\mathbf{x}_0, \mathbf{u}_0}$$

Subtracting out the equilibrium we get a linear differential equation in the perturbation variables $\delta\mathbf{x}$ and $\delta\mathbf{u}$:

$$\delta\dot{\mathbf{x}} = \mathbf{A}\delta\mathbf{x} + \mathbf{B}\delta\mathbf{u} \quad (4.11)$$

The state vector and the input vector are

$$\mathbf{x} = \begin{bmatrix} \theta_1 \\ \theta_2 \\ \theta_3 \\ \omega_r \\ \omega_g \\ \Delta\phi \\ T_g \\ x_t \\ \dot{x}_t \\ x_{f1} \\ \dot{x}_{f1} \\ x_{e1} \\ \dot{x}_{e1} \\ x_{f2} \\ \dot{x}_{f2} \\ x_{e2} \\ \dot{x}_{e2} \\ x_{f3} \\ \dot{x}_{f3} \\ x_{e3} \\ \dot{x}_{e3} \end{bmatrix} \quad \text{and } \mathbf{u} = \begin{bmatrix} \theta_{ref,1} \\ \theta_{ref,2} \\ \theta_{ref,3} \\ T_{ref} \end{bmatrix}$$

and in addition we have a disturbance vector consisting of the wind speeds for each blade \mathbf{d}

$$\mathbf{d} = \begin{bmatrix} V_1 \\ V_2 \\ V_3 \end{bmatrix}$$

Taking the derivative of the differential equations with respect to the state vector, input vector and disturbance vector yields the equations:

$$\delta\dot{\theta}_k = -\frac{1}{\tau_\theta} \cdot \delta\theta_k + \frac{1}{\tau_\theta} \cdot \delta\theta_{ref,k} \quad (4.12)$$

where $k = 1,2,3$ respectively for the three pitch actuators.

The aerodynamic forcing functions are calculated using BEMT as described in section 3.2. Notice in the following, that every output from the BEM code is only given as the contribution from one single blade.

For the drive-train the equations can thus be written as:

$$\begin{aligned} \delta\dot{\omega}_r = & + \frac{1}{J_r} \sum_{n=1}^3 \frac{\partial T_r(V, \omega_r, \theta)}{\partial \theta} \Big|_{V_0, \omega_{r0}, \theta_0} \cdot \delta\theta_n + \frac{1}{J_r} \left(-D_s + 3 \cdot \frac{\partial T_r(V, \omega_r, \theta)}{\partial \omega_r} \Big|_{V_0, \omega_{r0}, \theta_0} \right) \cdot \delta\omega_r \\ & + \frac{D_s}{J_r \cdot N_g} \cdot \delta\omega_g - \frac{K_s}{J_r} \cdot \delta\Delta\phi + \frac{1}{J_r} \sum_{n=1}^3 \frac{\partial T_r(V, \omega_r, \theta)}{\partial V} \Big|_{V_0, \omega_{r0}, \theta_0} \cdot \delta V_n \end{aligned} \quad (4.13)$$

$$\delta\dot{\omega}_g = \frac{D_s}{J_g \cdot N_g} \cdot \delta\omega_r - \frac{D_s}{J_g \cdot N_g^2} \cdot \delta\omega_g + \frac{K_s}{J_g \cdot N_g} \cdot \delta\Delta\phi - \frac{1}{J_g} \cdot \delta T_g \quad (4.14)$$

$$\delta\Delta\phi = \delta\omega_r - \frac{1}{N_g} \cdot \delta\omega_g \quad (4.15)$$

For the generator the equation is

$$\delta\dot{T}_g = -\frac{1}{\tau_g} \cdot \delta T_g + \frac{1}{\tau_g} \cdot \delta T_{ref} \quad (4.16)$$

The tower mass spring damper system is given by:

$$\begin{aligned} \delta\ddot{x}_t = & \frac{1}{m_t} \sum_{n=1}^3 \left. \frac{\partial F_t(V, \omega_r, \theta)}{\partial \theta} \right|_{V_0, \omega_{r0}, \theta_0} \cdot \delta\theta_n + \frac{3}{m_t} \cdot \left. \frac{\partial F_t(V, \omega_r, \theta)}{\partial \omega_r} \right|_{V_0, \omega_{r0}, \theta_0} \cdot \delta\omega_r - \frac{k_t}{m_t} \delta x_t \\ & - \left(\frac{c_t}{m_t} + \frac{3}{m_t} \left. \frac{\partial F_t(V, \omega_r, \theta)}{\partial V} \right|_{V_0, \omega_{r0}, \theta_0} \right) \cdot \delta\dot{x}_t - \frac{V_{sc}}{m_t} \sum_{n=1}^3 \left. \frac{\partial F_t(V, \omega_r, \theta)}{\partial V} \right|_{V_0, \omega_{r0}, \theta_0} \cdot \cos(\theta_0) \cdot \delta\dot{x}_{f,n} \\ & - \frac{V_{sc}}{m_t} \sum_{n=1}^3 \left. \frac{\partial F_t(V, \omega_r, \theta)}{\partial V} \right|_{V_0, \omega_{r0}, \theta_0} \cdot \sin(\theta_0) \cdot \delta\dot{y}_{e,n} + \frac{1}{m_t} \sum_{n=1}^3 \left. \frac{\partial F_t(V, \omega_r, \theta)}{\partial V} \right|_{V_0, \omega_{r0}, \theta_0} \cdot \delta V_n \quad (4.17) \end{aligned}$$

As the blade velocity in the linear model denotes the tip velocity, a velocity scaling factor V_{sc} was used to get the average blade velocity. As the pitch angle operates at low angles ($<20^\circ$), the flapwise deflection is the dominating blade mode influencing the equivalent wind speed. The scaling factor is a simple relation between the average velocity and the tip velocity, which for a 3rd order polynomial is $V_{sc} = 0.25$.

The flapwise blade dynamics for each blade $k = 1, 2, 3$ are then given by:

$$\begin{aligned} \delta\ddot{x}_{f,k} = & \frac{1}{m_f} \left. \frac{\partial F_f(V, \omega_r, \theta)}{\partial \theta} \right|_{V_0, \omega_{r0}, \theta_0} \cdot \delta\theta_k + \frac{1}{m_f} \left. \frac{\partial F_f(V, \omega_r, \theta)}{\partial \omega_r} \right|_{V_0, \omega_{r0}, \theta_0} \cdot \delta\omega_r \\ & - \frac{1}{m_f} \left. \frac{\partial F_f(V, \omega_r, \theta)}{\partial V} \right|_{V_0, \omega_{r0}, \theta_0} \cdot \delta\dot{x}_t - \frac{k_f}{m_f} \cdot \delta x_{f,k} \\ & - \left(\frac{c_f}{m_f} + \frac{V_{sc}}{m_f} \left. \frac{\partial F_f(V, \omega_r, \theta)}{\partial V} \right|_{V_0, \omega_{r0}, \theta_0} \cdot \cos(\theta_0) \right) \cdot \delta\dot{x}_{f,k} - \frac{k_f}{m_f} \cdot K_{E2F} \cdot \delta y_{e,k} \\ & - \left(\frac{c_f}{m_f} \cdot K_{E2F} + \frac{V_{sc}}{m_f} \left. \frac{\partial F_f(V, \omega_r, \theta)}{\partial V} \right|_{V_0, \omega_{r0}, \theta_0} \cdot \sin(\theta_0) \right) \cdot \delta\dot{y}_{e,k} \\ & + \frac{1}{m_f} \left. \frac{\partial F_f(V, \omega_r, \theta)}{\partial V} \right|_{V_0, \omega_{r0}, \theta_0} \cdot \delta V_k \quad (4.18) \end{aligned}$$

and similarly for edgewise blade dynamics

$$\begin{aligned}
\delta y_{e,k} = & \frac{1}{m_e} \frac{\partial F_e(V, \omega_r, \theta)}{\partial V} \Big|_{V_0, \omega_{r0}, \theta_0} \cdot \delta \theta_k + \frac{1}{m_e} \frac{\partial F_e(V, \omega_r, \theta)}{\partial V} \Big|_{V_0, \omega_{r0}, \theta_0} \cdot \delta \omega_r \\
& - \frac{1}{m_e} \frac{\partial F_f(V, \omega_r, \theta)}{\partial V} \Big|_{V_0, \omega_{r0}, \theta_0} \cdot \delta \dot{x}_t - \frac{k_e}{m_e} \cdot K_{F2E} \cdot \delta x_{f,k} \\
& - \left(\frac{c_e}{m_e} \cdot K_{F2E} + \frac{V_{sc}}{m_e} \frac{\partial F_e(V, \omega_r, \theta)}{\partial V} \Big|_{V_0, \omega_{r0}, \theta_0} \cdot \cos(\theta_0) \right) \cdot \dot{x}_{f,k} - \frac{k_e}{m_e} \delta y_{e,k} \\
& - \left(\frac{c_e}{m_e} + \frac{V_{sc}}{m_e} \frac{\partial F_e(V, \omega_r, \theta)}{\partial V} \Big|_{V_0, \omega_{r0}, \theta_0} \cdot \sin(\theta_0) \right) \delta y_{e,k} + \frac{1}{m_e} \frac{\partial F_e(V, \omega_r, \theta)}{\partial V} \Big|_{V_0, \omega_{r0}, \theta_0} \cdot \delta V_n \quad (4.19)
\end{aligned}$$

From these equations the state space matrices can be formed and are shown in appendix on page 93.

The outputs of the system are

$$\mathbf{y} = \begin{bmatrix} \theta_1 \\ \theta_2 \\ \theta_3 \\ \omega_r \\ \omega_g \\ \Delta\phi \\ P_e \\ M_{b1f} \\ M_{b1e} \\ M_{b2f} \\ M_{b2e} \\ M_{b3f} \\ M_{b3e} \end{bmatrix}$$

Notice, that the operating point have been denoted by Op for more compact notation.

The power is calculated from

$$P_e = T_g \cdot \omega_g \cdot \eta_g \quad (4.20)$$

However, this equation is non-linear in the states ω_g and T_g . Again using a first order taylor series expansion yields:

$$\delta P_e \approx \eta_g \cdot \omega_{g0} \cdot \delta T_g + T_{g0} \cdot \eta_g \cdot \delta \omega_g \quad (4.21)$$

Where $\delta P_e = P_e - P_0$ and P_0 is the rated power. T_{g0} is the generator torque when the turbine is operating at rated mechanical power and rated speed, that is:

$$T_{g0} = \frac{P_{rated}}{\eta_g \cdot \omega_{g,rated}} \quad (4.22)$$

The resulting output matrix can be seen in appendix on page 94.

The partial derivatives of the aerodynamics given in the presented equations, represent the slopes of the respective functions at the linearization point. Central differences have been used to calculate the slopes. In figure 4.1 the edgewise moment as a function of wind speed is plotted around the operating point at 16 m/s (for operating points, see table 5.1 in section 5.1). Along with the BEM output the linear approximation with the slope calculated at the operating point is shown.

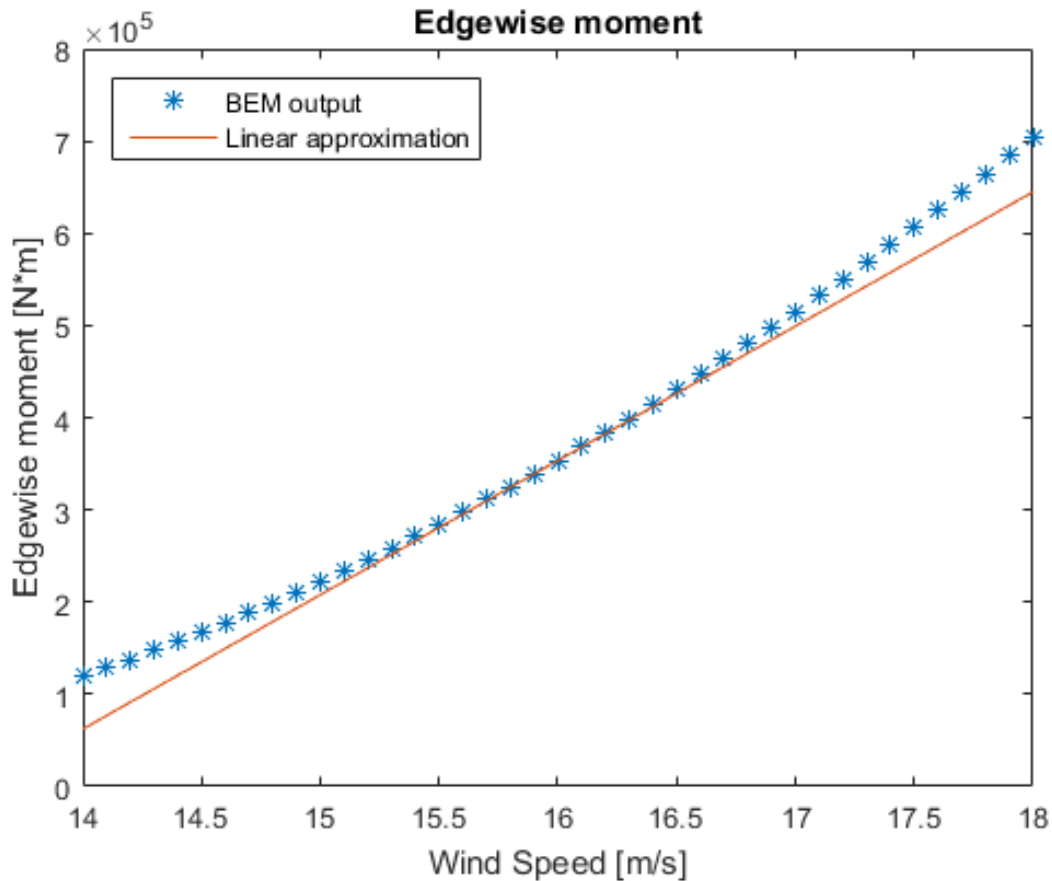


Figure 4.1: Linear approximation of the edgewise moment.

For more plots of the linear approximations at this operating point, see appendix A.3.

4.1 Model Validation

To make sure that the linear model gives sufficient outputs, it has been compared to the non-linear model and FAST. For the validation a step wind was used ($V_0 = 16\text{m/s}$ for $t < 80\text{s}$ and $V_0 = 17\text{m/s}$ for $t > 80\text{s}$) with a uniform distribution, since it shows the dynamics of the system without disturbance.

In figure 4.2 the step response of the tower can be seen.

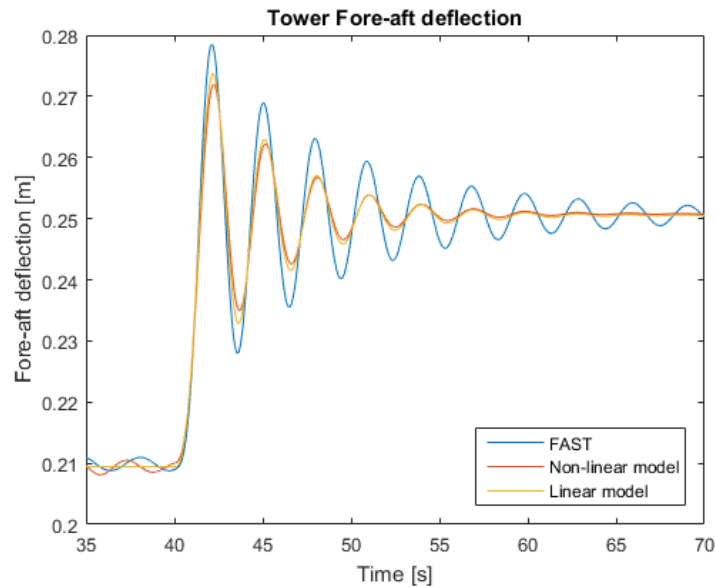


Figure 4.2: Dynamics of Tower deflection using step wind.

It can be seen that the dynamics of the linear model fit very well to the dynamics of the non-linear model. But it can also be seen that both models vary a bit from FAST, which has less damping on the tower. But the results of this step response were still chosen to be sufficient for the development of a controller.

In figure 4.3 the deflection of the blades can be seen. Due to the uniform wind fields, all three blades behave the same, so only the dynamics of a single blade are shown.

here it can be seen, that the linear model still shows some dynamics, but less than the dynamics of the non-linear model. It can also be seen, that FAST includes more dynamics, containing different frequencies, as it is more complex than the developed models in this project.

The comparison of the blade root moments between the different models can be seen in figure 4.4 .

As the blade root moments are calculated by means of the blade tip deflection, they show similar dynamics. But here it has to be mentioned, that the blade root moment sensors were tuned to give similar steady state values as in FAST, as they are necessary for the use in MPC.

A.4

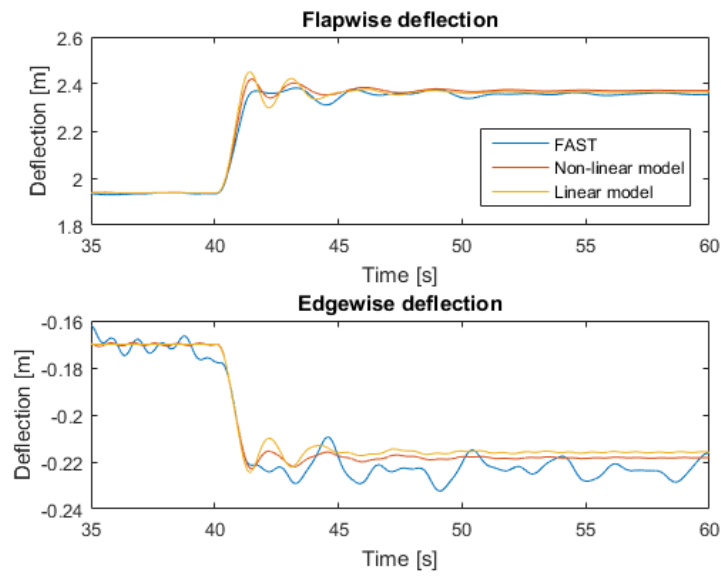


Figure 4.3: Dynamics of blade deflection using step wind.

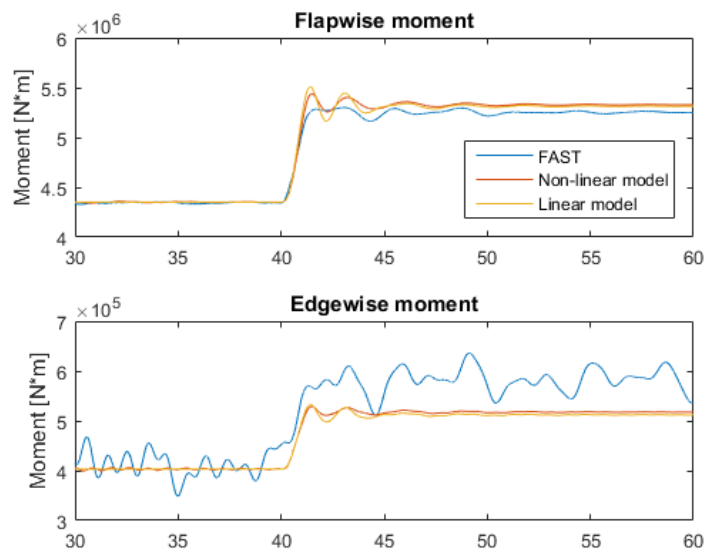


Figure 4.4: Blade root moment sensor output.

Chapter 5

Collective Pitch Control

In order to be able to evaluate the effectiveness of the individual pitch control systems a baseline collective pitch control system is needed. As the generator speed is needed for the collective pitch control, a filter has been implemented, which is described in section 5.0.1. The design of the collective pitch control is described in section 5.1, where a gain-scheduled PI-controller is derived and tested.

5.0.1 Filtering

As the collective pitch controller relies on the feedback from the generator speed, it has to be filtered. This is done by a simple difference equation, given as

$$y[n] = (1 - \alpha)u[n] + \alpha y[n - 1] \quad (5.1)$$

with

$$\alpha = e^{-2\pi T_s f_s} \quad (5.2)$$

where

- y is the output
- u is the input
- n is the actual time step
- $n - 1$ is the previous time step
- T_s is the sampling time
- f_s is the corner frequency, given as 0.25 Hz in section 2.2

As provided by [3].

The difference equation thereby gives

$$y[n] = (1 - \alpha)u[n] + \alpha y[n - 1] \quad (5.3)$$

$$y[n] - \alpha y[n - 1] = (1 - \alpha)u[n] \quad (5.4)$$

$$Y(z)[1 - \alpha z^{-1}] = U(z)[1 - \alpha] \quad (5.5)$$

$$\frac{Y(z)}{U(z)} = \frac{1 - \alpha}{1 - \alpha z^{-1}} \quad (5.6)$$

$$\frac{Y(z)}{U(z)} = \frac{(1 - \alpha)z}{z - \alpha} \quad (5.7)$$

which is implemented in simulink to filter the generator speed.

5.1 Collective Pitch Control using PI

The objective of the collective pitch controller is to keep the rotational speed of the generator constant at rated speed in region 3. This is implemented as a gain scheduled PI-control on the error between the filtered generator speed and the rated generator speed.

To design the control a simple model based on a stiff drive-train is utilized so that the angular rotation of the shaft is kept as the only degree of freedom.

The equation of motion can be written from a simple free-body diagram

$$\tau_{Aero} - N_{Gear}\tau_{Gen} = I_{Rotor}\frac{d}{dt}(\Omega) + I_{Gen}\frac{d}{dt}(N_{Gear}\Omega)N_{Gear} \quad (5.8)$$

$$= (I_{Rotor} + N_{Gear}^2 I_{Gen})\frac{d}{dt}(\Omega_0 + \Delta\Omega) = I_{Drivetrain}\dot{\Omega} \quad (5.9)$$

Where

- τ_{Aero} is the aerodynamic torque acting on the rotor
- τ_{Gen} is the generator torque acting on the high-speed shaft
- N_{Gear} is the high gear ratio
- I_{Rotor} is the rotor moment of inertia
- I_{Gen} is the generator moment of inertia
- $I_{Drivetrain}$ is the drive-train moment of inertia transferred to the low-speed shaft
- Ω is the low-speed shaft rotational speed and Ω_0 is the rated low-speed shaft rotational speed

- $\Delta\Omega$ is a small perturbation of the low-speed shaft rotational speed about the rated speed
- $\Delta\dot{\Omega}$ is the low-speed shaft rotational acceleration

In region 3 the objective of the generator-torque controller is to keep the generator power at the rated power. Therefore, the generator torque is inverse proportional to the generator speed in region 3:

$$\tau_{Gen}(N_{Gear}\Omega) = \frac{P_0}{N_{Gear}\Omega} \quad (5.10)$$

where P_0 is the rated mechanical power.

In general the aerodynamic torque is a function of the rotor rotational speed, the pitch angle and the wind speed. Assuming that the variation of aerodynamic torque with rotor speed is negligible in region 3, and for a given constant wind speed it will be a function of only pitch angle:

$$\tau_{Aero} = \frac{P(\theta, \Omega_0)}{\Omega_0} \quad (5.11)$$

Where

- P is the mechanical power
- θ is the rotor collective blade pitch angle

A linearisation of these two equations using a first order Taylor series expansion yields:

$$\tau_{Gen} \approx \frac{P_0}{N_{Gear}\Omega_0} - \frac{P_0}{N_{Gear}\Omega_0^2} \Delta\Omega \quad (5.12)$$

$$\tau_{Aero} \approx \frac{P_0}{\Omega_0} + \frac{1}{\Omega_0} \left. \frac{\partial P}{\partial \theta} \right|_{\theta_0} \Delta\theta \quad (5.13)$$

Where θ_0 is the linearisation/operating point and $\Delta\theta$ is a small perturbation about the operating point.

The perturbation in pitch angle around the operating point is related to the PID controller by:

$$\Delta\theta = K_P N_{Gear} \Delta\Omega + K_I \int_{t_0}^t N_{Gear} \Delta\Omega dt + K_D N_{Gear} \Delta\dot{\Omega} \quad (5.14)$$

where K_P , K_I and K_D are the proportional, integral and derivative gains, respectively and t_0 is the time at which the speed error occurs.

Substituting $\dot{\phi} = \Delta\Omega$ in equation 5.14 yields.

$$\Delta\theta = K_P N_{Gear} \dot{\phi} + K_I N_{Gear} \phi + K_D N_{Gear} \ddot{\phi} \quad (5.15)$$

The part from the integration part stems from the fact that

$$\int_{t_0}^t \Delta\Omega dt = \int_{t_0}^t \frac{\Delta d\psi}{dt} dt = \int_{t_0}^t d\Delta\psi = \Delta\psi(t) - \Delta\psi(t_0) = \Delta\psi(t) = \phi \quad (5.16)$$

Where $\Delta\psi(t_0) = 0$ in the steady state.

By combining eqs. 5.9, 5.13, 5.12 and 5.15 the drivetrain controlled by PID turns into the second order system:

$$\underbrace{\left(I_{Drivetrain} + \frac{1}{\Omega_0} \left(-\frac{\partial P}{\partial \theta}\right) N_{Gear} K_D\right)}_{M_\phi} \ddot{\phi} + \underbrace{\left(\frac{1}{\Omega_0} \left(-\frac{\partial P}{\partial \theta}\right) N_{Gear} K_P - \frac{P_0}{\Omega_0^2}\right)}_{C_\phi} \dot{\phi} + \underbrace{\frac{1}{\Omega_0} \left(-\frac{\partial P}{\partial \theta}\right) N_{Gear} K_I}_{K_\phi} \phi = 0 \quad (5.17)$$

With natural frequency and damping ratio given by:

$$\omega_{\phi n} = \sqrt{\frac{K_\phi}{M_\phi}} \quad (5.18)$$

$$\zeta_\phi = \frac{C_\phi}{2M_\phi\omega_{\phi n}} \quad (5.19)$$

In region 3, the sensitivity of aerodynamic power to the rotor-collective blade pitch angle, $\frac{\partial P}{\partial \theta}$, is negative. Thus, with positive control gains the following can be noticed from the second order differential equation:

- The derivative term increases the effective inertia of the drive-train
- The proportional term adds damping
- The integral term adds to the stiffness or restoring

Also, note that the generator-torque controller introduces a term of $-\frac{P_0}{\Omega_0^2}$ which decreases the effective damping. This negative damping can be compensated by the proportional term in the PI controller.

Solving for K_P in the expression for C_ϕ yields

$$K_P = \frac{2\zeta_\phi\omega_{\phi n}\Omega_0 + \frac{P_0}{\Omega_0} + 2\zeta_\phi\omega_{\phi n}\left(-\frac{\partial P}{\partial \theta}\right)N_{Gear}K_D}{N_{Gear}\left(-\frac{\partial P}{\partial \theta}\right)} \quad (5.20)$$

Similarly for K_I

$$K_I = \frac{I_{Drivetrain}\Omega_0\omega_{\phi n}^2 + \omega_{\phi n}^2\frac{1}{\Omega_0}\left(-\frac{\partial P}{\partial \theta}\right)N_{Gear}K_D}{N_{Gear}\left(-\frac{\partial P}{\partial \theta}\right)} \quad (5.21)$$

It is chosen to make a PI-controller and thus setting $K_D = 0$ the equations for the two control gains become:

Wind Speed [m/s]	Pitch angle θ [deg]
11.29	0
11.4	1.18
12	3.91
13	6.59
14	8.66
15	10.44
16	12.06
17	13.55
18	14.94
19	16.26
20	17.52
21	18.74
22	19.93
23	21.06
24	22.17
25	23.23

Table 5.1: Operating Points used to find sensitivity of power to pitch angle.

$$K_P = \frac{2I_{Drivetrain}\zeta_\phi\omega_{\phi n}\Omega_0 + \frac{P_0}{\Omega_0}}{N_{Gear}\left(-\frac{\partial P}{\partial \theta}\right)} \quad (5.22)$$

$$K_I = \frac{I_{Drivetrain}\Omega_0\omega_{\phi n}^2}{N_{Gear}\left(-\frac{\partial P}{\partial \theta}\right)} \quad (5.23)$$

The natural frequency $\omega_{\phi n} = 0.6$ and a damping ratio $\zeta_\phi = 0.7$ was used as in [3].

The only unknown is now the sensitivity of power to pitch angle $\frac{\partial P}{\partial \theta}$. In order to find this for different wind speeds in region 3, the pitch angles at which rated power is achieved with rated rotational speed was found. The operation points were found in Simulink using the BEMT code by setting the rotor rotational speed to its rated value of 12.1 RPM and using the integral of the power error as the pitch signal until steady state pitch was reached. The results can be seen in table 5.1

The sensitivity of power to pitch angle $\frac{\partial P}{\partial \theta}$ was found by perturbing the pitch angle a small value above and below the operating points and applying a central difference to approximate the derivative. The BEMT code was modified to use the Frozen Wake assumption during the perturbation, which simply means that the induced velocities calculated at the operating points were held constant in the perturbed calculations of power. As seen in figure 5.1 the power sensitivity to collective pitch angle is negative in the above rated region. A best linear fit is used as the sensitivity function for simplicity.

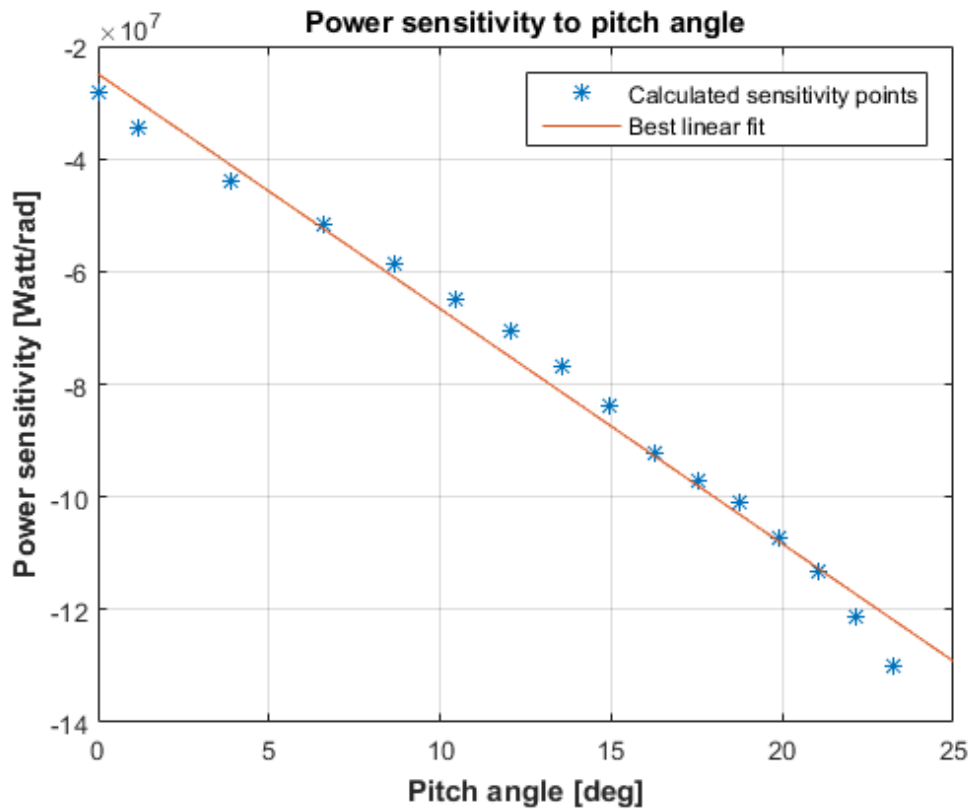


Figure 5.1: Plot of the calculated points of power sensitivity to pitch and the corresponding best linear fit.

Inserting the sensitivity function into the derived equations 5.22 and 5.23 for the gains yields the proportional and integral gains seen in figure 5.2.

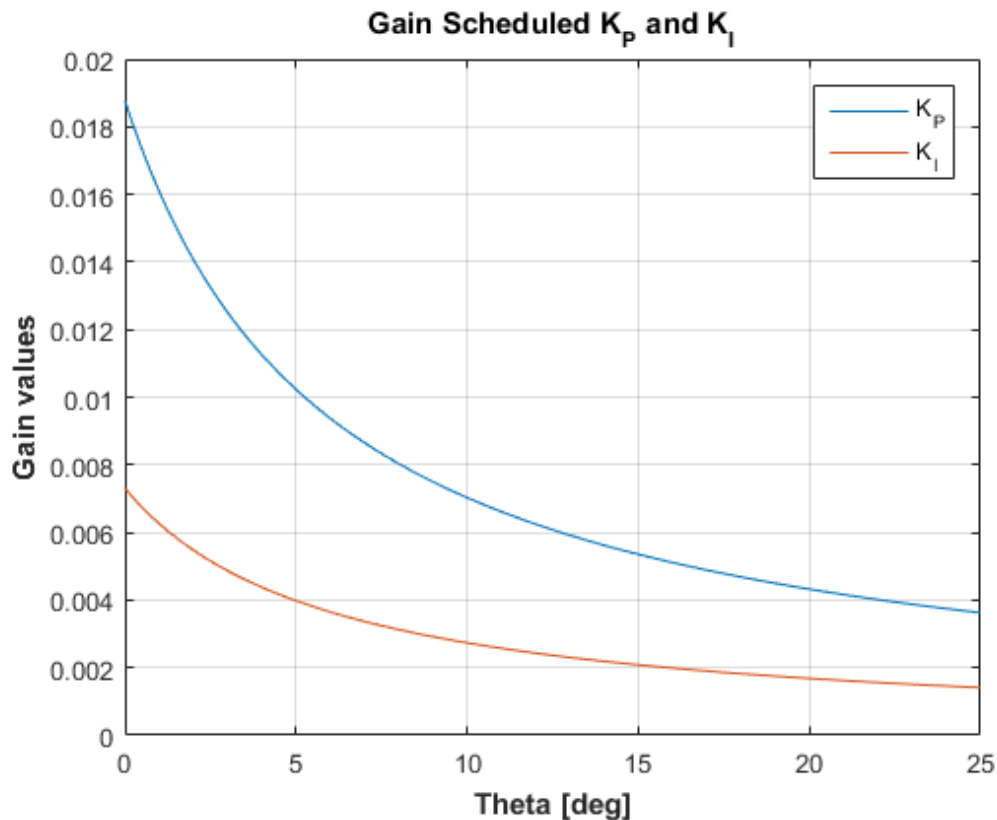


Figure 5.2: Plot of gain scheduled proportional and integral gains.

5.1.1 Test of Collective Pitch Control

Before using the collective pitch controller as baseline for individual control, it has been tested on a step wind ($V_0 = 15\text{m/s}$ for $t < 80\text{s}$ and $V_0 = 17\text{m/s}$ for $t > 80\text{s}$). Here it was found, that the controller reacted aggressive and the pitch angle was fluctuating too much, which could be a disadvantage when using it as a baseline for individual pitch control. Therefore it was chosen to scale the gain scheduled functions given from previous section. In figure 5.3 a comparison can be seen with the original gains (as shown in figure 5.2), a scaling of 0.5 and a scaling of 0.3.

Here it can be seen that the original controller (blue curve) is aggressive, as the pitch angle oscillates several times before settling. The controller with scaling factor 0.3 (yellow curve) shows a much smoother curve - which also means a slower reaction time of the controller, which could lead to too much delay at turbulent wind. Therefore it was chosen to scale the gains given from previous section by 0.5 (red curve), as it shows both a reasonable oscillations and response time.

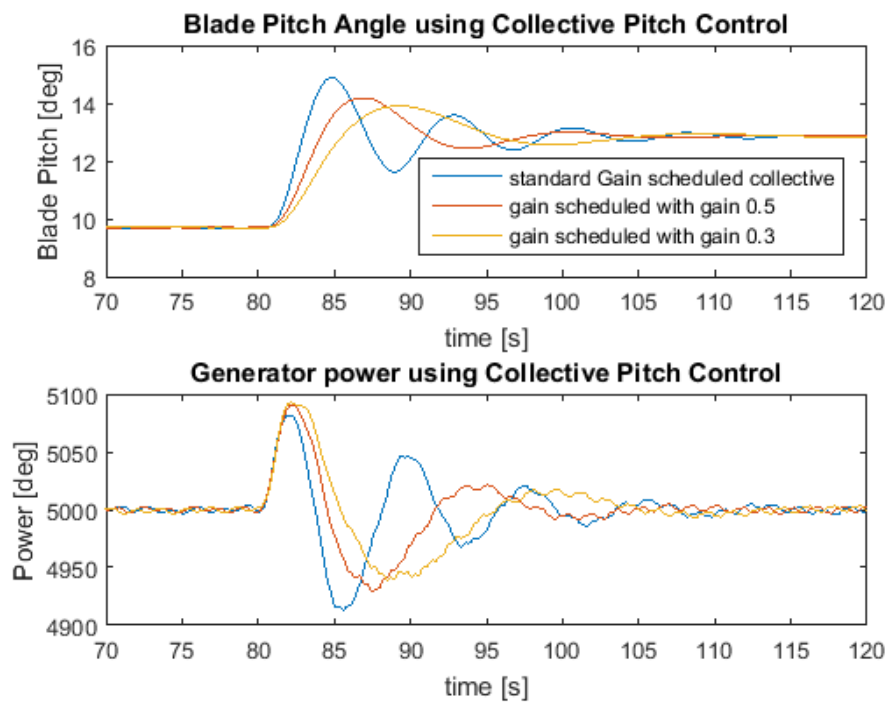


Figure 5.3: Test of gain scheduled PI controller.

Chapter 6

Individual Pitch Control

6.1 Individual Pitch Control using PI

The purpose of the individual pitch control in this project has been, to even out the forces on the rotor, which should reduce the loads on the hub of the rotor and thereby also reduce loads on main bearing. Here it has been decided to focus on the moments acting on the hub in tilt (moment around the y-axis) and yaw direction (moment around z-axis).

Therefore the loads on the hub are estimated by means of the blade root moments and then two reference angles are found, which are used to pitch the blades individually [2].

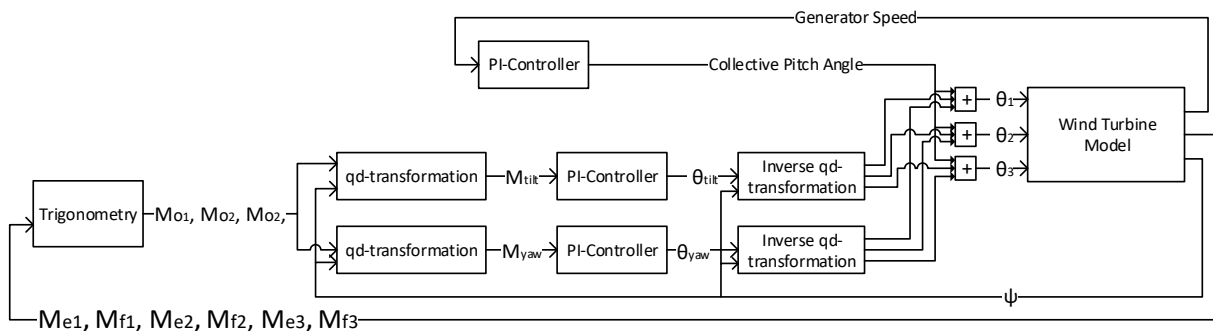


Figure 6.1: Control structure for individual PI pitch control.

6.1.1 Find loads on Hub

As described in section 3.9, the blade root moments in flap- and edgewise direction are known. Firstly, the moments have to be calculated from edge- and flapwise direction into in- and out-of-plane moments.

$M_{e,b}$:	the edgewise root bending moment of blade b
$M_{f,b}$:	the flapwise root bending moment of blade b
$M_{o,b}$:	the out-of-plane root bending moment of blade b
M_{tilt} :	the tilt-moment around the hub (moment about y-axis)
M_{yaw} :	the yaw-moment around the hub (moment about z-axis)
θ_{tilt} :	influence angle used to eliminate tilt-moment on hub
θ_{yaw} :	influence angle used to eliminate yaw-moment on hub
θ_b :	pitch angle given to blade b

Table 6.1: Description of the nomenclature used in figure 6.1.

$$M_{o,b} = M_{f,b} \cdot \cos(\theta_b) - M_{e,b} \cdot \sin(\theta_b) \quad (6.1)$$

$$M_{i,b} = M_{e,b} \cdot \cos(\theta_b) + M_{f,b} \cdot \sin(\theta_b) \quad (6.2)$$

where $b = 1, 2, 3$, denoting the no. of the blade.

Here it is assumed that the moment on the root of the blade is the same as the moment in the origin of the hub, although the distance between the origin of the hub and the root of each blade is equal to the radius of the hub.

The Tilt moment (moment around the y-axis) is given as

$$M_{tilt} = M_{o,1} \cdot \cos(\psi_1) + M_{o,2} \cdot \cos(\psi_2) + M_{o,3} \cdot \cos(\psi_3) \quad (6.3)$$

While the Yaw moment (moment around the z-axis) is given as

$$M_{yaw} = M_{o,1} \cdot \sin(\psi_1) + M_{o,2} \cdot \sin(\psi_2) + M_{o,3} \cdot \sin(\psi_3) \quad (6.4)$$

This calculation is also often referred to as qd-transformation, which is known from electrical machines.

As the blades on the rotor are equally spaced, it is known that

$$\psi_2 = \psi_1 + 120^\circ \quad (6.5)$$

$$\psi_3 = \psi_1 + 240^\circ \quad (6.6)$$

This makes it easier to implement, as only the angle of blade no. 1 is needed.

6.1.2 Filtering

The filtering of the tilt- and yaw moments play an important role when implementing a PI controller. As the pitch angle of each blade should not vary more often than twice pr. rotation, the moment on the tilt and yaw direction were chosen to be filtered. As filter there was implemented a difference equation, as described in section 5.0.1.

The corner frequency was chosen to be half of the frequency, each blade passes the same spot at the rotor. Thereby the corner frequency is given as

$$f_s = \frac{12.1 \text{ rpm}}{60 \text{ sec}} \cdot 0.5 = 0.1 \text{ Hz} \quad (6.7)$$

6.1.3 Control Strategy

For the individual pitch control of the wind turbine, the collective pitch control was chosen to give the reference pitch angle. To even out the moment in both the tilt and yaw direction, it was chosen to let the pitch angle vary within each rotation, where 4 reference angles were found. Those 4 angles can be seen in figure 6.2.

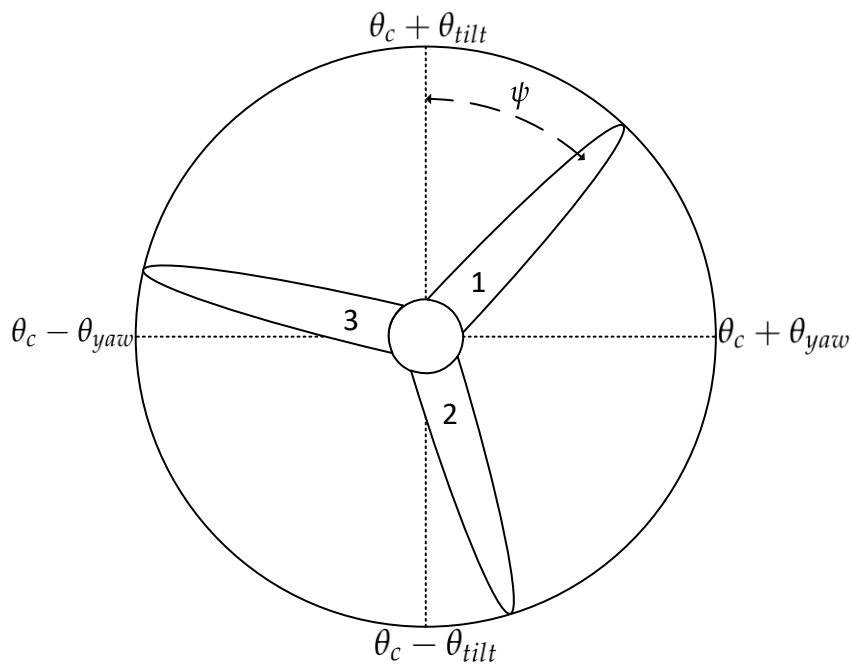


Figure 6.2: Illustration of individual pitch control method using PI.

the values for Δ_{tilt} and Δ_{yaw} are found by the help of 2 PI-controllers.

$$\theta_{tilt} = K_p \cdot M_{tilt} + K_i \int_0^t M_{tilt} dt \quad (6.8)$$

$$\theta_{yaw} = K_p \cdot M_{yaw} + K_i \int_0^t M_{yaw} dt \quad (6.9)$$

The proportional- and Integral gain were found by intentional tuning, where following gain was found to be sufficient for the system:

- $K_p = 2 \cdot 10^{-6}$
- $K_i = 4 \cdot 10^{-7}$

The calculation for the final pitch angle of each blade is calculated as following

$$\theta_1 = \theta_c + \theta_{tilt} \cdot \cos(\psi_1) + \theta_{yaw} \cdot \sin(\psi_1) \quad (6.10)$$

$$\theta_2 = \theta_c + \theta_{tilt} \cdot \cos(\psi_1 + 120^\circ) + \theta_{yaw} \cdot \sin(\psi_1 + 120^\circ) \quad (6.11)$$

$$\theta_3 = \theta_c + \theta_{tilt} \cdot \cos(\psi_1 + 240^\circ) + \theta_{yaw} \cdot \sin(\psi_1 + 240^\circ) \quad (6.12)$$

This calculation is also often referred to as inverse qd-transformation.

6.2 Comparison between Collective PI and Individual PI Control

To validate the effect of the individual pitch PI-controller, it is compared to the collective pitch PI-controller described in section 5.1. To do this, two different simulations has been carried out using FAST.

- **In the first simulation**, only the collective pitch controller described in previous chapter is used.
- **In the second simulation**, the collective pitch controller has been used as a baseline and the individual pitch controller described in this sections has been added.

To make sure that both controllers are tested on a verified system, they were tested on a certified set-up in FAST.

As wind input, a wind speed of 17 m/s (at hub height) with turbulence and vertical shear (with a power law exponent of 0.2) was chosen. The wind speed at hub height can be seen in figure 6.3.

The pitch angles and the pitch rates given by the controllers can be seen in figure 6.4.

Here it can be seen that the pitch angles of all 3 blades from the second simulation fluctuate around the collective pitch angle used in the first simulation.

As the pitching rate of the blade is limited, it is necessary to analyse the blade pitch rates, which are shown in figure 6.4.

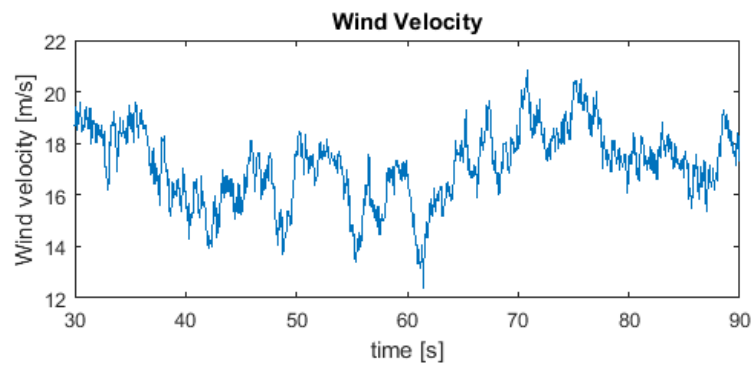


Figure 6.3: Wind speed at hub height used for verification.

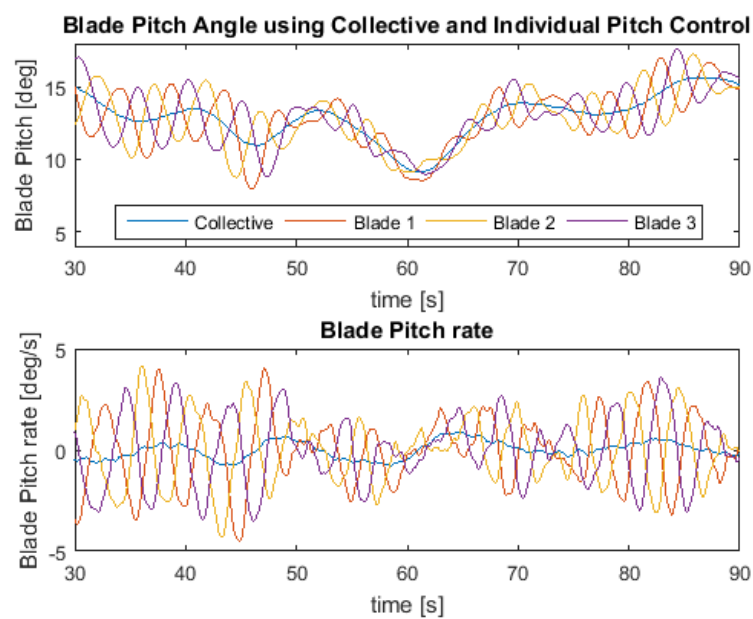


Figure 6.4: Pitch angle and pitch rate using collective and individual pitch control.

Here it can be seen that the blades are pitching with a rate of more than 4 deg/s when using individual pitch control, whereas the collective pitch controller does not exceed a pitch rate of 1 deg/s .

Loads on Turbine

To validate the performance of the different controllers, the performance and damage on the wind turbine has to be investigated. The individual pitch control was expected to have an influence on the following parts of the wind turbine:

- Tower loads

- Load on blades (edgewise moment and flapwise moment)
- Load on pitch bearings
- Load on hub
- Torsion of low-speed-shaft
- Produced power output

This report does not include a detailed analysis of the fatigue of the wind turbine. Only the results and comments regarding fatigue are given in this section.

6.2.1 Tower loads

The tower fore-aft deflection and the rotor thrust can be seen in figure 6.5

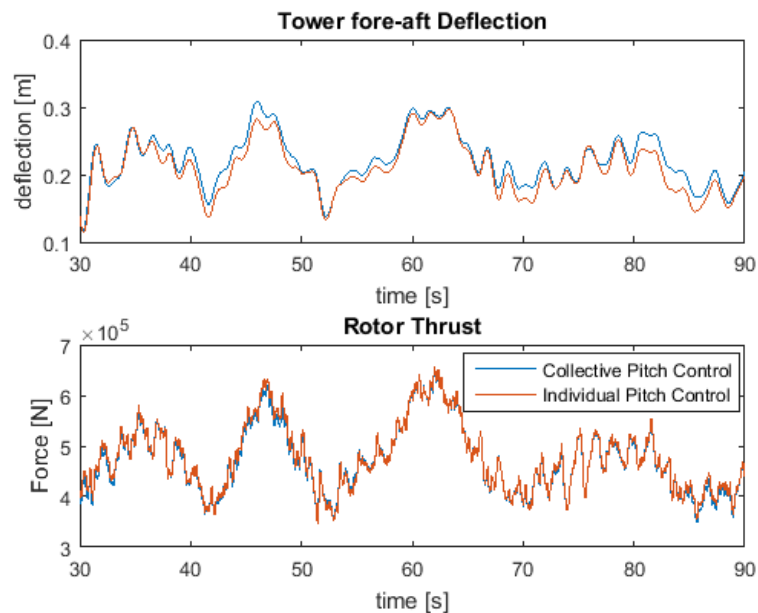


Figure 6.5: Comparison of tower deflection and the rotor thrust.

Here it can be seen, that the fore-aft deflection of the tower has decreased when using individual pitch control, while the rotor thrust has increased a very little - this could lead to confusion, as the fore-aft deflection could be expected to be proportional to the rotor thrust. The reason to this behaviour is, that the equivalent point of pressure using collective pitch is located in the upper half of the rotor plane and thereby leads to an additional tilt moment acting on the hub. The use of individual pitch control lowers the equivalent pressure point, as it tries to even out the loads on the rotor. More about the moments acting on the hub can be

seen in subsection 6.2.4. The average reduction in deflection of the tower has been calculated to be 0.011 m.

6.2.2 Load on Blades

The Flap- and Edgewise deflection of all three blades can be seen in figure 6.6.

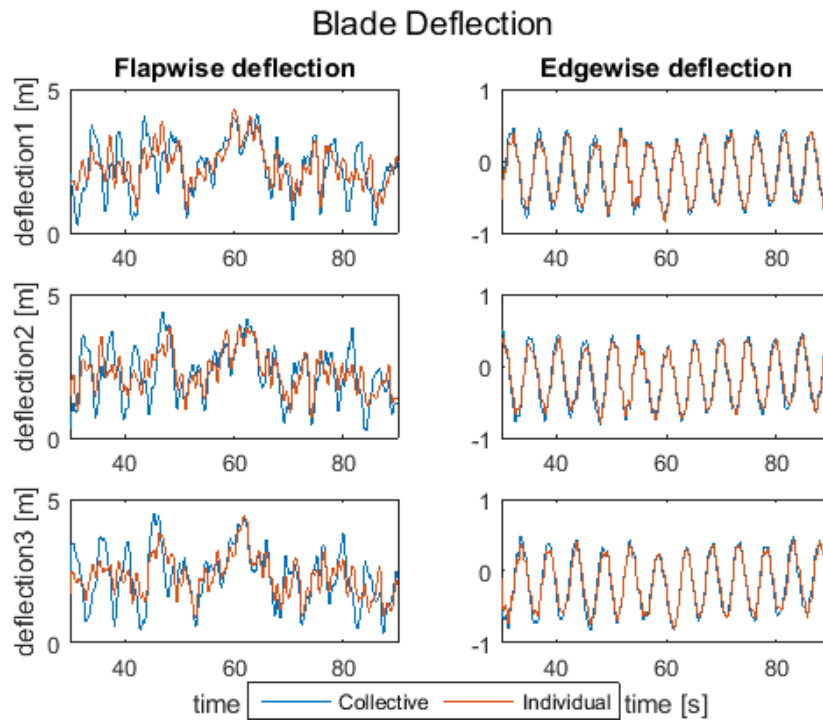


Figure 6.6: Flap- and edgewise blade deflection for blade 1, 2 and 3.

Here it can be seen, that the amplitude of the edgewise deflection almost is not affected by the individual pitch controller. The reason to this is, that the edgewise deflection mainly is caused due to gravity. The flapwise deflection shows approximately the same mean deflection level in both simulations, but here the amplitude is lowered when using individual pitch control.

Additional to the deflection, a FFT analysis of the blade movement has been carried out, which can be seen in figure 6.7.

Here it can be seen, that individual pitch control does not have a big influence on the edgewise deflection. The peak at 0.2 Hz is equal to the rotor frequency and is thereby caused by gravity.

The FFT analysis of the flapwise deflection shows a damping at the rotor frequency when using individual pitch control.

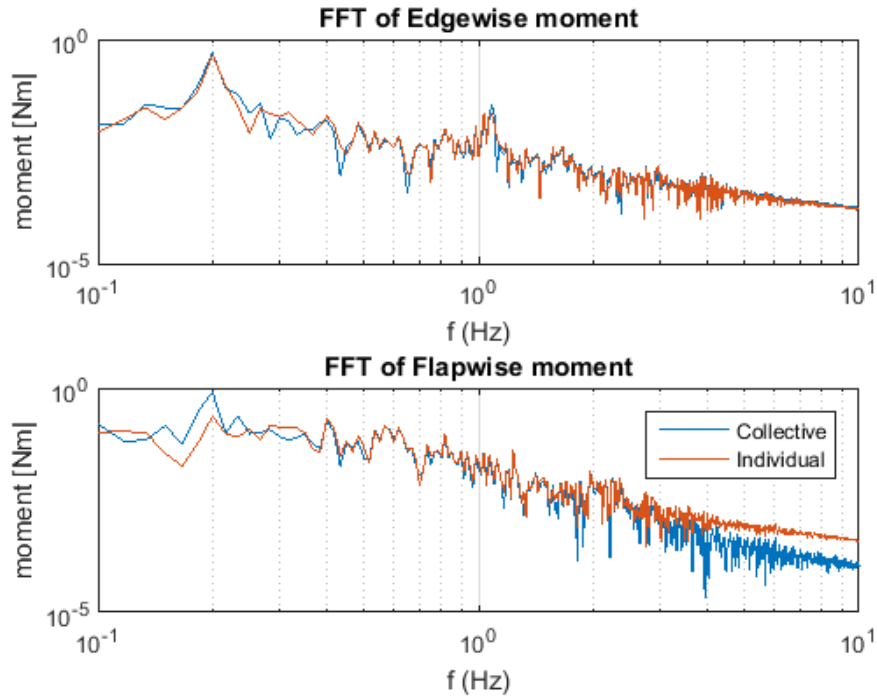


Figure 6.7: FFT analysis of blade deflection.

6.2.3 Load on Pitch Bearings

Using Individual pitch control causes the blades to be pitched constantly to eliminate the tilt- and yaw moment on the main bearing.

A simple method to estimate the fatigue damage of the pitch bearings is given as [12]

$$D_{\theta} \approx \int_y^{t+T} M_B^k(t) |\dot{\theta}(t)| dt \quad (6.13)$$

where

- D_{θ} is the total damage on the bearings of the blade
- M_B is the total moment on the blade bearing (root bending moment)
- k is the Wöhler exponential, for the most bearings given as $k = 3$ [7]

while the total blade moment is given by means of the flapwise and edgewise root bending moment

$$M_B = \sqrt{M_f^2 + M_e^2} \quad (6.14)$$

Here damage has increased by 169% when using individual pitch control (compared to collective pitch control). But here it has to be mentioned, that shear forces are not taken into consideration, which also could have an effect on the fatigue of the pitch bearings.

6.2.4 Load on Hub

The Tilt and Yaw loads on the Hub can be seen in figure 6.8.

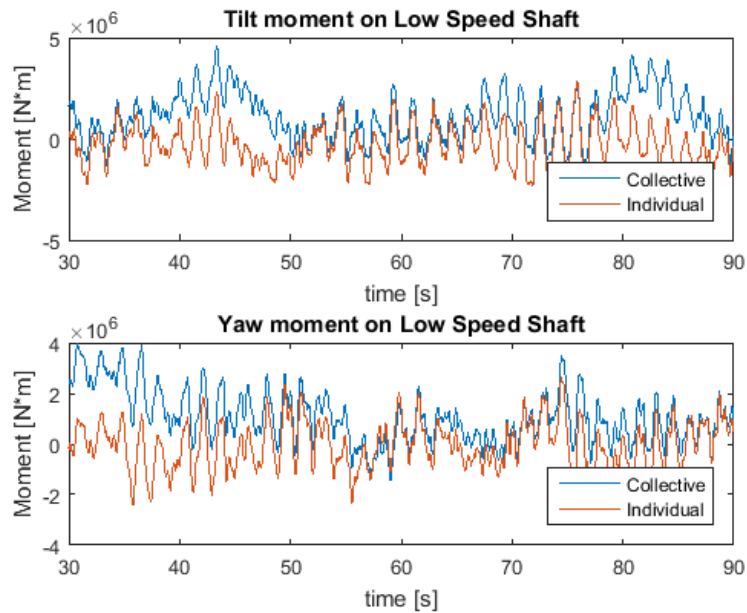


Figure 6.8: tilt- and yaw moments on hub using collective and individual pitch control.

Here it can be seen that the loads on the hub caused by shear wind has decreased significantly by the help of individual pitch control.

The total moment on the hub has been calculated as in equation 6.14 and then the average and the standard deviation of the total moment on the hub were calculated:

	mean value	standard deviation
Collective pitch	$1.6373 \cdot 10^6$	$3.1981 \cdot 10^5$
Individual pitch	$4.686 \cdot 10^5$	$1.52 \cdot 10^5$

6.2.5 Load on Low-Speed-Shaft

The torsion of the low speed shaft can be seen in figure 6.9.

Here it can be seen, that the individual pitch control does not have a significant impact on the amplitude of the torsion.

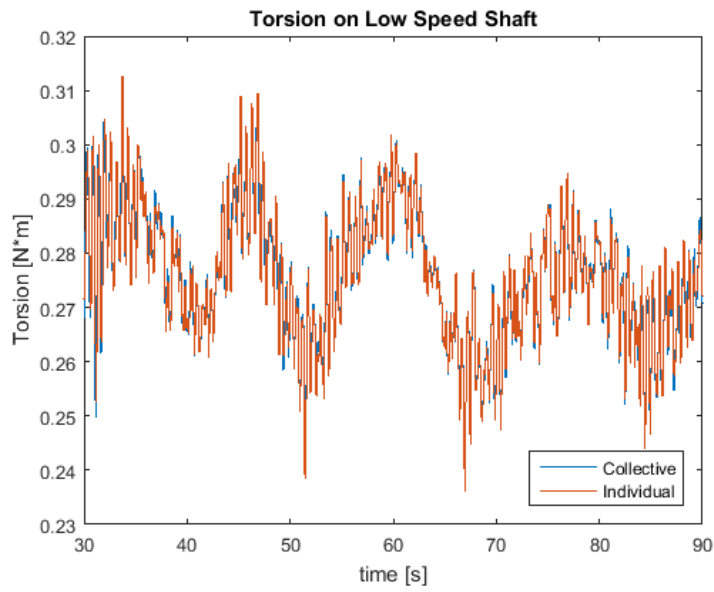


Figure 6.9: Comparison of torsion of low-speed-shaft.

6.2.6 Power output

To be sure that the use of individual pitch control does not influence the performance of the wind turbine, the power output has been compared, as seen in figure 6.10.

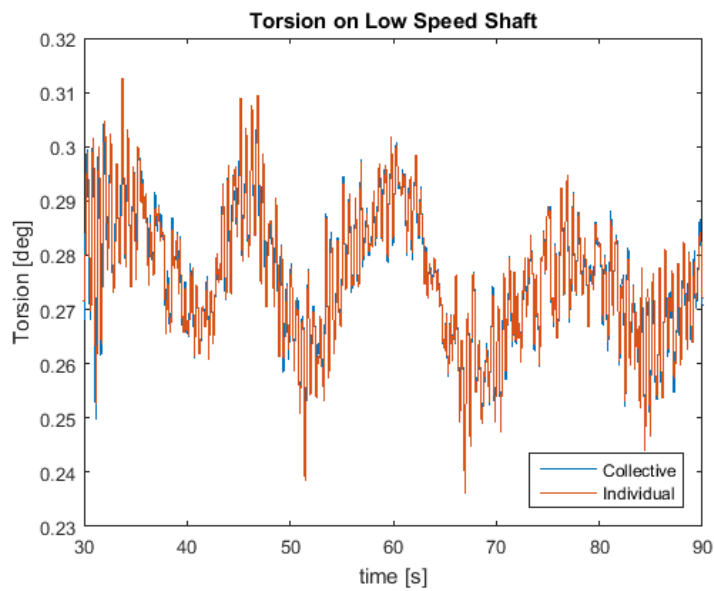


Figure 6.10: Comparison of power output.

Here it can be seen, that the use of the individual pitch controller does not affect the power output significant.

6.3 Individual Pitch Control using MPC

The implementation of MPC has not been successful in this project, as it was not possible to stabilize the power output or generator torque, since the blade pitch angle did not stabilize the rotor speed.

In figure 6.11 and 6.12 the pitch angle and the rotor speed can be seen, respectively.

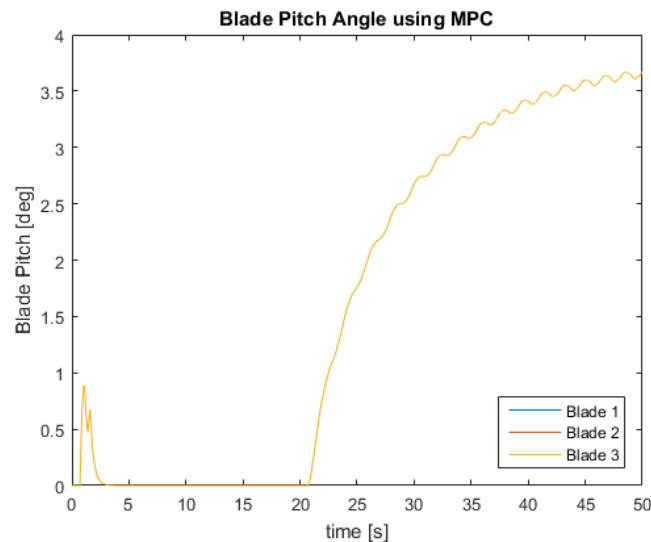


Figure 6.11: Blade pitch angle using MPC.

As it can be seen, the rotor speed increases above the rated rotor speed, while the pitch angle still remains zero. This leads to further increase of the rotor speed, until the blade pitch angle given into the system increases. As the rotor speed is far from the operating regions, the system was concluded to be unstable. Due to time limitations, it was not possible to stabilize the system using MPC.

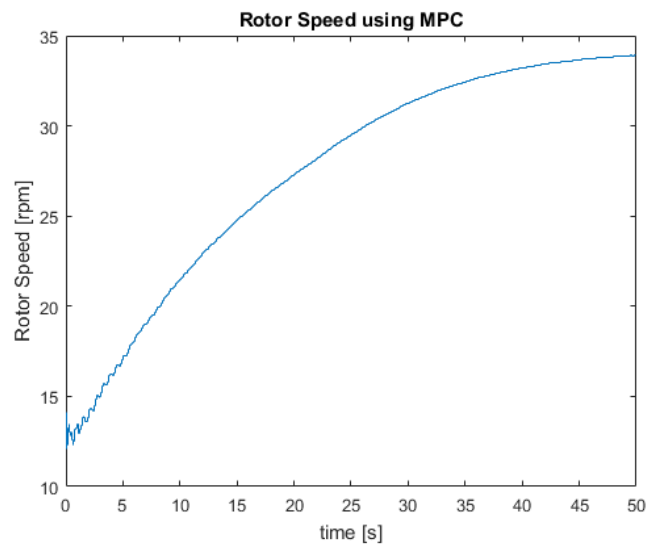


Figure 6.12: Rotor speed using MPC.

Chapter 7

Discussion

A wind turbine is a very complex structure, that reacts on aerodynamic forces from the wind. This makes it complicated to develop a good model which is valid in reality. The non-linear model, which has been developed in this project contains some of the basic structural dynamics, which were simplified to mass-spring-damper systems. For the blades it is very clear that the edge- and flapwise deflection influence each other in way more complex manner in FAST than in the developed models. Here it also has to mentioned, that the twist in the blade was not implemented in the development of the structural model of the blades, but only in the calculation of the aerodynamic forces in the blade element momentum theory (BEMT). The edge- and flapwise deflection were modelled in such a way, that they influence each other - but the influence coefficients were tuned by hand, so the final deflection fits to the deflection given by FAST. This approach was chosen to be sufficient for the development of a control system, but could be improved. The model was only validated within windspeed reaching from 16 to 17 m/s, which does not mean, that it is valid at wind speeds below or over the mentioned area.

The collective PI controller developed in this project was based on a gain scheduling which uses a very simple model with a stiff drive-train. Furthermore the control was scaled intentionally based on a step response of the wind. Due to the lack of experience and knowledge with wind turbines, this choice of controller is not necessarily the best possible collective pitch controller. But since the collective pitch controller is used as a basis for the individual PI controller, it was chosen to avoid to make the collective PI controller more aggressive.

The individual PI controller used in this project was tuned intentionally. Here it could be beneficial to have some more experience and knowledge about wind turbines to tune and validate the performance of the individual pitch controller.

The individual PI controller has the purpose to eliminate the uneven loads on the rotor, caused by shear wind. As the pitch angle of the blades varies much more compared to collective pitch, it could have a valuable effect on the lifetime of the pitch bearings, compared to collective pitch. When using turbulent wind conditions, the amount of shear could vary, which could have a significant effect. Here it can be mentioned, that sometimes (for example in figure 6.8 at the time between 45 and 50 seconds) the average tilt moment within one rotation is negative.

This means, that the individual pitch controller controls the pitch level of the blades too much and thereby reduces the lifetime of the pitch actuators without any benefit. Here it could be more beneficial to have a simple P-controller to avoid those kind of unfavourable situations. In this case the design of the filter in section 6.1.2 could be improved, ending up with a controller that both could reduce the loads on the main shaft, without reducing the lifetime of the pitch actuator as much as an individual PI controller. In addition, a big acceleration of a pitch actuator also leads to a twist moment in the blade, which not has been taken into consideration in this project - but could reduce the lifetime of the blade.

The developed MPC controller was neither capable of stabilizing the generator speed or the power output. This means, that the use of MPC can not be validated, as the use of MPC has not been implemented successfully.

Chapter 8

Conclusion

The non-linear model in this project was successfully developed and validated, whereafter the linear model was derived and compared to FAST. Here both models showed some reasonable outputs, which were chosen to be sufficient for the development of control systems.

The collective- and individual PI controller have successfully been implemented in the aero-elastic simulation software FAST, together with a turbulent wind field generated in TurbSim. Here the implementation of the collective PI controller has shown to be able to maintain a stable power output and was therefore chosen to be sufficient for further use as a baseline controller for individual pitch control. The individual PI controller was tuned intentionally and has shown to be able to even out the loads on the rotor of the wind turbine in both tilt and yaw direction. As the pitch controller was used to pitch all 3 blades individually, the fatigue of the pitch bearings will be increased and thereby reducing lifetime of those. This concludes, that the lifetime of some components could be increased, while the lifetime of other components could be decreased. On the other hand, the wrong use of individual pitch control could lead to a total reduction of lifetime of the wind turbine, by increasing loads on some parts without reducing loads sufficient on other parts - and thereby increase overall cost of the wind turbine. Even though an estimation of the lifetime not has been given, it leads to the conclusion that further research could benefit the total lifetime, or lead to the use of cheaper components and thereby reduce overall cost of the wind turbine.

As the use of MPC was not successfully implemented, the benefits and disadvantage of it can not be concluded.

Bibliography

- [1] Allan J. Larsen et al. *Individueel pitchregulering af vindmølle*. Technical University of Denmark, 2006.
- [2] E.A. Bossanyi et al. "Individual Blade Pitch Control for Load Reduction". In: *Wind Energy Volume 6* (2002).
- [3] Jason Jonkman et al. *Definition of a 5-MW Reference Wind Turbine for Offshore System Development*. National Renewable Energy Laboratory, 2009.
- [4] Johannes Friis et al. "Repetitive Model Predictive Approach to Individual Pitch Control of Wind Turbines". In: *2011 50th IEEE Conference on Decision and Control* (2011).
- [5] Jose de Jesus Barradas-Berglnd et al. "Fatigue damage estimation and data-based control for wind turbines". In: *IET Control and applications* (2014).
- [6] Mahmood Mirzaei et al. "An MPC approach to individual pitch control of wind turbines using uncertain LIDAR measurements". In: *2013 European Control Conference (ECC)*.
- [7] Tony Burton et al. *Wind Energy Handbook*. Wiley, 2001.
- [8] Yunqian Zhang et al. "Mitigation of Fatigue Loads Using Individual Pitch Control of Wind Turbines Based on FAST". In: *46th International Universities' Power Engineering Conference, UPEC 2011*.
- [9] Zhongzhou Yang et al. "Individual Pitch Control for Wind Turbine Load Reduction Including Wake Modeling". In: *Wind Engineering Volume 35* (2011).
- [10] Office of Energy Efficiency and Renewable Energy. *Schematic diagram of a modern horizontal-axis, three-bladed wind turbine*. https://commons.wikimedia.org/wiki/File:EERE_illustr_large_turbine.gif. 2006.
- [11] Gene F. Franklin. *Feedback Control of Dynamic Systems*. 6. ed. Pearson, 2010.
- [12] Keld Hammerum. *A Fatigue Approach to Wind Turbine Control*. Technical University of Denmark, 2006.
- [13] Martin O. L. Hansen. *Aerodynamics of Wind Turbines*. 3. ed. Routledge, 2015.
- [14] Søren R.K. Nielsen. *Vibration Theory, Vol. 1: linear vibration theory. (3rd edition ed.)* Aalborg University, 2004.

- [15] NREL. *FAST source code file: dependencies/AeroDyn/BEMTUncoupled.f90 line 472 to 492*. 2017.

Appendix A

Appendix

During this project, several MATLAB and SIMULINK files were developed. Here is given a list of the used files in this project:

Appendix/FAST/... should contain NREL's aeroelastic computer-aided engineering (CAE) tool FAST, which in this project is used to simulate a wind turbine. As the source files were too big for the AAU database, it is necessary for the reader to download them from the NREL website and place the bin-files in this folder.

For chapter 3 the following files, including their explanation, are:

- .../Appendix/Modelling...*
- .../BladeMode_estimation.m*: identify the blade mode shapes
- .../DOFtest.m*: identify the importance of the different DOF's
- .../Parameter_estimation_Edgewise.m*: estimation of parameters for the edgewise DOF
- .../Parameter_estimation_Flapwise.m*: estimation of parameters for the flapwise DOF
- .../Parameter_estimation_Generator.m*: estimation of timeconstant for the generator
- .../Parameter_estimation_Tower_K.m*: estimation of spring constant for the tower
- .../Parameter_estimation_Tower_omega_zeta.m*: estimation of ω and ζ for the tower
- .../Turbine_regions.m*: to show operation regions (section 2.2)
- .../FAST_only.mdl*: contains the SFunction to run FAST
- .../ModelverificationDriveTrain.slx*: contains the model of the drive train
- .../ParameterEstimationGenerator.slx*: contains the model of the generator

The Collective and individual control systems were implemented in the folder "*Appendix/Controller_verification*" where

.../CertTest26/ contains the setup of the wind turbine model. This folder contains the original files given from NREL's setup for the 5 MW wind turbine. The only change that has been done in this folder is the settings for the wind input used, as the original wind data only contained wind speeds around 12 m/s.

.../Controller_Collective.m is used to compare different collective PI controller gains, as discussed in section 5.1.

.../Controller_Individual.m is used to compare the individual PI controller to the individual PI controller in section 6.2.

.../FAST_Collective.mdl and *.../FAST_Individual.mdl* contain the SFunction to use FAST and the implementation of the collective, and individual PI controller, respectively.

Appendix/Collective pitch gain scheduling/... contains the files used to find the gain scheduled functions in section 5.1

Appendix/Model Validation/... contains the validation of the linear and nonlinear model, where *.../Main_Validation.m* contains the constants used for both the linear and non-linear model. Furthermore it contains the state space matrices for the linear model.

.../Turbine_model.slx contains the simplified and clear version of the nonlinear model (Notice that it is necessary to run "*Main_validation.m*" to load constants into workspace.

Appendix/Controller_verification_MPC/... contains all files used for the development and testing of the MPC, which has not been implemented successfully.

A.1 BEMT Verification

In figure A.1 the rotor speed is shown for the simulations. It is seen that the rotor speed is 12.1 m/s which is the rated speed of the NREL 5 MW wind turbine as discussed in section 2.2. The same rotor speed is naturally given to the BEM-MATLAB function implemented in simulink as seen in figure ??.

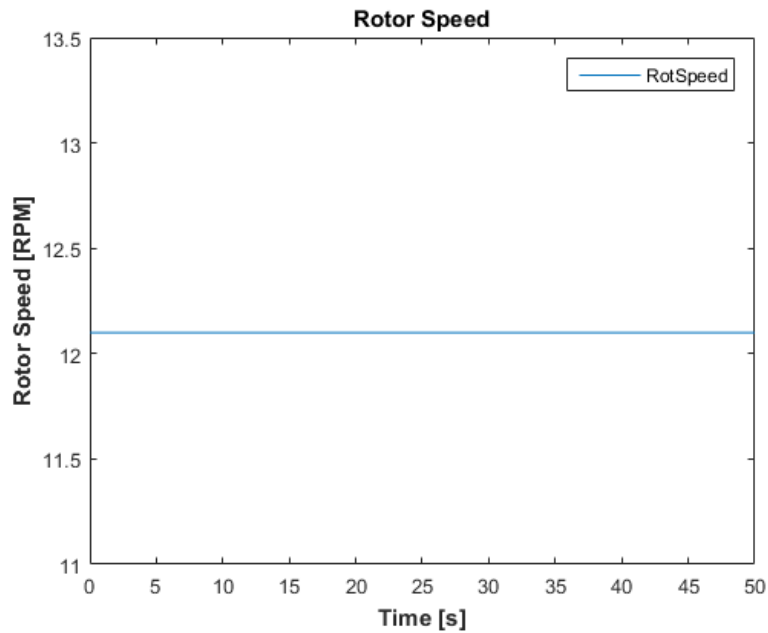


Figure A.1: Rotor speed as commanded in FAST.

The pitch angle command ramp signal is shown in figure A.2. The initial pitch angle is -20 deg, and the ramp has a slope of 1 deg/s. The simulation was run for 50 s to achieve a pitch varying from -20 deg to 30 deg.

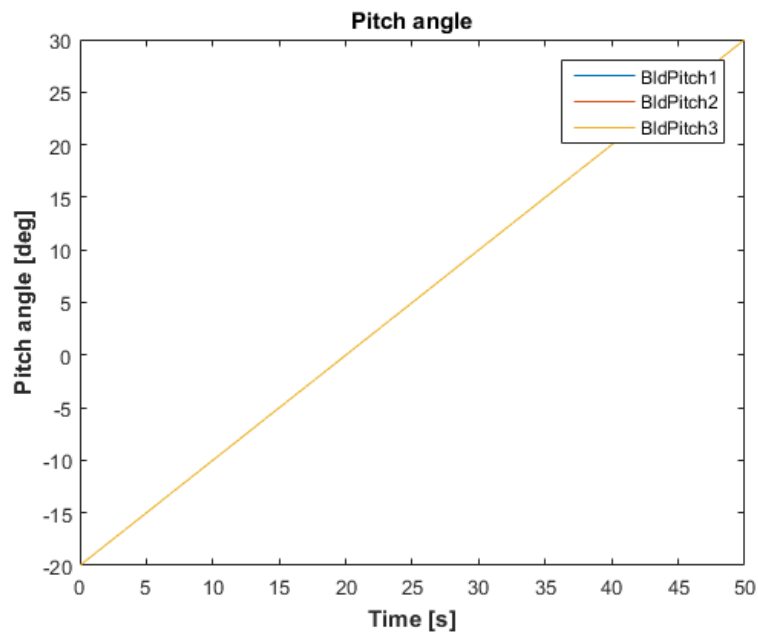


Figure A.2: Pitch angle ramp used for validation.

In figure A.3 the comparison between the aerodynamic thrust force calculated from Aerodyn and the thrust force calculated in Simulink is shown. The free-stream wind speed is a uniform wind field of 12 m/s for simplicity. The upper plot gives the thrust force from both Aerodyn and Simulink and the lower plot gives the Simulink calculation's deviation from the Aerodyn output in percent. As seen the two simulation results are so close to each other that the two cannot be distinguished in the upper plot. The deviation is very close to zero percent and the spikes seen are caused because of the simulation curves zero crossings. The smaller spike is due to spikes occurring in the Aerodyn calculation as seen in figure A.4.

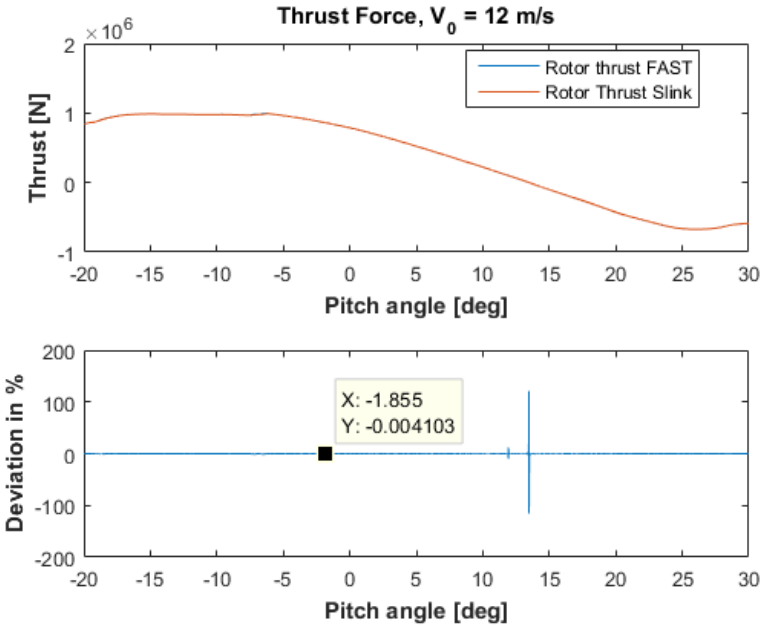


Figure A.3: Aerodynamic Thrust comparison between Aerodyn and the simulink BEM model.

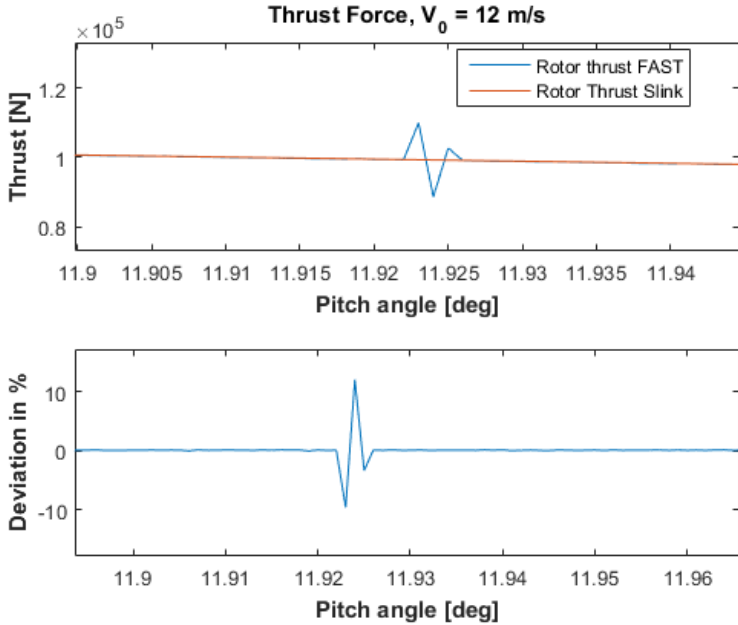


Figure A.4: Aerodynamic Thrust comparison between Aerodyn and the simulink BEM model.

The comparison between the FAST Aerodyn modules aerodynamic torque calculation and the torque calculation from Simulink is shown in figure A.5 again with 12 m/s uniform wind.

Once again the two curves are indistinguishable and the deviation in percent is seen to be close to zero, except for the two zero crossings resulting in the two spikes seen.

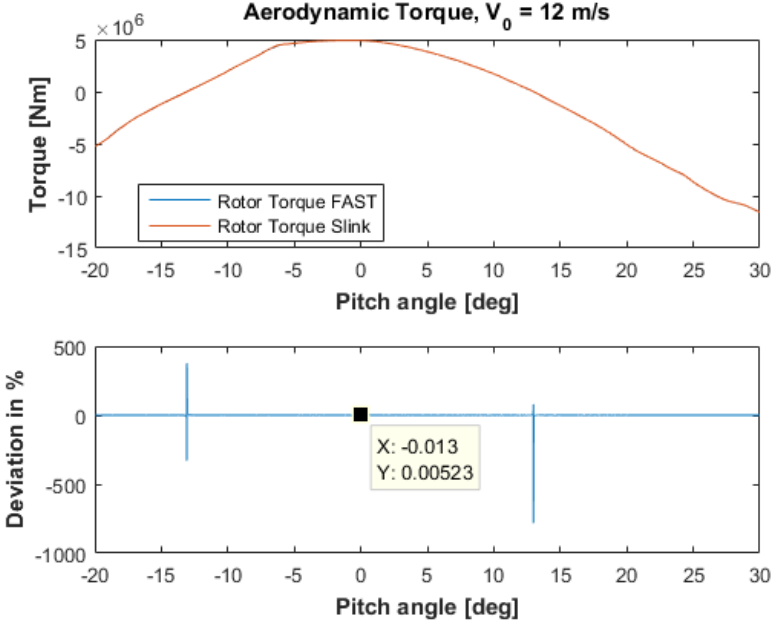


Figure A.5: Comparison between aerodynamic torque calculated by FAST Aerodyn module and BEM code in Simulink/MATLAB function.

The in-plane and out-of plane moments are shown in figures A.6 and A.7, respectively. In FAST, gravity has been unchecked to make sure that the in-plane moment is due to aerodynamic forces only. Again the simulation in Simulink is very identical to the simulation run with FAST.

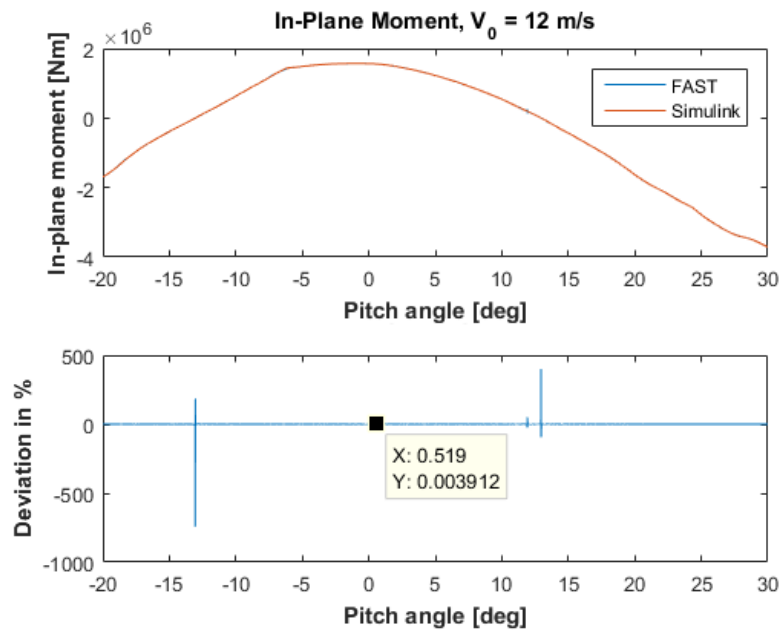


Figure A.6: In-plane bending moment comparison with Elastodyn.

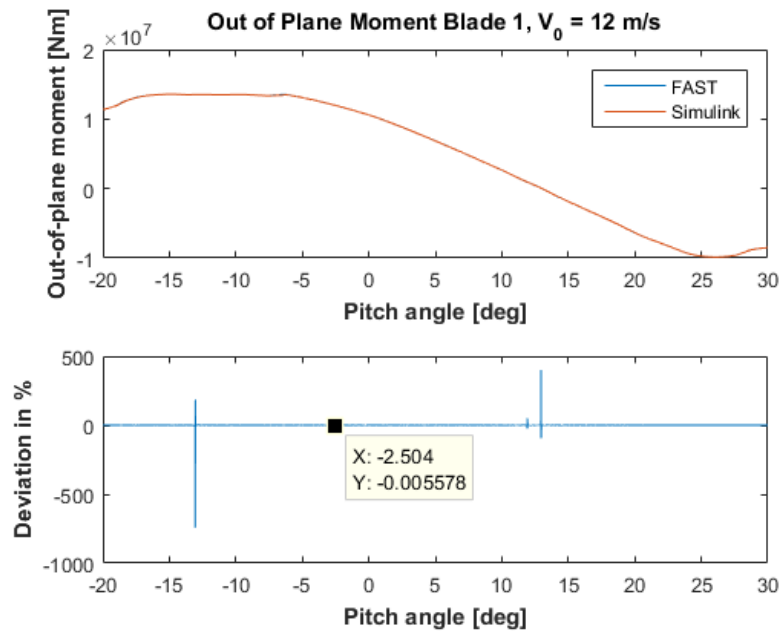


Figure A.7: Out-of plane bending moment comparison with Elastodyn.

The BEM-code block cannot be validated on a single wind speed and simulations have therefore been carried out at 14, 16 and 18 m/s also. In figures A.8, A.9 and A.10 the plots

for aerodynamic thrust, aerodynamic torque, in-plane and out-of plane moment are shown together for wind speeds of 14, 16 and 18 m/s, respectively. Once again the curves from Simulink are as good as identical with the simulation curves from FAST.

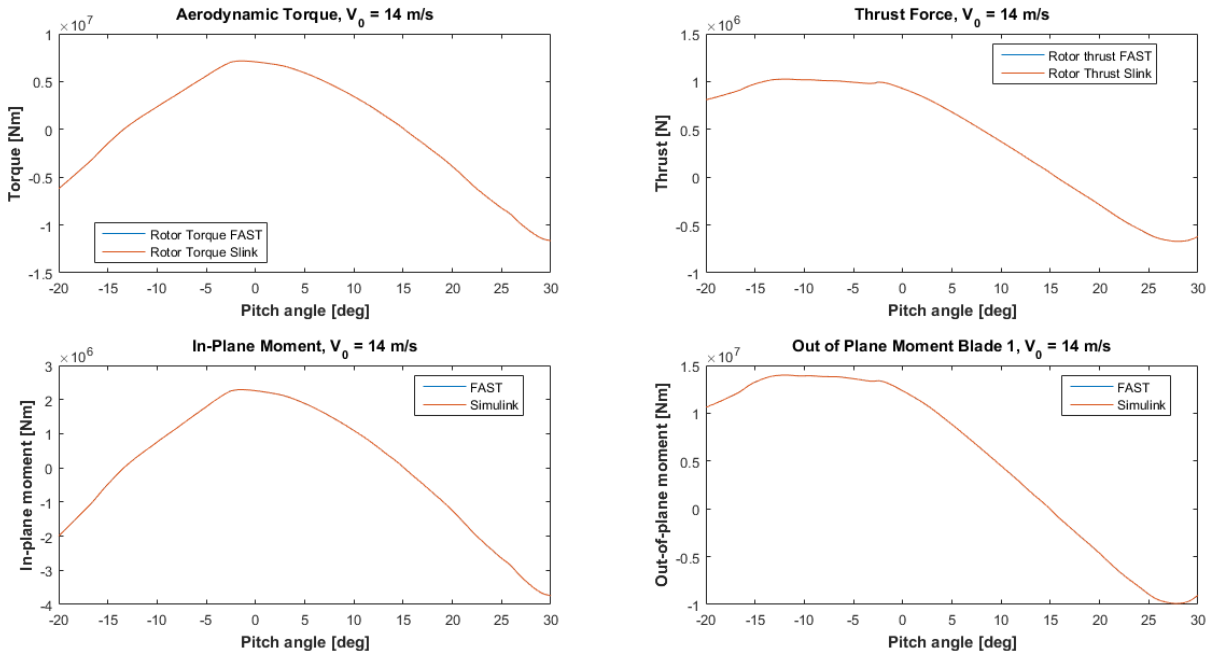


Figure A.8: Comparison at 14 m/s.

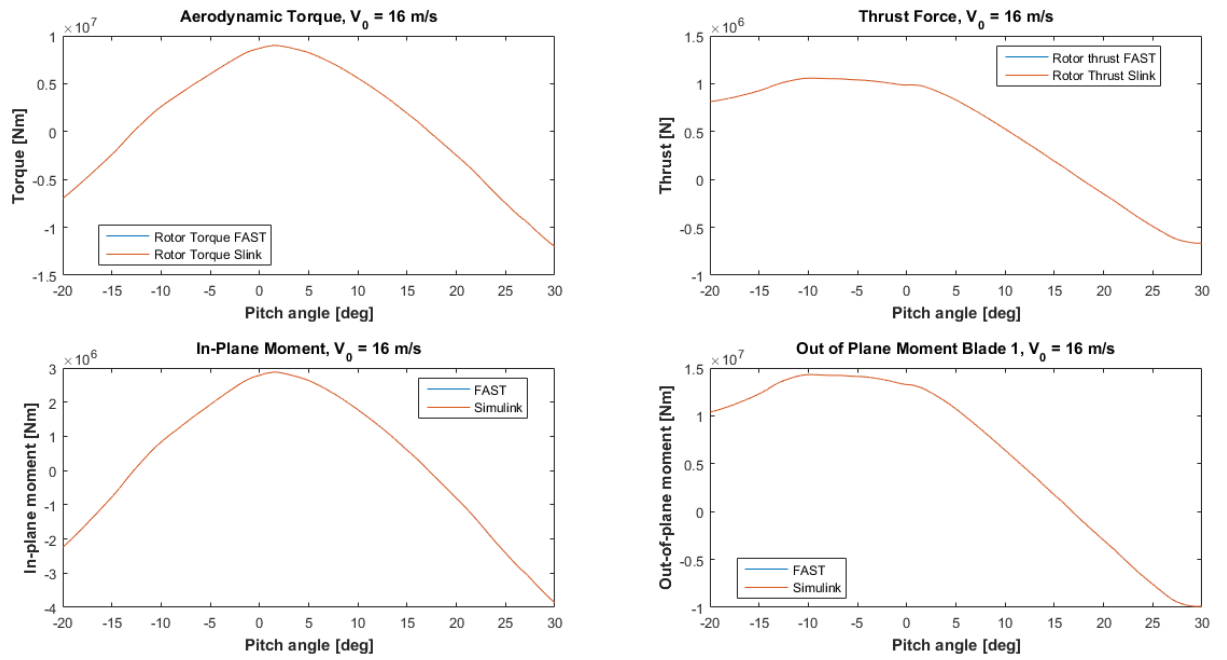


Figure A.9: Comparison at 16 m/s.

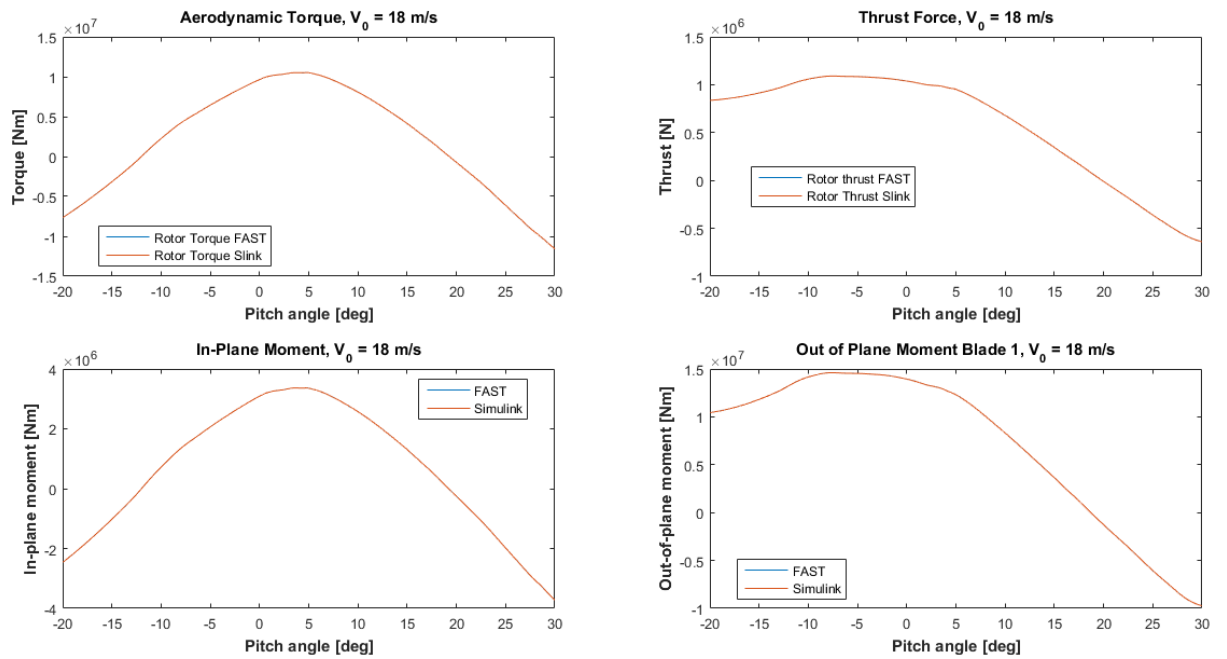


Figure A.10: Comparison at 18 m/s.

Thus, the BEM-coded is deemed acceptable for implementation in the model.

A.2 Drive Train Tuning

As the most parameters for the model of the drive train were given in the datasheet of the 5MW wind turbine, where the generator mass moment of inertia J_g , the equivalent drive-shaft torsional-spring constant K_s and -damping constant D_s were given, the rotor inertia J_r was estimated by the second mass moment of inertia of the blades and the moment of inertia from the hub.

To make sure that the drivetrain model works well, a comparison between the drivetrain in FAST and the modelled drivetrain has been carried out. The inputs into the drive train are the aerodynamic torque from the rotor and torque given from the generator. Both inputs were taken from a test in FAST, where all DOFs were activated and a step wind was used as input ($V_0 = 16m/s$ for $t < 40s$ and $V_0 = 17m/s$ for $t > 40s$).

The outputs from the drive train model are the rotor speed and the generator speed. The rotor speed given from FAST and the simulated rotor speed including the error between them can be seen in figure A.11. Respectively, The generator speed given by FAST is compared with the generator speed calculated in simulink is shown in figure A.12, where also the error between them is shown.

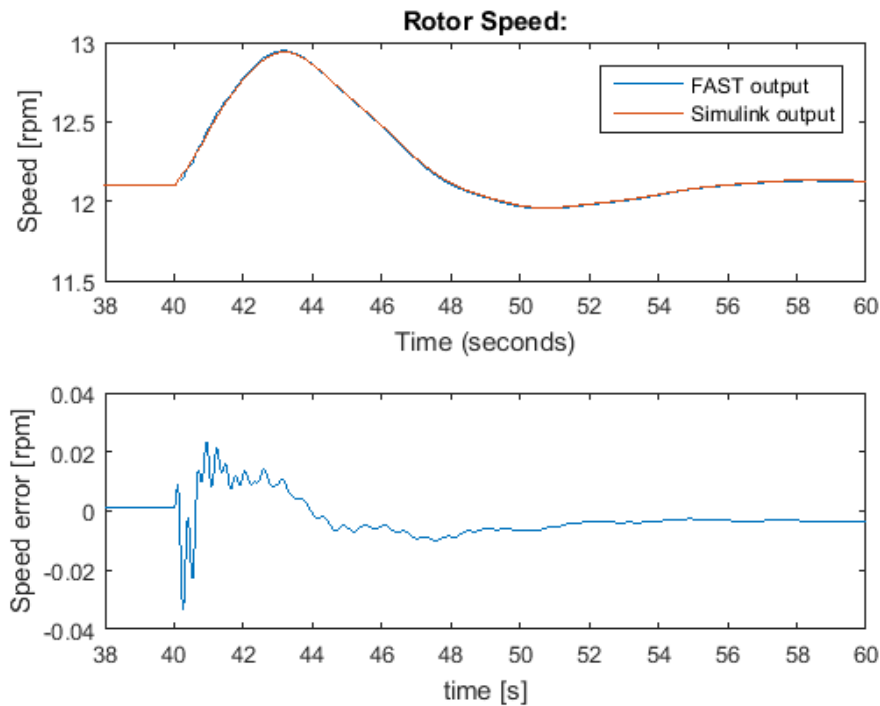


Figure A.11: Generator speed before Tuning.

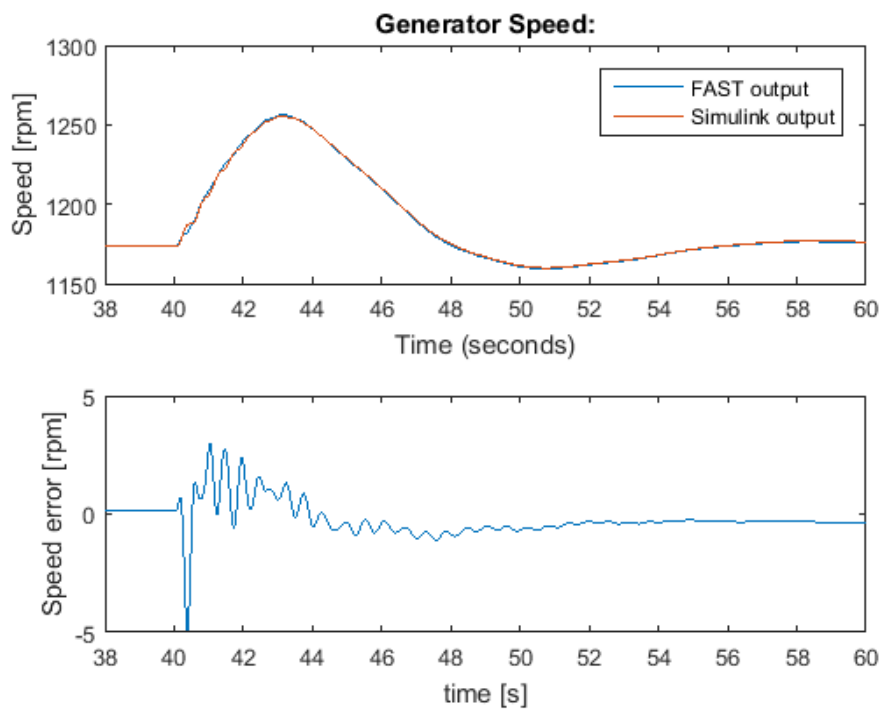


Figure A.12: Generator speed before Tuning.

A.3 BEM Linear Approximations

In this appendix the remaining linear approximations of the BEM calculations are shown graphically for the operating point ($V = 16 \text{ m/s}$, $\theta = 12.06 \text{ deg}$, $\omega_r = 12.1 \text{ RPM}$).

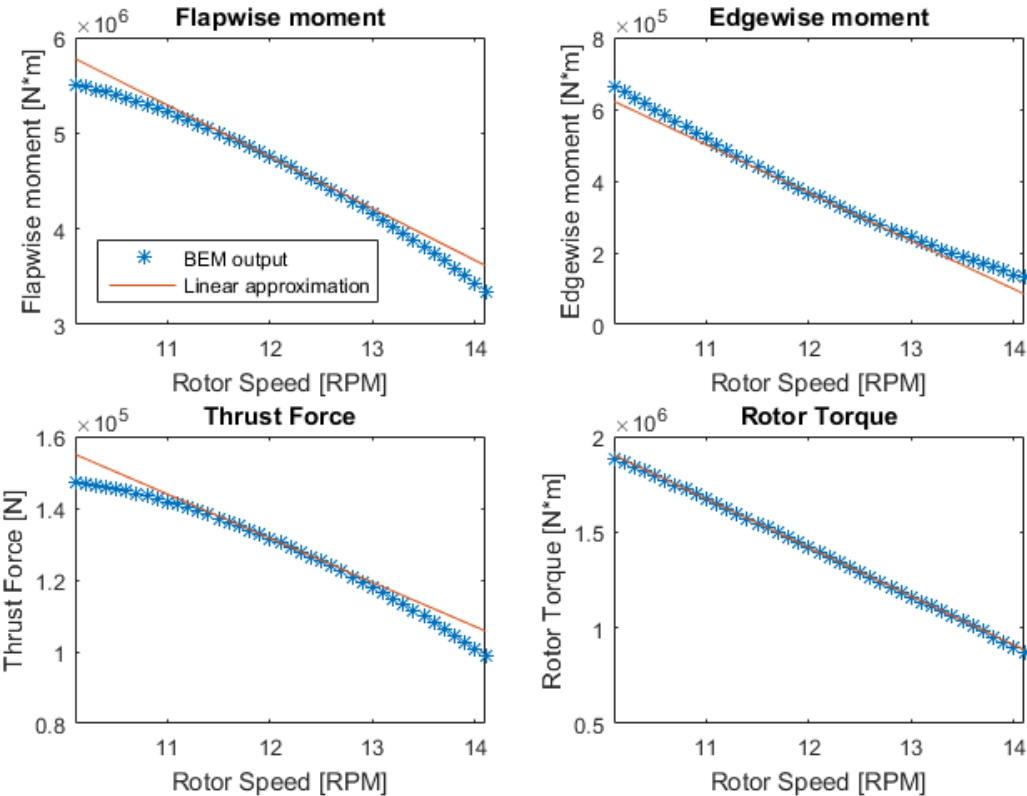


Figure A.13: Linear approximation with respect to rotor speed.

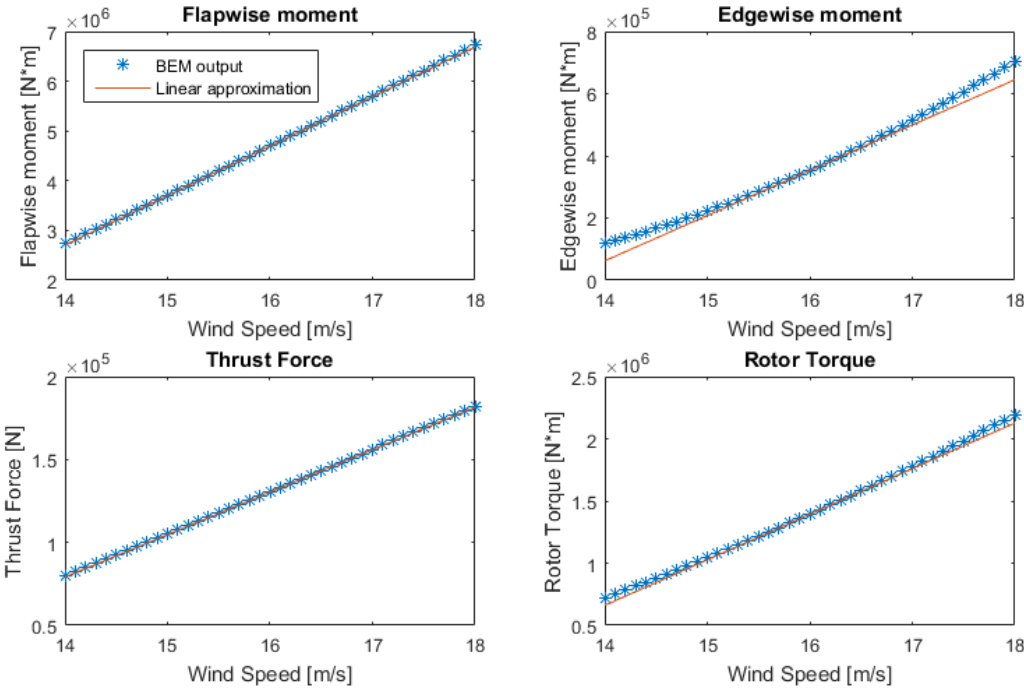


Figure A.14: Linear approximation with respect to wind speed.

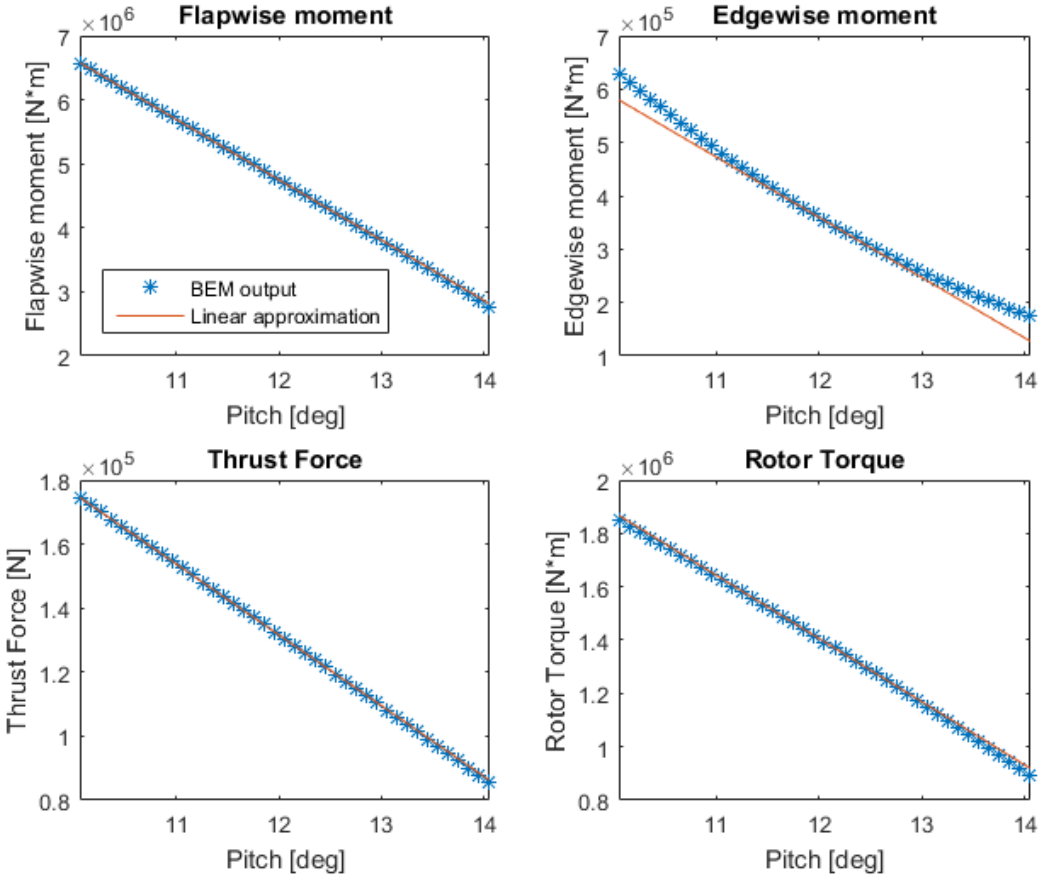


Figure A.15: Linear approximation with respect to pitch angle.

A.4 Validation of Linearization

In this appendix the remaining linear validations are given, where the pitch input has been given a step from 12.0568 (since it was the pitch angle found to fit for 16 m/s) to 13.0568.

It is shown that the blade deflection and blade root bending moment differs significant in the linear model, compared to the non-linear model and FAST, but due to time limitations it was chosen to be acceptable.

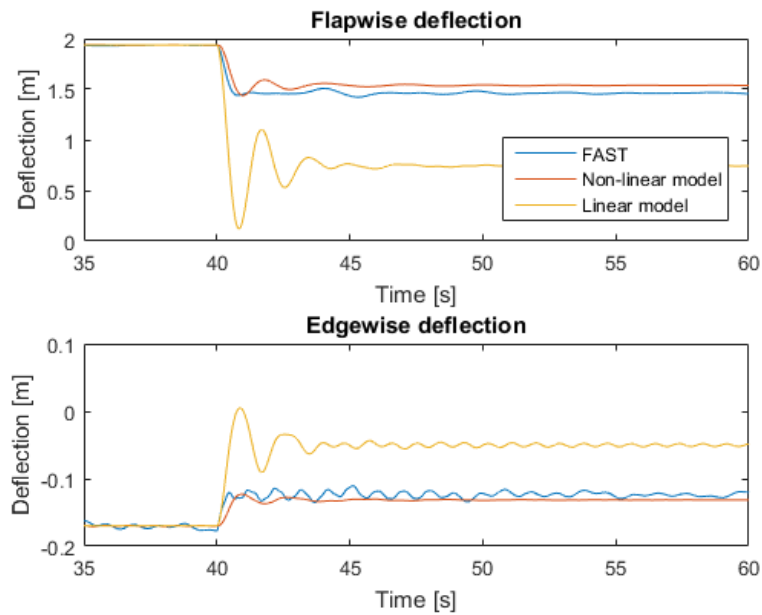


Figure A.16: Blade dynamics with respect to pitch step.

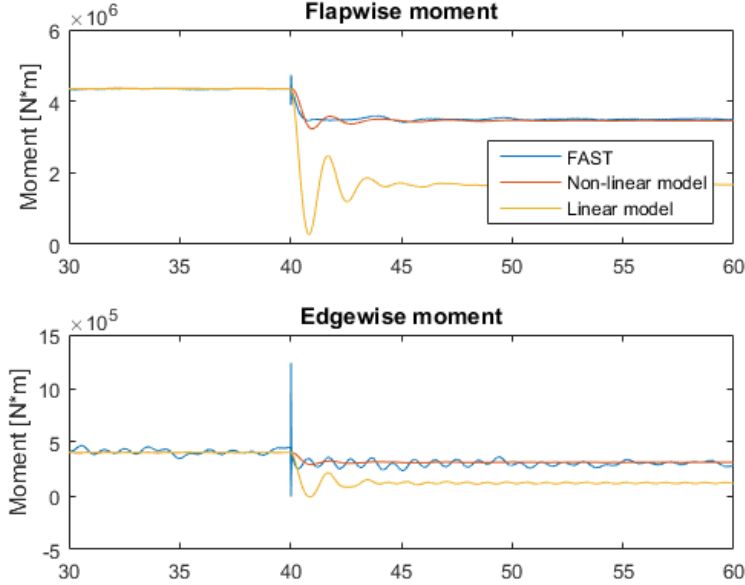


Figure A.17: blade root bending moment with respect to pitch step.

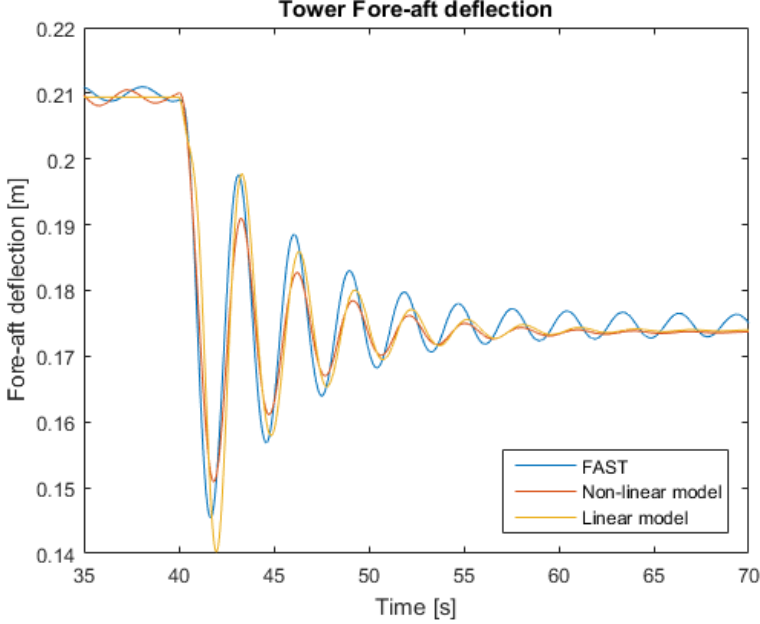


Figure A.18: Tower dynamics with respect to pitch step.

